NTNU
Kunnskap for en bedre verden

Norwegian University of Science and Technology
Department of Engineering Cybernetics
Masters Thesis

Energy consumption model route planning for an UAV with electro-thermal icing protection system

Author:
Man Ken Michael Cheung

Supervisors:
Dr. Tor Arne Johansen
Dr. Richard Hann

June, 2021

Abstract

To accommodate the huge growth in the unmanned aerial vehicle (UAV) industry, research in to dealing with icing is required. This is to make it safe enough for UAVs to operate in highly populated areas. In a pre-existing path planning algorithm for UAVs, particle swarm optimisation (PSO) was used. The algorithm also considers hybrid engine, aerodynamic performance degradation and icing protection system (IPS) energy consumption. In this thesis, the goal is to expand the electro-thermal icing protection system (IPS) part of the algorithm by using experimental and computational data for the performance degradation and energy consumption due to icing. The experimental data comes from having access to icing wind tunnel (IWT) data. The computational data comes from computational fluid dynamics (CFD) simulations, by using commercial software such as LEWICE and FENSAP-ICE. It also implements 3D data usage which comes from CFD models, to compare with 2D data to see the validity in only using 2D data. Lastly, it implements propeller degradation to give more accurate results when the IPS is disabled. This gave, as expected, higher energy consumption than having IPS available. Comparisons were made between anti-icing and de-icing to observe which mode was optimal. The data was implemented by assuming linear relationships and with linear interpolation. Both trilinear and bilinear interpolation methods were used. For the propeller IPS consumption, the data was extrapolated with air temperature through the convection equation and adding a safety margin. For 2D and 3D data usage, 3D was found to consistently give lower power requirements despite having larger drag characteristics. This 2D and 3D power disparity issue was identified with the equation used to calculate required thrust. When 3D data is used, the UAV is operating at a lower angle of attack, leading to the thrust equation to yield lower power requirements. The results became more consistent by implementing changes to the Angle of Attack (AoA). 3D data usage now gave higher energy consumption with the ratio between 2D and 3D being close to the drag ratio of the two datasets. As for comparing anti-icing and de-icing, de-icing does generally yields lower power consumption and was found to be the best balance between energy consumption and flight time for the given weather conditions, but was inconclusive overall. Anti-icing has higher power ratings at low icing severity, while de-icing overtakes anti-icing if the icing is severe enough. The results did not show when de-icing power ratings overtakes anti-icing power ratings. Hence, the results did not show how severe icing needs to be for this to happen. Further investigations is required. Testing should be performed in more varied weather conditions for more conclusive answers. The IPS mode tests were found to be most beneficial when optimising for time compared to optimising for energy. It uses the IPS to its fullest by allowing periodic icing to get the best flight time. This is not the case when optimising for energy as using the IPS consumes energy and the algorithm tries to find an alternative path to avoid IPS usage.

Acknowledgements

I would like to express my gratitude to my supervisors, Dr. Richard Hann and Dr. Tor Arne Johansen for their support, suggestions, guidance and advice during the writing of this thesis.

List of Tables

List of Figures

Abbreviations

UAV - Unmanned Aerial Vehicle

IPS - Icing Protection System

bVLoS - beyond Visual Line of Sight

IWC - Icing Wind Tunnel

CFD - Computational Fluid Dynamics

AoA - Angle of Attack

PSO - Particle Swarm Optimisation

MET - Meteorological Institute

IMU - Inertial Measurement Unit

LWC - Liquid Water Content

MVD - Median Volume Diameter

ENU - East-North-UP

NED - North-East-Down

BWB - Blended Wing Body

MAC - Mean Aerodynamic Chord

TR - Taper Ratio

AR - Aspect Ratio

sUAV - small UAV

RPM - Revolutions Per Minute

LUT - Look-Up Table

Units

Ah- Ampere-hours

Wh - Watt-hours

kWh - kilo-Watt-hours

m - meters

W - Watts

m/s - meters per second

kg - kilogram

Table of Contents

1 Introduction

1.1 Background and Motivations

The growth of the unmanned aerial vehicle (UAV) industry has been significant in the past few years and is expected to grow even further in the future. According to Global UAV market forecasts, the expected market growth is close to triple between 2018-2029 [11]. To be able to fully exploit this growth and hence expand this market to its fullest potential, there are number of challenges that needs to be addressed, as reviewed by Hann and Johansen [12]. These include applications in cold climates and in the topic of aircraft icing. There is a drive among a few industries, such as the automobile industry, that wants to offer air taxis, automated air package deliveries in retail or scientific applications, such as surveillance, monitoring and data gathering for research purposes. UAV icing then becomes important to deal with as it is critical for safety of passengers in air taxis, or safety of bystanders when drones are out for package delivery. It is important to ensure that drones are able to achieve their missions by being able to deal with icing that can occur in all, but the hottest of climates. Hence, there has been a research drive to look further into UAV icing to be able to deal with issues that can show up. It is important to note that there is a distinction between unmanned and manned flight icing. This thesis will specifically deal with unmanned flight icing. This is because there has been extensive research into manned flight icing conditions, but with a gap in knowledge for unmanned flight icing. There are key differences between manned and unmanned flight. Firstly, manned aircraft will usually have more resources at their disposal, mainly having a larger power capacity in form of fuel, while unmanned vehicles will most likely be battery powered or hybrid. This particularly applies to small unmanned vehicles, as there exist drones that are quite large and have the capacity to carry as much fuel as some manned aircrafts. With this extra capacity, icing protection systems (IPS) can deal with any potential icing on the aircraft in a less restrictive manner. It is also easier for the pilot to spot if any icing has occurred and can better control the IPS and use only as much energy as required. Commercial size aircraft will have additional measures available to them, such as being able to fly at high enough altitudes where icing is less frequent and be able to identify most conditions where icing can occur. Additionally, with larger aircrafts, the ice will be a very small percentage of the total weight of the plane and will have less effect on energy consumption overall.

For small UAVs, the measures to avoid icing as mentioned, will either not be applicable or be less effective. This is particularly the case for UAVs that operate beyond visual line of sight (bVLoS), as most systems will need to be automated [13]. The IPS use will be much more restricted due to having much less energy capacity. If the UAV is within line of sight, visual inspection for icing is possible, but when the UAV is bVLoS other methods is required to effectively detect the presence of ice. This can be done using optics, temperature measurements, atmospheric measurements or general change in aerodynamic performance [13]. The change in aerodynamic performance can be detected by the autopilot as requiring more energy to maintain a set velocity or requiring a change in angle of attack (AoA). The IPS has two modes and is only turned on when icing conditions is detected. The two modes are anti-icing and de-icing. The two modes will be discussed more at length in their respective section, but the main difference between the two is that for anti-icing the IPS is permanently on when in icing condition, while for de-icing it is cyclical, which allows a certain amount of ice build up. The question of which mode to use will be part of the investigation of this thesis. Particularly, de-icing is the more complex of the two, as it will have to take into account both IPS de-icing mode and thrust increase due to performance degradation due to ice. Hence, the focus will be on making existing models more accurate by using experimental data [14]. The work in this thesis will form some of the basis for future PhD work. The energy consumption model will contain simplistic models that will form the foundation for more accurate models in the future. Icing then, is something that warrants further research to sufficiently deal with the challenges that arise from it. This thesis will be a part of the research effort that goes into finding a solution to the icing problem for UAVs. It will contain every aspect of icing, seeking to improve the accuracy of current methods and be able to develop more robust solutions.

1.2 Previous Work

The work by Narum [10] is based on Hovenburgs PhD [15] in terms of information and data. The program made by Narum will be presented in detail with changes in the coming chapters. The program in question is a mission planning program for fixed wing UAVs in icing and wind conditions. The program also includes a hybrid power and battery model to calculate the energy capacity and its use. The hybrid power and battery model will be the only part that will remain unchanged. Narum achieved this by incorporating meteorological and aircraft performance data together with Particle Swarm Optimisation (PSO) to allow the UAV to plan for a best path to achieve its mission. The thesis by Narum [10] compared different missions, such as comparing the UAV with and without IPS and minimizing either flight duration or energy consumption through cost function minimisation. Due to the many topics covered by Narum in his thesis, he did not go into much detail for several topics and some of the models used inaccurate relationship, such as the equation for IPS energy consumption. This thesis aims to expand and improve upon the work done by Narum [10], implementing more accurate models, as well as having a more rigorous explanation of the aerodynamics of UAVs and how icing affects it. This thesis will in general try to explain the physics behind most of the topics covered. It will start from the basics such that no previous knowledge is required and will try to explain up to the level required to understand everything that is performed.

The work done in this thesis is run simultaneously with Tiller [16], which also aims to improve upon the work by Narum, but looking at a different aspect of the work. In an unpublished project report by Tiller [17], he built upon the algorithm developed by Narum [5] and looked at improving how forecasting is performed by grouping the data into an ensemble, which predicts the weather 5 times before averaging, lowering uncertainty and gives more realistic results. This is because the weather is not possible to predict deterministically, hence predicting several times will make the simulation more robust. This is also how weather forecasts are performed by meteorological institutes worldwide. Additionally, the PSO will be made more consistent, as the current PSO yields different solution each time due to part of it being random. By adding a seed, it is possible to get reproducible results, given the same variables. However, although it is made more comparable, it does give the disadvantage of not being able to run several times to find a better solution. The PSO still has a degree of randomness, but the results are now reproducible. A new seed will need to be provided for each run to explore for better solution. In the masters thesis by Tiller [16], he includes a more rigorous mathematical formulation on the PSO. He also rebuilds and updates the algorithm from scratch, such as making the PSO more adventurous by exploring for more solutions. More details on this will be presented in chapter 5 on path planning. This thesis will use Narums [5] algorithm with the improvements made in Tillers [17] project report and focus on incorporating an energy consumption model that is more accurate, by making a model built upon experimental data measured from an icing wind tunnel (IWT). Most of the data is either acquired through experiments using an icing wind tunnel or by numerical modelling through computational fluid dynamics (CFD) software such as LEWICE and FENSAP-ICE.

1.3 Objectives

The overarching objective of this thesis is to build an energy consumption model that combines IPS energy consumption and aircraft performance degradation. Breaking down this main objective, several objectives need to be fulfilled. The first is to complete a literature review over aerodynamics, icing conditions, IPS and weather models. The bulk of the thesis will be in constructing and documenting the energy consumption model itself. Documentation is something that was lacking in Narums thesis and this thesis will provide a comprehensive documentation that enable better understanding of the algorithm for future collaborators. The energy consumption model will use experimental data to improve the IPS energy consumption model and aircraft performance degradation model. The aircraft performance degradation that results from icing on the wing, will look into 2D icing data of the aircraft wing. 3D clean experimental and computational data is also available and will be compared with the 2D clean data results. The denotation clean is to differentiate between icing or no icing data. The clean data is used to determine if the 2D data is reasonable to use instead of 3D data as real life application uses 3D data. Hence, it becomes

important to check if using 3D data is required in the simulations. Data on propeller degradation will also be used as it is a part of the aircraft performance model. The propeller degradation will affect the thrust generation, which can make it much more sensitive to degradation and will be analysed further. The IPS experimental data contains both anti-icing and de-icing power loads that will be implemented into their respective models and compared. It will be determined whether or not de-icing is worth using over anti-icing. An important note is that for propeller IPS only anti-icing mode is assumed to be available. The reason for this will be explained in its respective section. The main results from this thesis will try to compare the results with previous work and see if it is possible to give a more accurate representation on the path planning algorithm.

1.4 Limitations

Ideally, by using the experimental data, more accurate models will be employed to get a more accurate relationship as shown by the data. However, due to time constraint, simple relationships will be prioritised, with linear or quadratic interpolation for easier implementation. Although it will not be as accurate, it should still manage to improve upon pre-existing models and hence is a worthwhile endeavour.

1.5 Thesis Outline

Chapter 2 will start with introducing the atmospheric model and how key parameters will be estimated if necessary. The chapter will also cover the most important parameters that leads to icing, as it will be important to understand how icing occurs to deal with it or avoid it when the UAV is in the air. Chapter 3 will follow up with presenting the aerodynamic performance model. The chapter will present what influence efficiency and fuel consumption of the aircraft as well as how these are modelled. Chapter 3 also looks into the general theory of flight and how icing can impact the aerodynamic performance, then talk about how icing will affect the performance. To be able to understand how the performance degrades, the aircraft specifications will need to be presented as to ascertain the baseline. The chapter will then end with how ice affects the performance of the aircraft and which parameter is most fit to represent this degradation as to be implemented into the optimisation program. Chapter 4 will move into the actual energy consumption model starting with how the data was acquired and combining the data into a single model. It will then look into the IPS energy consumption and discuss anti-icing and de-icing modes. Chapter 5 will look into the guidance, navigation and control of the aircraft, essentially looking into the autopilot that will decide on how the UAV will behave to fulfil its mission. To do this some aspects on path following methods will be discussed. This chapter is mostly for the sake of completeness as the optimisation program will have aspects of control that needs to be discussed for a better understanding. Chapter 6 will cover the simulation platform and what methods is used for simulation. This chapter will cover PSO, cost function and implementation of the energy consumption model. Chapter 7 will have the results and analysis of the implemented model. This thesis ends with the conclusion in Chapter 8 and future work in chapter 9.

2 Atmospheric Model and Icing Conditions

The atmospheric model estimates parameters vital to aircraft performance and icing conditions. Most parameters will be used directly from Norwegian Meteorological Institute (MET), mostly parameters regarding icing, while the rest will be estimated based on empirical relationships. The models used will mostly be unchanged, except for the weather ensemble method for processing meteorological data for forecasting as implemented by [17], who made changes to the initial meteorological model by Narum [10]. The ensemble method used is to reduce the variance seen in the data by predicting the weather multiple times, creating an ensemble, before averaging out. By using this method a more realistic forecast is possible. This chapter will give a quick look over some of the unchanged parameter estimation used and how they affect aircraft performance and icing conditions. Any details on the ensemble method will be referred to project report by Tiller [17].

2.1 Pressure Estimation

There exist a simple pressure equation that is widely used called the barometric equation [18]. Although the accuracy of said equation can be questionable after certain altitudes, the equation still estimates to a reasonable accuracy in terms of the simplicity of the equation. The simplicity also leads to it being very cheap to implement. The pressure is important to calculate as it affects lift, drag and ice accumulation. It is not used directly, but is important to calculate the air density, which is directly used in the lift and drag equations. The equation is:

$$P = P_0(\frac{T_0}{T_0 + L_0 h})^{\frac{gM}{R_u L_0}} \tag{1}$$

Here, P is the pressure at given altitude, P_0 is reference pressure at sea level, T_0 is reference sea level temperature, L_0 is lapse rate at T_0, g is gravity, M is Molar Mass of air, R_u is universal gas constant and h is altitude.

2.2 Air Density

The air density is calculated by using the ideal gas equation given by:

$$\rho = \frac{MP}{R_u T} \tag{2}$$

with ρ being density and T is temperature at a given altitude and the rest are as given in the pressure equation. The air density is an important metric as lift and drag is directly proportional to this. The reason why air density affects lift and drag is just how much air an object would encounter moving through the air. The faster an object moves, the more volume of air it would encounter, making it harder to move through, hence an increase in drag occurs. Lift is generated by a pressure differential, but also by how much air is around to lift it. Lift increases at the same rate as drag with regards to air density. However, drag is the deciding factor, as it increases faster than lift because the air streamline is applied in the same line as drag. However, the faster drag increase is encapsulated in the drag coefficient and not the air density. The air hits the aircraft frame, converting all the energy to pressure, also called stagnation pressure, which is a significant drag component. For lift it only looks at the pressure differential between top and bottom of the aircraft without stagnation and hence the overall energy conversion is much less [19].

2.3 Icing Conditions

Although research into UAV icing has only seen increased effort in the past few years, research into icing on commercial aircrafts are plentiful and icing physics are generally well understood. There has only been some areas that have seen little research as the conditions were rarely reached in commercial flights, such as low Reynolds number conditions, ice mass or energy consumption

measures [12]. All icing on aircrafts are initiated by supercooled liquids, that is liquids that are below freezing [20]. Supercooled liquids occurs because the liquids require impurities or surfaces to propagate freezing. Supercooled liquids are of similar nature when boiling pure water without impurities, such as no bubbles forming to show that it is boiling, which can be a hazard. The droplets impacting a solid surface such as an aircraft is enough to force this transition, which is the basic explanation for this phenomena. Icing conditions can be boiled down to three key parameters. Temperature, liquid water content (LWC) and median volume diameter (MVD), all of which are directly or indirectly measured or calculated from MET data.

2.3.1 Temperature

The temperature determines how quickly the droplets freeze, with lower temperature leading to larger freeze rates, entrapping air and generally conserving airfoil shape, called Rime Ice. For higher temperatures, this process is delayed, allowing uneven distribution and giving more uneven surfaces called glaze ice. Glaze ice formation is affected in combination with temperature and wind, as the wind is able to distribute the water in unpredictable ways. This leads to glaze ice being driven by convective heat transfer [20]. Other characteristics of glaze ice, at high enough temperatures, is the presence of a water layer. This water layer stems from the initial freezing ice delays further freezing as latent heat is released. The thickness of the water layer depends mostly on the temperature, with some dependence on convective heat transfer. The temperature determines if the latent heat released is enough to overcome the freeze rates due to cool temperatures. Freezing rates usually overcomes the latent heat below -5 degrees C and the water layer will freeze entirely [21]. This phenomena affects the IPS energy consumption, which will be discussed in the IPS chapter.

The different ice types can be observed in Figure 1. The combined temperature, wind effect and splashing effects can lead to horn ice and is the worst case scenario in terms of aircraft performance, as you would expect from having large vertical protrusion. MVD of the droplets particularly affects splashing, with larger droplets splashing more. However, larger droplets and splashing is a topic for future work and not considered in this thesis. The drag of an object is mostly related to the object form, or how many points that leads to a stagnation point. For example if you move a plate vertically through air, you will feel a more resistance than if the plate was sideways [22]. Hence, any large vertical protrusion or extension will add to drag quicker than small additions. In general, glaze ice leads to more irregular ice formations as can be observed on the left graph in Figure 1.

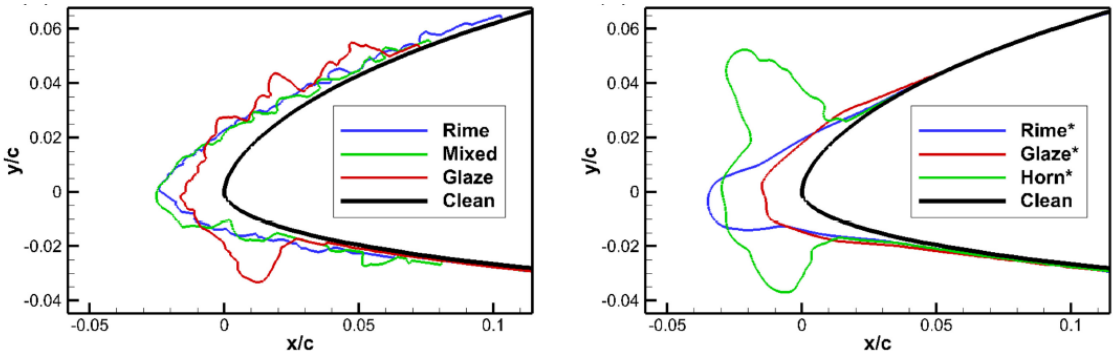

Figure 1: Left figure shows how different ice types forms on the airfoil experimentally. Right figure are shapes built numerically and shows what is meant with ice horns with exaggerated ice horn structures. Source: [1]

2.3.2 Liquid Water Content

LWC is how much water is contained within the air per unit volume, with typical values ranging from 0.1-3 g/m^3 [20]. The equation used to calculate LWC is the same equation used by Narum [10], which converts MET LWC mixing ratio into LWC:

$$LWC = \frac{LWC_m P}{R_d T} \tag{3}$$

where LWC_m is the MET mixing ratio and R_d is specific dry gas constant. LWC is not used directly to determine aircraft performance in this thesis, but is used to identify icing condition during the flight optimisation and for calculating MVD. Some of the physical interpretation of LWC on icing, is simply if there is any water present for icing to occur. The LWC determines how large water droplets can form, which makes it important in calculating MVD. Figure 2 shows how LWC, MVD and temperature are related to each other and how knowing two parameters fixes the third. In the case of performance degradation, the lift and drag coefficient will be determined by MVD and temperature since LWC is fixed by the other two parameters. The AoA is also a parameter, but is the parameter that needs to be calculated and can be controlled by the user.

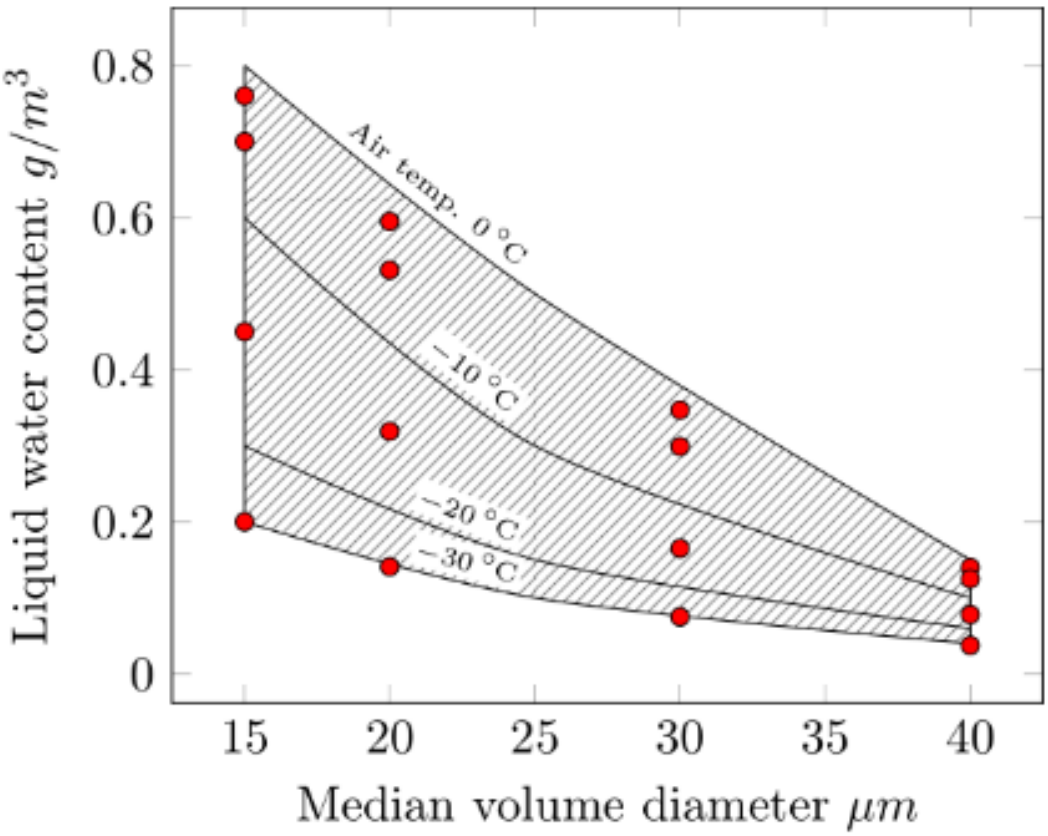

Figure 2: Icing cases with red dots indicating test cases where the data used in the next chapter was extracted from. The figure also relates how temperature, LWC and MVD are related to each other. Source: [2]

2.3.3 Median Volume Diameter

MVD is a statistical measure on water droplet size, hence the word median. MVD tries to simplify the statistical distribution into a single number. For the full MVD equation with its shape and slope parameter consult Narum [10]. The droplet size is important in terms of the trajectory, as a heavier droplet will be less inclined to follow the streamline. This is important in relation to airfoils, as smaller droplets will follow the streamline. The smallest droplet will then not impact the airfoil at all and allow it to follow the streamline all the way through without freezing, unless significant vertical ice accretions are already present for the droplets to hit. Larger droplets will follow the streamline less and hence large droplets will generally impact the airfoil more often,

leading to more icing. Droplet size will also determine the maximum speed due of the droplets due to inertia. Speed determines any splash effects that can freeze the droplets further downstream, altering mass balance of the aircraft [20]. In general, ice accretions on UAV have significant impact on mass and performance and will greatly impact the UAV.

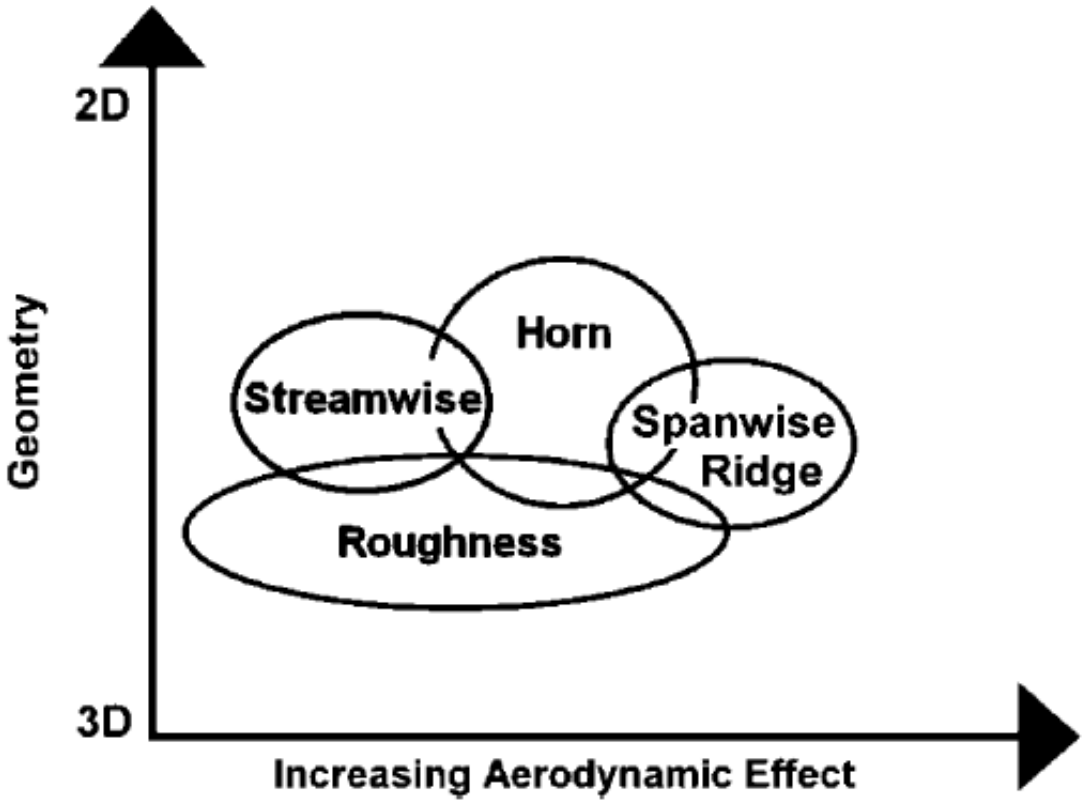

Figure 3: Aerodynamic Performance effect for ice geometries plus roughness. Source: [3]

2.4 Roughness

Roughness is defined as the height of formed "domes" on the airfoil surface. Roughness incurs more friction on the aircraft surface and this affects boundary layer physics. A generally rough surface can trip the flow to transition into turbulent flow earlier than a smooth surface due to friction. This can lead to increased drag and vibrations and can be significant in degrading performance [23, 24]. The roughness of the ice accretion can be quite random, but perfect reproducibility is generally not required, as the physics itself is quite well understood [3]. However, most models accounts for roughness simplistically by assigning it a constant value [25]. Hence, there have also been research efforts into modelling and simulation of roughness effects and to be able to give more accurate roughness values to be able to predict the effect of roughness on icing more accurately [25, 26]. Although not much can be done with how rough the ice becomes, Ice Protection Systems (IPS) can be used to remove the ice, it is an important parameter in understanding some of the drag physics, which is why a small comment is presented here. If the boundary layer is tripped into transition due to roughness, drag will automatically increase. As the topic of roughness is quite involved, no further discussions will be presented in this thesis. Figure 3 shows what kind of effect ice geometry plus roughness have on aerodynamic performance.

2.5 Wind Influence

The work by Narum [10] also incorporates wind to the optimisation model. For a small UAV, wind has a significant effect the aircraft. It can have both a positive and negative effect, such as being

able to ride the wind (tailwind) or having to consume more power to overcome the wind force (headwind). This depends on which direction the wind is blowing and wind maps are available for different altitudes. Several other effects are also present, such as thermal columns that contribute to lift or cross winds that can blow the aircraft off course. Wind is the one phenomena that can affect the UAV the most, even more than icing in some situations [4]. Wind physics and how some of these effects occur is, however, out of scope of this thesis and will not be discussed further.

Wind also introduces additional velocity component in the equation of motion of the aircraft. This velocity component makes the general control problem more complex, as heading and course will no longer be the same and needs to be taken into account. Heading is where the aircraft points, while course becomes the where the velocity vector of the aircraft points. Airspeed and ground speed also become separate speeds, with ground speed being the speed that indicates the speed to a desired destination. The wind influence will be encapsulated in the equation of motion. The equation of motion will be introduced in the next section together with the wind components.

3 Aerodynamic Performance Model

3.1 Aircraft Equation of Motion

As part of the aircraft performance model, the equation of motion for the UAV needs to be defined to be able to know the position and velocity of the aircraft in relation to the earth. Additionally, all aerodynamic forces depend on the airspeed and the direction of movement of which needs to be defined. The equation of motion is defined in the East-North-Up (ENU) frame of reference. Meaning the x-axis points north, y-axis point east and z-axis point down towards the earth. The air velocity is defined as:

$$\overrightarrow{\mathbf{V}_a} = \overrightarrow{\mathbf{V}_g} - \overrightarrow{\mathbf{V}_w} \tag{4}$$

Where V_a is the air velocity, V_g is the ground velocity and V_w is wind velocity. These velocity vectors are all three element vectors, denoting velocity in the x,y and z-direction. Of these it is the ground velocity that determines how fast it will reach its destination and it can be observed how wind can influence UAV velocities significantly. The air velocity is the result of the aircraft thrust. Ground velocity is then greatly affected by the wind velocity and can both contribute to slowing down or speeding up the UAV in terms of reaching its destination. From Beard and Mclain [4], they mention that wind can account for 20-50% of the air velocity for UAVs and it becomes vital to correctly utilise wind maps to the advantage of reduced flight time or reduced energy consumption. To expand upon the equation of motion, the position and its rates of the aircraft needs to be related with the airspeed, which is given by:

$$\dot{h} = \|\overrightarrow{\mathbf{V}_g}\| * sin(\gamma) \tag{5}$$

where $\dot{h}$ is the climbing rate, h is altitude and γ is the ground flight path angle. Ground flight path angle is specified because air flight path angle γ_a exists due to wind, which lead to the concept that where the plane points is not necessarily where the aircraft is moving relative to earth. The components of Eq.(4) refers to vectors. These vectors are defined by the speed multiplied by the direction vector:

$$\overrightarrow{\mathbf{V}_g} = \|\overrightarrow{\mathbf{V}_g}\| * \begin{bmatrix} cos(\chi)sin(\gamma) \\ sin(\chi)cos(\gamma) \\ -sin(\gamma) \end{bmatrix} \tag{6}$$

$$\overrightarrow{\mathbf{V}_a} = \|\overrightarrow{\mathbf{V}_a}\| * \begin{bmatrix} cos(\psi)sin(\gamma_a) \\ sin(\psi)cos(\gamma_a) \\ -sin(\gamma_a) \end{bmatrix} \tag{7}$$

and the wind velocity vector:

$$\overrightarrow{\mathbf{V}_w} = \begin{bmatrix} w_n \\ w_e \\ w_d \end{bmatrix} \tag{8}$$

where χ is the course angle (where the aircraft is travelling in relation to the earth) in Eq.(6) and w_n, w_e and w_d are the wind components for ENU coordinates respectively in Eq.(8), denoting the positive direction. The simplest course relationship is given by x and y ENU coordinates at time step i:

$$\chi = \psi + \beta \tag{9}$$

where β is defined by:

$$\beta = arcsin(\frac{V_w}{V_a sin(psi_w - \chi)}) \tag{10}$$

where ψ is the heading angle (where the aircraft nose is pointing) and β is the crab angle induced by the wind and ψ_w is the wind direction. Additionally, for the vertical plane the pitch angle θ (tilt in relation to ground speed) is calculated through air relative flight path angle γ_a and angle of attack α (tilt in relation to airspeed). The angle of attack is an important parameter that determines the lift and drag coefficient of the aircraft. The angle relations are given by:

$$\gamma_a = arcsin(\frac{V_g sin(\gamma) + w_d}{V_a}) \tag{11}$$

$$\theta = \gamma_a + \alpha \tag{12}$$

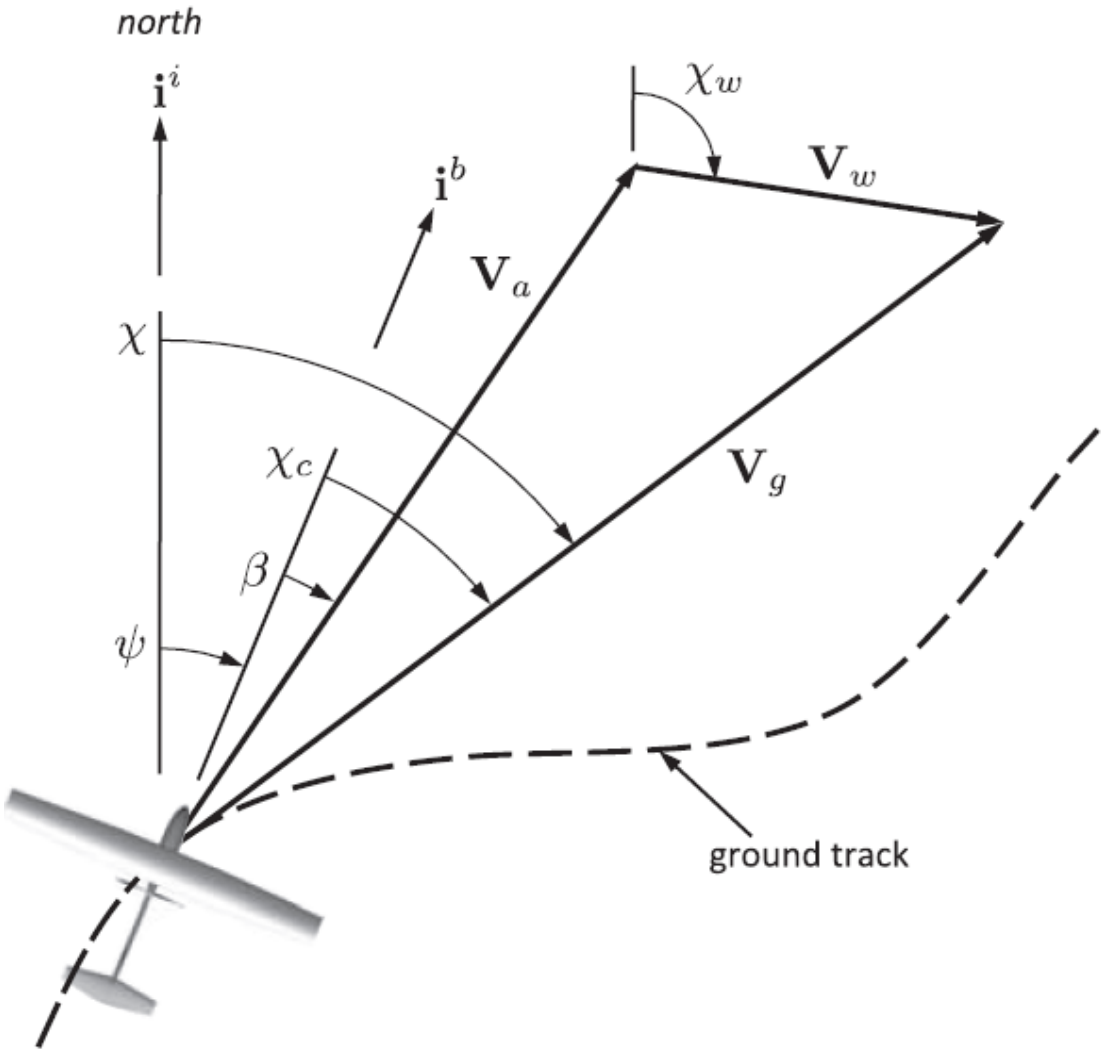

Figure 4: Horizontal plane angle description of the aircraft. Source: [4]

Figure 4-5 show how the angles are related in the horizontal and vertical plane, giving a better overview of fundamental angles for aircrafts in general. It is important to note that without wind, course and heading will be the same, as well as AoA and pitch angle. The wind component is a vital component to include as the UAV would drift towards undesirable destinations otherwise. Finally, it is possible to calculate an estimated discretized flight time, which will be important with regards to IPS usage and general energy consumption metrics [4]:

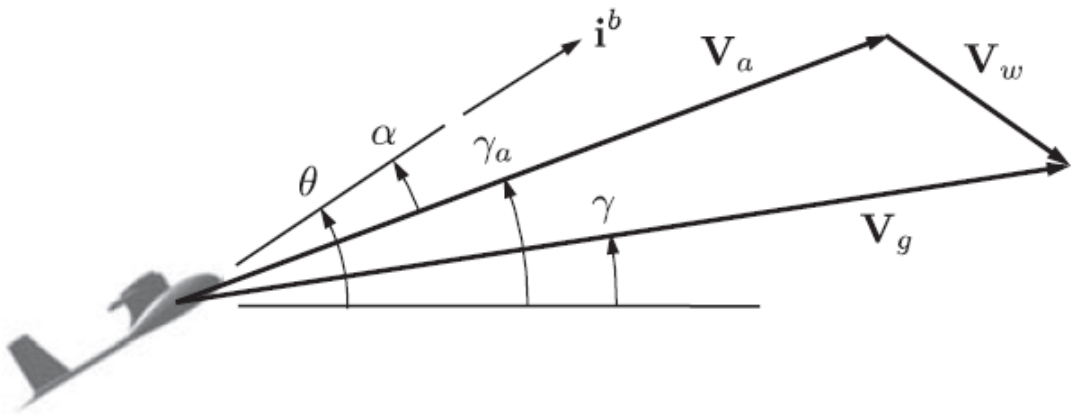

Figure 5: Vertical plane angle description of the aircraft. Source: [4]

$$t_i = \frac{L_i}{V_g cos(\gamma)} \tag{13}$$

where t_i is the estimated flight time at time step i, L_i is the distance to destination. The flight time is calculated between waypoints and L_i is distance to next waypoint. As a final note, the discretized steps are divided between waypoint to waypoint. As the simulation is currently set up, the conditions between each waypoint is assumed constant, such as whether or not icing is present, velocities and so on. This simplifies the simulation considerably, although in the future it might be desirable to make the simulation more accurate by allowing variable conditions between each step.

3.2 Aerodynamic Forces

To better understand how aircraft performance degrades, a first step is to look into what defines performance for an aircraft. This chapter will explain the physics behind these parameters and why they would be affected by icing. In fact, a measurement on aircraft performance is quite easily described by three coefficients, lift, drag and thrust. Lift and drag is generated by pressure differentials due to the aircraft moving through air, while thrust is generated by the engine or motor. The weight is a gravity force that is of particular interest when icing is considered, due to the ice mass accumulation. This will be discussed at the end of the chapter. Figure 6 shows the main force distribution of an aircraft. It can be observed that depending on the AoA, the lift can contribute a force component to the drag or thrust component in the figure.

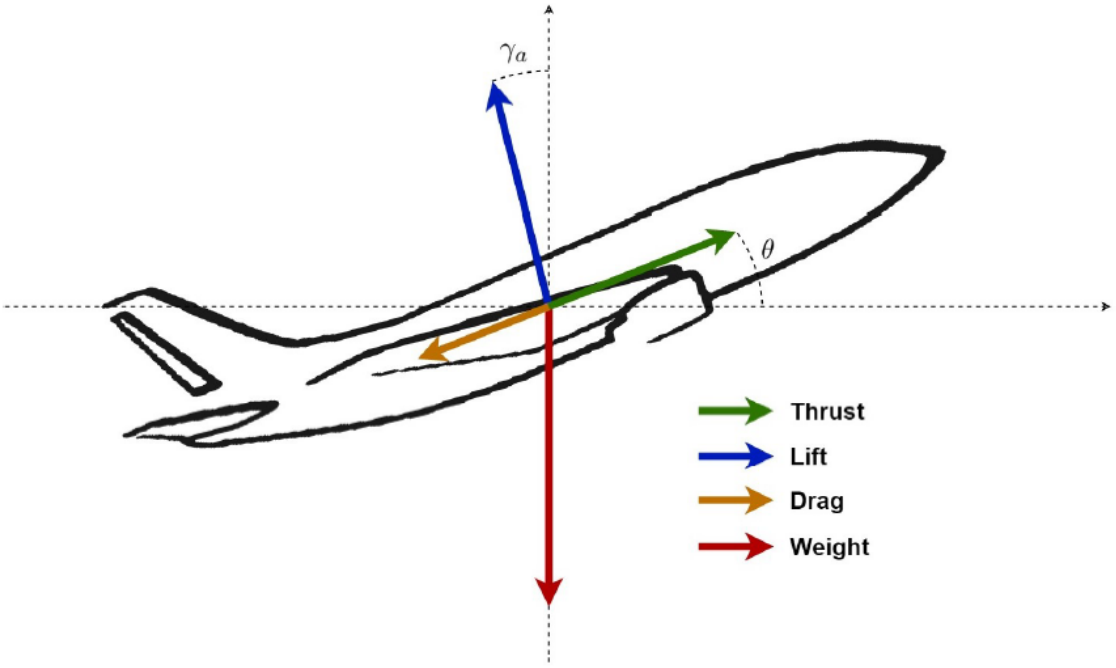

Figure 6: Main force distribution for an aircraft. Source: [5]

When it comes to the aircraft shape, the major contributor to lift is mainly the wings, while the whole aircraft is important when it comes to drag. However, the wings is the most sensitive to performance changes when icing occurs, when it comes to both lift and drag. The propeller is the most important when thrust is involved and influences the UAV the most, which will be demonstrated for the case when IPS is disabled. It will show why using an IPS on the propeller is vital for success. Hence, this chapter will mainly focus on the wing and propellers when describing the related parameters. It is still important to note that the fuselage does play a role in lift and drag. Hence, a few comments is in order pertaining the fuselage. Although the fuselage is less important when it comes to lift, all objects usually have some positive lift characteristic, which include the fuselage. The loss of some of the wing area and hence lift of the wing-body configuration is almost compensated by the positive fuselage lift characteristic [22]. The fuselage impact drag significantly due to its vertical size in relation to the wing. The classical wing-body configuration also adds additional weight due to having three distinct parts that is usually bolted together, which adds weight for every bolt used. This is however not usually a problem for small UAVs as molding it into a single piece is simpler than for large aircraft. As noted by Anderson [22], the lift generated is not as simple as adding the lift of two objects together due to the complexity of how the flow changes when two objects gets assembled together. There are additional components that are not taken into account here, such as the tail rudder and elevators. However, the combination of lift from all components can only be found by extensive testing and is out of the scope of this paper.

It does benefit making the fuselage as aerodynamic as possible as to minimize fuel consump-

tion. This applies more in regards to commercial aircraft, but does still play a role on small UAVs. There have been designs both in manned and unmanned aircraft to make the aircraft body more streamlined, such as having a fuselage that blends in with the wings as shown in Figure 7, a so called blended wing body (BWB) aircraft. There are advantages and disadvantages of the design, with the advantage of having less drag, but not having a dedicated rudder which reduces stability. Given how conservative the aerospace industry is, such designs will take time to implement. Hence, it is more common to see it applied to UAVs where safety is not as strict. In any case, the fuselage is not as detrimental to performance as one would expect, but does impede fuel consumption metrics. To start with the three coefficients related to the wing shape will be discussed.

Figure 7: Blended Wing Body concept design. Source: [6]

3.2.1 Pressure Coefficient

The pressure coefficient is a dimensionless parameter that compares streamline pressure and pressure by the airfoil surface. Figure 8 shows a typical pressure distribution graph of an airfoil, the sideways distance on the x-axis and C_p on the y-axis. To generate lift, the pressure under the airfoil is higher than the pressure above. This generates an upward force on the wing. For this reason, it is normal to flip the y-axis such that the positive pressure coefficient is under the airfoil. A positive C_p denotes that the specific point by the airfoil is larger than the freestream pressure and vice-versa. The equation that governs this relation is given by Eq. 14, where p is pressure at a specific airfoil position, p_∞ is freestream pressure far away from the airfoil, ρ is the air density of the freestream and V_∞ is the streamline speed [22].

$$C_p = \frac{p - p_\infty}{\frac{1}{2}\rho_\infty V_\infty} \tag{14}$$

The lift coefficient encapsulates all the information of the pressure distribution curve and is essentially the area encapsulated by the curve. What the pressure distribution is useful for is to identify which part chordwise of the airfoil that exhibit unusual C_p. For example in Figure 8, it is possible to pinpoint where the flow gets disturbed by the x/c axis, x being the x-value along the wing and c being the chord, close to the leading edge in this icing case. The pressure distribution of the iced case gives a huge penalty to C_p and hence lift, most likely due to ice horns forming as can be seen in Figure 1 [3]. By looking at the pressure distribution, it is possible to identify where the ice is forming and how to efficiently deal with the ice. It is also possible to predict the type of ice with glaze ice and ice horns usually giving larger penalties, but it is not always possible to identify this from the pressure distribution nonetheless. Rime ice usually preserves the shape of the airfoil and usually give smaller penalties to lift and drag. Glaze ice gives more unusual shapes and hence larger penalties. The ice horns usually forms under glaze or mixed ice conditions, which give the largest penalties [**?**]. There is a difference between mixed and glaze ice performance

degradation for experimental and computational results. It is possible that CFD have a tougher time in measuring mixed ice types as it is highly irregular, and hence show larger losses for mixed ice types. In actual experiments glaze ice generally gives larger penalties than mixed ice [1]. The main difference for when these two types of ice form is the temperature, with rime ice usually forming at colder temperatures and glaze ice forming closer to freezing point of water and mixed ice anywhere inbetween [1]. The physics behind rime and glaze ice is how quickly the supercooled liquid freezes. The colder it is the faster it freezes and hence entrap the surrounding air with it, preserving the airfoil shape and hence creates rime ice. For glaze ice, there might be a slight delay until the droplets freeze, creating uneven shapes as the droplet manages to unevenly distribute across the airfoil before freezing by forming a water layer, as well as letting air escape. The release of latent heat also affects the process as explained in an earlier chapter, which all contribute to the complexity of glaze ice. Rime ice in comparison is a relatively simple ice formation.

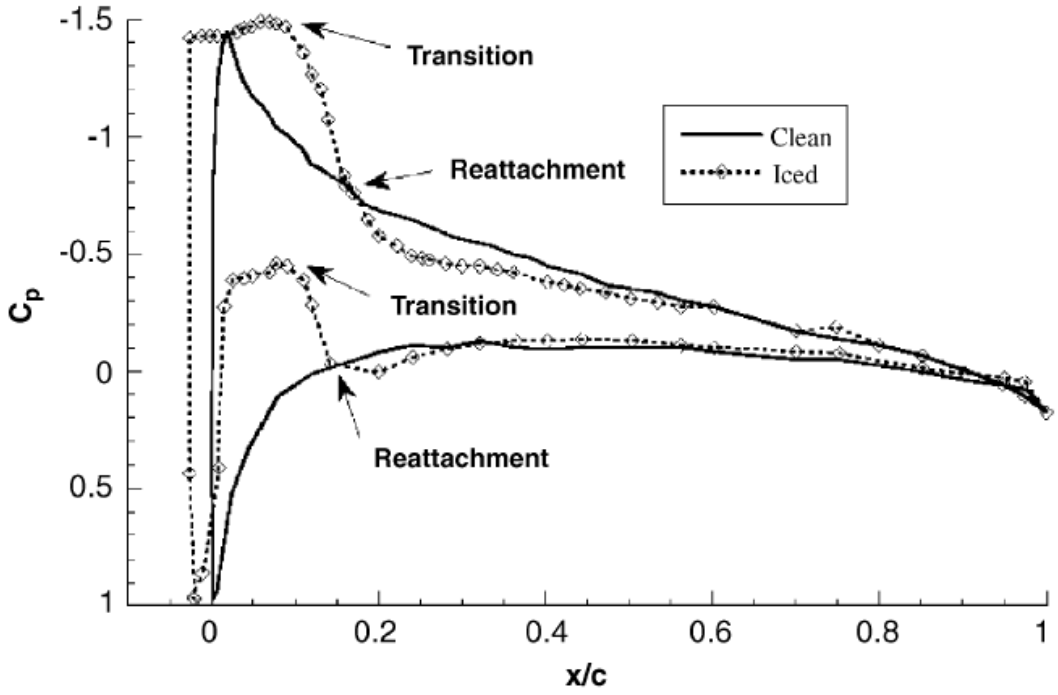

Figure 8: Comparison between clean and iced airfoil pressure distribution. Source: [3]

Since rime ice usually gives small penalties, the pressure distribution curve would be relatively well preserved in shape, but with a smaller area, when comparing clean and iced airfoils. For glaze ice, there are more cases of run off ice due to the existence of a water layer and wind carrying it further down towards the trailing edge. The ice can also reform when it is melted by the IPS at the leading edge and reforms further down towards the trailing edge. It should generally be easy to differentiate the two conditions with that in mind. There is also a third type of ice, which is a mix of the two types of ice and it can be observed to give a combination of characteristic pressure distributions. It is important to note that the pressure distribution is not really used while in flight, but is a more design oriented approach, such as where to locate the IPS heating elements. By looking at the pressure distribution curve, it can be observed that the majority of lift is generated close to the leading edge (larger area). This leads to a design focus in locating the IPS at the leading edge as the changes here are the most critical. The simulation software uses the parameters of the PX-31 UAV developed by Maritime Robotics and the IPS location is situated at the leading edge. This is after experimental investigations have been performed, during the process of designing an IPS for the PX-31 [13].

3.2.2 Lift Coefficient

The lift coefficient encapsulates most of the information from the pressure coefficient distribution, as mentioned earlier. Lift is also partially generated by shear stress distribution, but is relatively small compared to the pressure distribution and hence is not discussed further [22]. This section will focus on the lift coefficient of the wing as this is the main lifting surface. There are two lift coefficient equation that is especially useful in the design of an aircraft, the normal lift coefficient equation given by:

$$C_L = \frac{2L}{\rho u^2 S} \tag{15}$$

where C_L is the lift coefficient, L is the lift force, ρ is the density of air, u is streamline speed, and S is the surface area, usually the wing surface area. Due to the unconventional shape of the airfoil, the surface area equation is usually simplified to be mean aerodynamic chord (MAC) times wing length. The MAC is especially used for swept and tapered wings, due to variable chord length. This is usually a reasonable assumption as C_L decreases with increased surface area, and hence is the conservative solution. With the other parameters easy to calculate, the lift force depends on which part of the flight the aircraft is currently at, take-off, cruise or landing. Starting with the longest part of the flight, cruise mode is a steady-state mode where little change happens to the flight condition. However, the PSO will try to calculate an optimal path that tries to make use of tailwind or avoid icing if necessary to complete its objective in minimizing either flight time or energy consumption. Hence, the path will usually not be a straight path, but depends on the weather conditions. The standard of cruise being steady-state applies to commercial aircrafts more than UAVs. As UAVs have a more limited operating range, both in terms of energy capacity and cruise altitude, the cruise mode of the UAV will need to use of all its resources to satisfy its mission. Hence, the PSO will give projections that are usually more variable than commercial paths. In any case, the general cruise condition will need to satisfy certain requirements for steady flight.

The required lift force will be balanced against the weight of the aircraft to keep the aircraft at a stable altitude towards its destination. Climbs and descent that occur throughout the route, calculates the need for a change in lift coefficient as needed. This is generally achieved by changing the AoA. Take-off and landing is a more complex topic and can be covered by many articles alone and is hence out of the scope of this thesis, but a few comments on general requirements is useful for completeness. General lift force requirements on these two stages is to have a larger lift force than the weight of the aircraft to be able to reach cruise height. This is achieved by a combination of using flaps and elevators, max thrust by engines and increasing angle of attack to make the aircraft take-off. In the case of the PX-31, assisted take-off and landing is deployed by the users. As for landing, it is slightly opposite of take-off, where it glides down while adjusting for engine thrust, flaps and elevators as needed for to achieve a safe landing. The second lift coefficient equation is the section lift coefficient:

$$c_l = \frac{2l}{\rho u^2 L} \tag{16}$$

where l is lift force per unit span and L is reference length, usually the chord. The other parameters are the same as the other equation. This lift coefficient is more commonly graphed with angle of attack to get a better picture on how a certain airfoil shape performs per span, better known as the 2D lift coefficient. It is much easier this way to calculate the lift as it does not depend on the specific aircraft with their specific wing span and area, but only on the airfoil shape.

$$Re = \frac{\rho u L}{\mu} \tag{17}$$

One important aspect that has not been brought up yet is the Reynolds number, which is the ratio between inertial and viscous forces as seen in Eq. 17. For a wing the parameters are ρ for

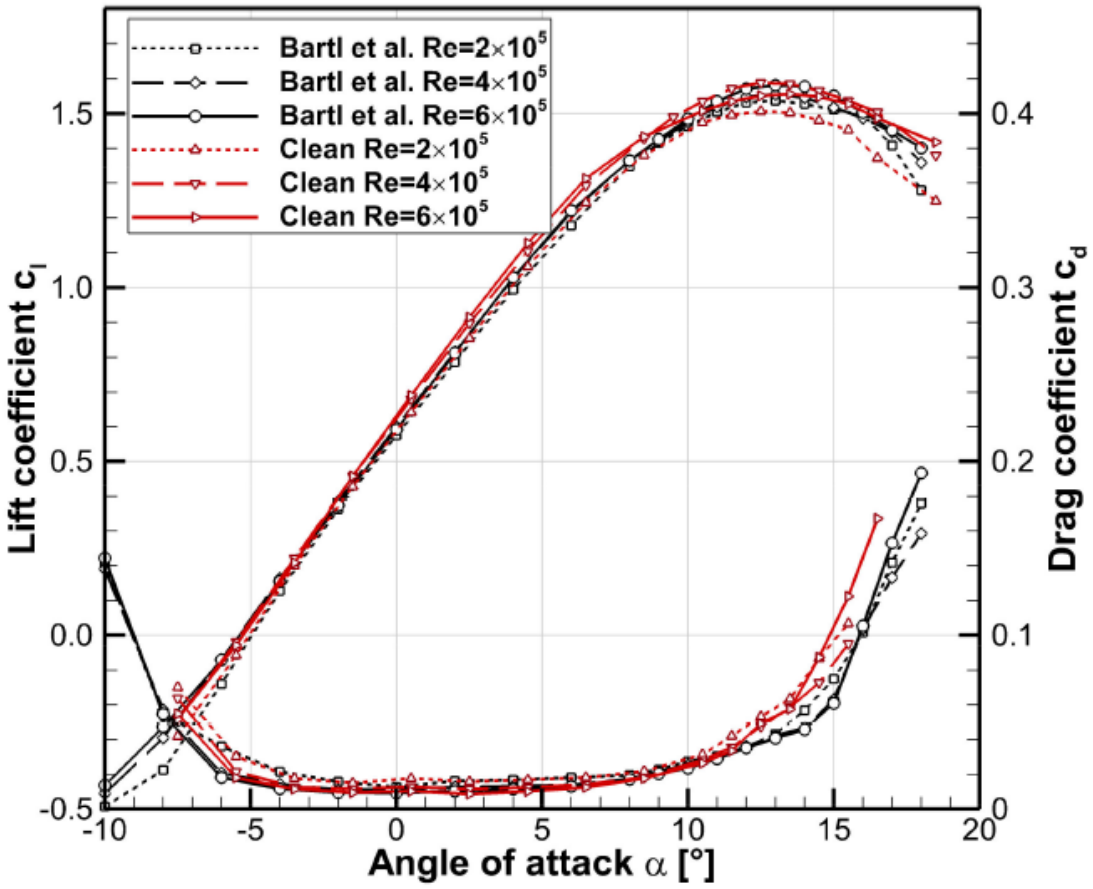

Figure 9: Curves over lift and drag coefficients plotted against angle of attack. The top curves are the curves for lift and bottom ones for drag. The curve shows typical lift coefficients for the operating Reynolds number range of UAVs. These curves are performance metrics for the S826 airfoil. Source: [1]

density of air, u flow velocity, L is chord length and μ is dynamic viscosity. Of these, only the velocity and chord length varies from aircraft to aircraft if operating at the same altitudes. It is an indicator on when the flow is very orderly, better known as laminar flow, or chaotic, better known as turbulent flow, or transitional flow which is somewhere inbetween. What is important with Reynolds number on the lift coefficient is that higher Reynolds number generally causes stall to be induced at increased AoA. This can be observed in Figure 9, where the curve starts changing slope and decreases. It is perhaps difficult to observe, but the curve does get pushed slightly left and down with reduced Reynolds number. This is particularly one of the challenges with icing on UAVs because UAVs generally have lower Reynolds numbers and research on low Reynolds number icing is not as extensive as for standard Reynolds numbers as reviewed by Hann and Johansen [12]. Reynolds numbers for commercial aircrafts are usually in order of ten times larger than what it is for UAVs as shown in Figure 9. Commercial aircrafts achieve higher Reynolds numbers due to their longer chord lengths and higher velocities. General commercial aircrafts have thus generally larger margin of errors due to their higher stall angles. The work by Hann [1] looks into low Reynolds number effect on lift and drag, which corroborate this lower Reynolds number effect. Hence, icing on UAVs is something that needs to be dealt with due to lower stall angles and how icing penalties are more severe for UAVs. The paper by Winslow et al. [27] looks at understanding the basics of low Reynolds number characteristics for non-icing conditions. It looks at even lower Reynolds numbers in the $10^4 - 10^5$ range or less, while the reference drone in this thesis is in the $10^5 - 10^6$ range. The conditions looked at by Winslow et al. [27] is concluded to be much more sensitive to boundary layer separation and other negative effects for flight. These results would be important

if sizes of drones becomes even smaller in the future, particularly for exploration or survey drones. Drones that have delivery duties will require larger sizes to have enough power to carry its payload and is as of now technologically restricted to be a certain size.

Finally, some comments on differences between 2D and 3D effects are in order. This is because both 2D and 3D clean data are available for use and discussing the differences is important for better understanding and to validate the use of 2D data. Most 2D effects have already been covered, as most of the theory covered above falls under 2D theory, especially the equations presented. 3D effects are a complicated topic and as this is not an aerodynamic paper, will avoid discussing it from basics, but rather focus on a specific phenomenon which does not require starting from basics. The phenomenon in question are tip vortices that result from circulation that occurs due to the higher pressure region below the wing compared to the pressure above the wing. This creates a sort of leakage at the tip of the wing. This vortex flow momentum is preserved as the aircraft moves forward, creating vortices and hence vortex drag. The flow loses energy due to the vortices, as the energy is converted into circular motion, which slows down the flow velocity and hence reduces lift. To compensate for the reduced lift, a higher AoA is required, and lift-induced drag (explained in the drag section) is dependent on the lift and induced downwash angle. This also leads to the tip being less effective at generating lift, creating a root-tip lift force difference that makes the root prone to require more maintenance [28]. Hence, the overall effect is problematic and measures have been taken to alleviate this problem, such as installing winglets at the wing tip, which was investigated and designed by Whitcomb [29] at NASA. Winglets have been a very successful solution and been incorporated to most commercial aircrafts. Winglets are a relatively simple solution. Imagine curving the wing tip upwards at a steep angle, but as a separate structure, such that the wing span stays the same. The winglet essentially forces the flow to travel a longer distance to the top of the wing. This quite successfully stops most of the vortices created as the flow generally lacks the energy to overcome this longer distance, improving performance. This does not eliminate 3D effects of course, but the 3D effect with the biggest impact have been solved. The addition of iced winglets are also unknown and might be worth investigating further for future work.

3.2.3 Drag Coefficient

The drag denotes the force that needs to be overcome such that the plane is able to move forward and how much thrust is required to do so. The interesting part is that the drag coefficient is made up of several components, such as interference drag, parasitic drag and lift induced drag. The wing is again the main focus as the changes will be the largest at the wings. Since the wing is the main focus, interference drag is ignored as it is the contribution from the interaction between the wing-body configuration. Because most of the UAV fuselage blends well with the wing area, this is a reasonable assumption, particularly when looking at the PX-31 where fuselage and wings are merged together in a manner where most corners are smooth. Hence, parasitic drag and lift induced drag remain and is given by the equation:

$$C_D = c_{d,e} + \frac{C_L^2}{\pi e AR} \tag{18}$$

where $c_{d,e}$ is the parasitic drag, C_L is the lift coefficient, e is Oswald efficiency factor, which is encapsulates the wing geometry, such as taper ratio (TR) and aspect ratio (AR). AR is the aspect ratio, which is the ratio between the span and MAC. The second part of Eq. 18 is the lift induced drag, which have a relatively simple geometrical explanation and a more complicated physical explanation, in this case the geometrical explanation will be used. The lift force is always perpendicular to the wing and if the wing is tilted slightly away from the horizontal plane, this tilt is called induced downwash angle, the lift force will also be tilted backwards. The lift force can then be decomposed into a x and y component, where the y component is lift force and x component is the drag force due to the tilt backwards. This is the effects of induced drag at its most basic form. There are all sorts of other effects that contribute to induced drag, such as tip vortices, downwash effects and how the airflow moves across the wing, can affect induced drag. These effects have been

described in the lift coefficient section when comparing 2D and 3D effects. In the strictest sense, the geometrical explanation on induced drag is the only 2D effect. This means that induced drag is in a strict sense only a 3D effect, because induced drag only happens in 2D when AoA increases, which is usually controlled by the pilot. When talking about 3D effects, induced drag can happen just by how the flow interacts with the wing without change in AoA, making it a complex 3D phenomena. In a strict sense induced drag is a 3D phenomena, but does have components even in 2D given certain controllable conditions.

However, since the lift induced drag is dependent on the lift it is of relatively little interest in terms of icing as it will be relatively similar between a clean and iced airfoil. Another point is that the required lift coefficient of the aircraft is relatively constant through the flight. In fact, if the aircraft uses fuel, the required lift reduces as fuel gets used up throughout its journey. The only way for the aircraft to increase its required lift is the gain from icing laying on the aircraft structure. Hence, the required lift is relatively constant and the lift induced drag does not really change between clean and iced conditions. That is not to say that the AoA will not need to change to maintain a desired lift, the main idea to take away is that lift performance degradation is relatively low compared to the drag increase. Hence, parasitic drag is the component that is most influenced by icing as it is term that encapsulates form drag (shape of the aircraft), friction (roughness) and pressure drag. Ice changes the form of the airfoil hence influencing pressure and form drag. Ice also changes the roughness of the aircraft and hence friction force. The form drag is the approach shape that the flow sees,for example looking directly at the nose of the aircraft you can see a silhouette, when this silhouette changes the form drag changes. If this frontal shape increases, the drag increases and vice versa. There are other factors that affect drag, such as whether or not he corners are smooth or not and roughness as mentioned earlier. However, the main point is that the silhouette seen by the streamline is the main drag indicator. This is why horn ice is the worst kind of icing as it changes the aircraft shape the most, adding noticeable vertical expansion of the silhouette. Additionally, horn ice also affects the pressure drag, leading to faster separation as observed in Figure 8. Pressure drag is the drag component that occurs when the flow meets an object and all the energy gets transformed into pressure otherwise known as stagnation points, forming a high pressure region that pushes the incoming object back [22]. The shape of the object influence how large this high pressure region becomes as it is determined by how well the flow can move around the object. For example a sphere will have one streamline that stops completely, while the other streamlines can move around it. Contrast this with a vertical wall, every streamline would stop at impact, creating a much larger pressure region. This also depends on how the overall air streamline approaches the aircraft, as crosswinds are possible, making the streamlines approach on an angle. This is part of the downwash effect mentioned earlier and aircrafts perform worse in this situation [19]. How quickly boundary separation occurs is also determined by the shape of the object. Boundary layer separation leads to a wake behind the object which leads to lower pressure behind the object that counteracts the high pressure frontal region less. Hence, it is important to maintain the designed airfoil shape to prevent separation and change in the leading edge to avoid increased high pressure region at front [22]. Drag is the main issue when it comes to icing as it can greatly increase thrust requirements to maintain cruise velocities. As the thrust increases, energy consumption increases, and as drag further increase the aircraft will inevitably slow down such that generated lift force decreases. To compensate, AoA will need to increase, but with reduced stall angle will lead to quicker stall. More details on ice influence will be presented by the end of this chapter, comparing lift and drag coefficients between clean and iced airfoils.

3.3 Thrust

Thrust can be generated by a variety of engines, but for small UAVs (sUAV) only a few choices are appropriate due to their size. Due to their size, only battery driven motors are appropriate as fuel carrying capacity is limited. The hybrid powertrain model implemented by Narum [5] uses an internal combustion engine to charge the batteries for more range. The motors are attached to a propeller that rotates. Similarly to the wings, the propeller blades are shaped to generate a force forward by the same pressure differential that generates lift for the wings. Propeller blades are generally more complex however, in addition to being airfoil shaped, it can twist from the root to

tip to take advantage of the different velocities along the blades between root and tip to generate more thrust. The propeller forces air to go through the propeller and generates thrust by creating a higher pressure differential behind the propeller and pushing the aircraft forward [4]. The power consumed by the generation of thrust is determined by the equation:

$$P_{prop} = T_{prop} V_a \tag{19}$$

where T_{prop} is the thrust generated by the propeller and V_a is aircraft airspeed. The energy consumed can be found by multiplying the power with time. The thrust is further broken down to the equation:

$$T_{prop} = F_D + mgsin(\theta) \tag{20}$$

$$F_D = \frac{1}{2}\rho C_d u^2 A \tag{21}$$

where F_D is the drag force, m is mass, g is acceleration of gravity and θ is pitch angle of the aircraft. Additionally, ρ is air density, C_d is drag coefficient, u is air velocity and A is cross-sectional area. Pitch angle is only the same as AoA if there is no presence of wind. Equation 20 assumes that cruise mode is reached and that it needs to overcome the drag and horizontal component of gravity to keep a steady-state velocity [5]. In the simulation, these two equation needs to be calculated at every time step to be able to adjust to any disturbances and hence be able to keep an optimal steady-state velocity. Additionally, the efficiency of the propeller is required and is given by:

$$\eta_{prop} = \frac{P_{propeller}}{P_{shaft}} \tag{22}$$

where P_{shaft} is the power delivered by the motor and $P_{propeller}$ is the actual power delivered to the propeller after all losses have been accounted for between the shaft and propeller. The propeller efficiency however is usually how efficient the propeller itself is at converting motor power to generating thrust. Similarly to what Narum [5] did in his thesis, the reference efficiency will be kept constant, although this efficiency will be changed from 50% to 65% after measurements from experimental data [7]. This efficiency is not directly mentioned in Fajts paper, but is provided by Fajt and experiments performed. Propeller efficiency usually depends on the velocity of the aircraft, but the average velocity of the aircraft at cruise is assumed to be constant, hence propeller efficiency can be assumed to be constant. This increase in propeller efficiency will give higher leeway on thrust. The propeller can just as easily experience icing as the wing, reducing its efficiency. In fact, the propeller degrades much quicker than the wing, which will be discussed in the performance degradation section. Assuming linear relationship, it is relatively easy to account for the drop in efficiency due to icing on the propeller, which gives the power requirement equation to be:

$$P_{propeller} = \frac{P_{shaft}}{\eta_{degradation} * \eta prop} \tag{23}$$

where $\eta_{degradation}$ is the degradation of the propeller due to icing. The degradation ranges from 0-1, where 1 is no degradation. The more severe icing is, the closer to 0 the degradation will be, and hence require more power. Propeller icing is more complex than this, but due to time constraints, the assumption of linear relationship is the best that can be done at this point. Further details on propeller icing will be given in the propeller icing chapter.

3.4 Aircraft Specifications

To be able to discuss the aircraft performance, the aircraft used will be presented. The aircraft is the PX-31, manufactured by Maritime Robotics. The PX-31 specifications are:

1. Cruise speed = 25 m/s
2. Max speed = 40 m/s
3. Stall speed = 14 m/s
4. Wing length = 3.2 meters
5. Max take off weight = 22 kg
6. Wing area = 0.81 m^2
7. Max flight time = 10-13 hours

There are however some differences between the chord used on the PX-31 and the simulation program, which will be used in this paper. The airfoil used in the algorithm is RG-15, but with a longer chord than what is used on the PX-31. The simulations and experiments uses a chord of 45 cm while the actual chord of the PX-31 is 27 cm, which with similar operating conditions, reduce the Reynolds number. This will inevitably reduce stall angle and change drag characteristics. Looking at Figure 9, the lift and drag gets a minimal performance reduction in the linear regions with lower Reynolds number. It only changes stall angle and the behaviour past stall angle. However, since operation close to stall will be avoided and with the coefficient relatively constant, the operating AoA is far away from stall. Hence, this is not a huge problem. The aircraft is designed to operate in laminar conditions, a stable and fuel efficient operating condition. If the flow gets tripped to turbulent during icing, the performance might get erratic. In this thesis, the flight flow be assumed to be laminar at all times. The performance degradation due to icing reflects some of the turbulence effects as the flow gets separated, which moves the lift and drag curves. Figure 10 shows the baseline aircraft, which is close to having being a BWB configuration. The PX-31 also have winglets installed to reduce vortex effects and hence reduces induced drag. Finally, the IPS is solely located at the leading edge with a width of 5 cm. This makes the IPS area:

$$IPS_{area} = IPS_{width} * WingLength = 0.05m * 3.2m = 0.16m^2 \tag{24}$$

This IPS area is used for multiplying with the IPS loads, since the IPS load is given in kW/m^2.

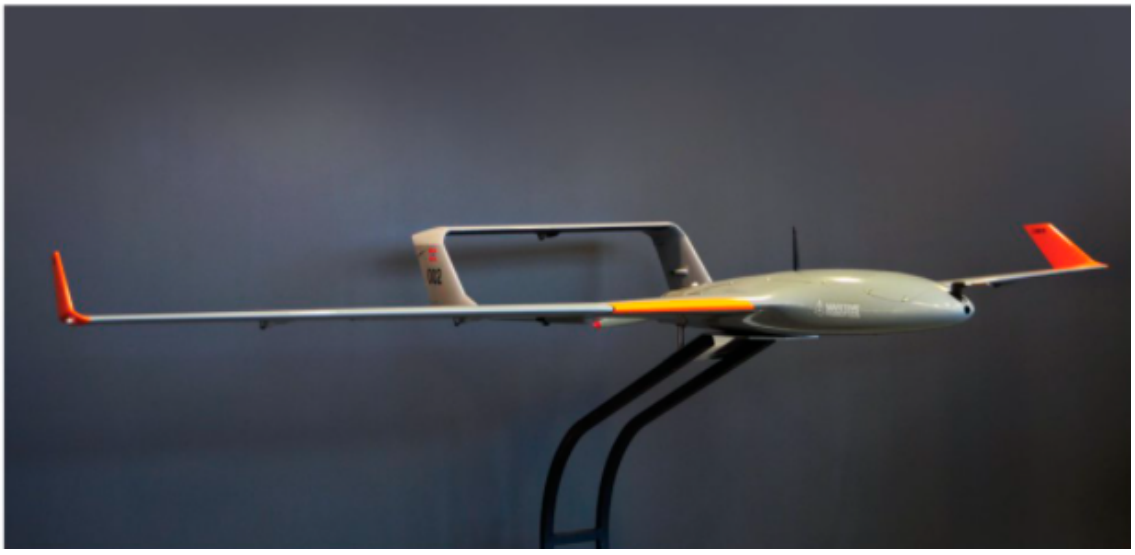

Figure 10: PX-31 UAV. Source: Maritime Robotics

3.4.1 Comments on the Validity of Collected Data and Application to the Actual Drone

A few comments on the validity of the data that will be used in this thesis is in order. This is due to the difference in chord length between experiments and actual chord length of the drone as mentioned previously. The chord length of the drone is almost half of the experimental chord used (27cm compared to 45 cm). Looking at Eq. 17, this drop in chord length will almost half the Reynolds number of the aircraft at the same conditions. The question is whether the Reynolds number will drop below 10^5, which is the sensitive region as indicated by Winslow et al [27]. Since the Reynolds number almost drops by half, the Reynolds number at operating conditions would be at around 10^5 to drop down to the 10^4 range. This is however in the lower ranges and will be assumed to not occur, as actual operation conditions is in the $3 * 10^5+$ range and hence will not drop below 10^5. This is assuming the same cruise speed. Hence, it can be assumed to be safe to apply the data to the actual drone, although with a slight penalty on stall, but as it currently operates far away from stall, it should be fine unless the UAV encounters the most severe of icing. Much of the data included, looks at a range of AoA values with its corresponding lift and drag coefficients. For most of the data included, the UAV operates at conditions far away from stall. This is not the case for temperatures close to freezing data where glaze ice is frequent occurrence, but will with IPS hopefully be able to deal with the hazardous conditions and never approach stall.

3.5 Aerodynamic Performance Degradation Due To Icing

This section will look into the performance degradation due to icing and will present graphs that compares clean and iced airfoils. A simple relationship will be assumed for all of them. Meaning, interpolation between the different icing conditions will be performed to get the value that correspond to certain condition. The data used will be presented and given a thorough analysis. This section will first look into the reference parameter for wing before comparing the clean airfoil with the 2D and 3D data.

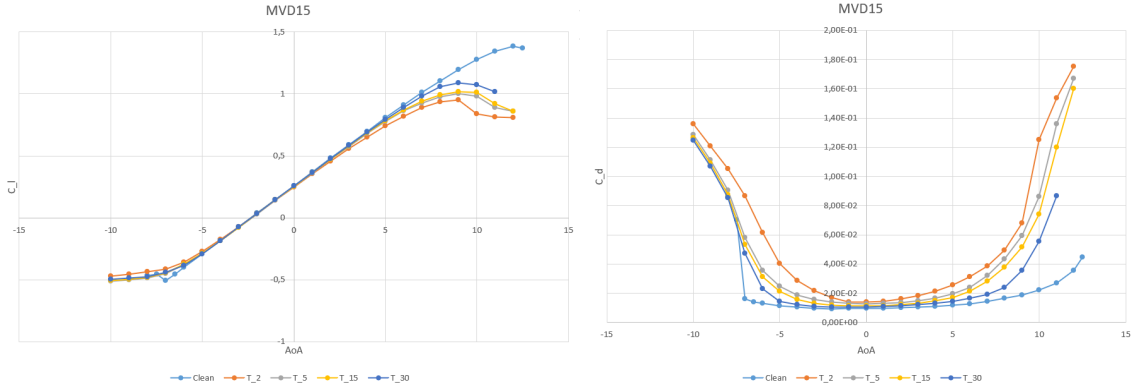

Figure 11: Lift and Drag Coefficient Curves MVD15 after 20 minutes of ice accumulation for different temperatures, with the lift curve to the left and drag curve to the right. Source: [7]

3.5.1 Comparison between Clean and Iced 2D Airfoil

A general look at the data show that a temperature decrease at a given droplet MVD has a larger stall angle than at temperatures closer to freezing point (warmer temperatures), there is a shrinkage in stall angle for glaze and hence operates in a tighter frame. This correspond well with what has been discussed earlier on rime and glaze ice. Rime ice occurs at colder temperatures, but keeps the airfoil shape much better than glaze ice that give more irregular shapes. An interesting observation is that for MVD 15-30 the same trend is seen, the performance degradation is at its worse at -2 degrees, but moves closer to clean airfoil performance with decreased temperatures. Drag is remarkably worse in the warmer temperature ranges. This corresponds well with the rime and glaze ice formation characteristics. This trend is the transition between glaze and rime ice [9]. At MVD 40 however the iced performance are close to overlapping for all temperatures. The same

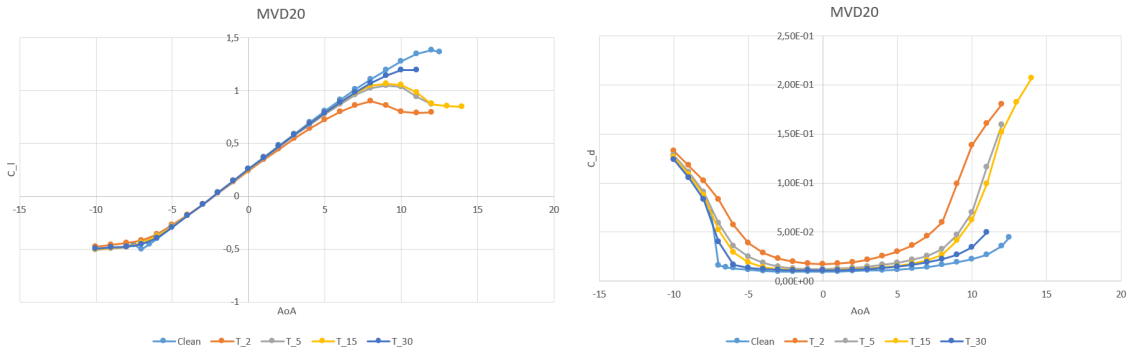

Figure 12: Lift and Drag Coefficient Curves MVD20 after 20 minutes of ice accumulation for different temperatures, with the lift curve to the left and drag curve to the right. Source: [7]

general trend is present, but the differences are negligible. This is because for lower MVD the LWC range is larger, while at MVD 40, LWC has much lower values, which yields more uniform ice accretion shapes. The results discussed can be seen in Figure 11-14 and the data represented is taken from the work by Fajt et al. [7]. The work by Fajt et al. looks at how meteorological conditions affect aircraft performance [7]. The results found are as presented earlier, with the performance degradation being at its worst at -2 degrees. Additionally, the LWC and MVD that leads to worst degradation is when it is high. The physics of this has been explained in the previous chapter. Similar findings in the data were found and corroborated in the PHD thesis by Hann [9]. As can be seen in Figure 11-14 the lift coefficient is relatively linear up until stall, which makes it easy to implement software wise. With the linear region in place, a maximum can be defined for the AoA in the optimisation for the linear region. Drag is slightly more complex as the plot is more complex, but does have three distinct regions. The two steep slope regions at the ends and a relatively linear region in the middle. The drag curve can be simplified as the AoA transitions correspond well with the lift curve stall angles. It then remains to find an accurate representation for when drag starts to increase, as a linear representation would underestimate actual drag values. This will essentially make drag lower than it should be and it would perhaps be more fitting to use quadratic interpolation. What method will be used will be presented in the simulation section.

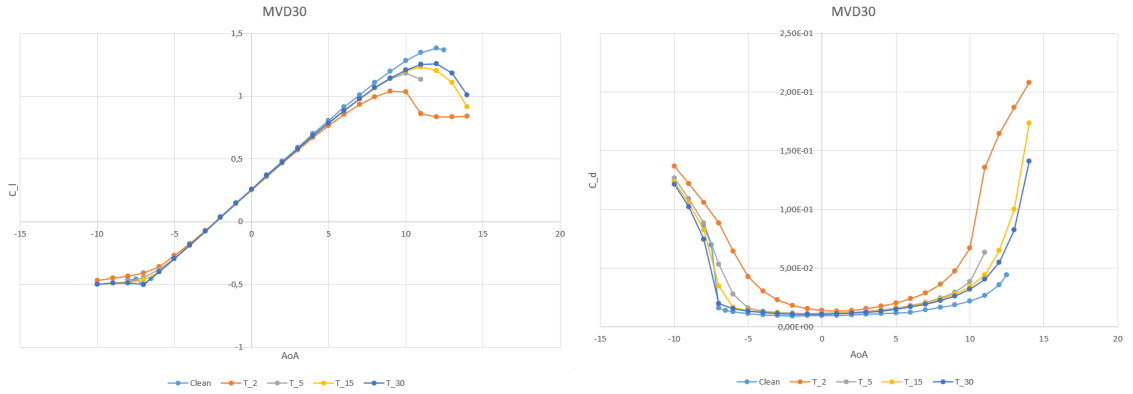

Figure 13: Lift and Drag Coefficient Curves for MVD30 after 20 minutes of ice accumulation for different temperatures, with the lift curve to the left and drag curve to the right. Source: [7]

3.5.2 Comparison between Clean 2D and 3D Airfoil

For this thesis, 2D and 3D data will only compare clean conditions as only clean data is available for both. This is for validation purposes and is to check if using 2D data is acceptable or if 3D data is required. If 3D data ends up not being applicable, using 2D data is most likely not accurate as 3D data reflects real life application more. Comparing the 2D and 3D data directly, the 3D lift

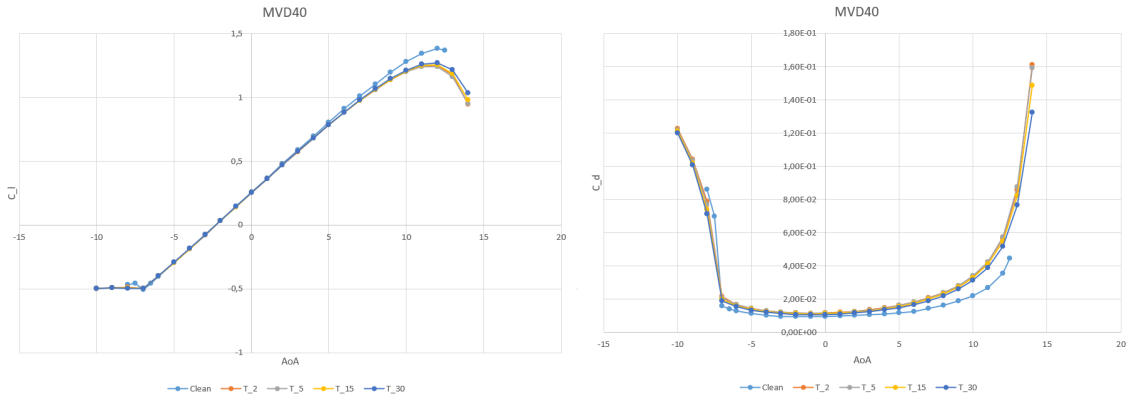

Figure 14: Lift and Drag Coefficient Curves for MVD40 after 20 minutes of ice accumulation for different temperatures, with the lift curve to the left and drag curve to the right. Source: [7]

coefficient is generally higher at lower AoA, but reaches lower peak lift coefficient. The drag is much higher when compared to 2D data, and higher by a significant margin for all AoA, which might reflect real life more, due to 3D effects such as downwash as mentioned earlier. The drag is anywhere between 3-10 times higher depending on the AoA for the 3D dataset. Due to the nature of CFD simulations where the 3D data comes from, the performance characteristics becomes worse at the ends of the curves close to stall. It might however be fine, as the operating range is at the lower range of AoA drag increase. The data supplied by Hann [1] only models half the aircraft.

Only the clean airfoil 3D data is currently available and while the 2D data gave sectional lift coefficient, the 3D data gives lift coefficient for an aircraft with reference area 1. To find the actual lift coefficient for the reference aircraft, the Mean Aerodynamic Chord (MAC) is multiplied by the wing span to find the surface area of the PX-31. The MAC is the averaged chord of the airfoil as most wing designs are seldom rectangular, but instead is tapered and swept. By using the MAC, a more accurate figure for the surface area is available. Depending on the wing, the MAC can be difficult to calculate, but in this case MAC is provided and hence the calculation of MAC will not be discussed further [22]. The surface area is given in chapter 3.4 in the aircraft specifications. Since only half the model is modelled, half the surface needs to be used. This half surface area is then divided with the lift coefficient data to give the 3D lift and drag coefficient of the actual aircraft. The 3D data available looks at two Reynolds numbers, with the higher Reynolds number corresponding to a higher lift force and stall angle as expected from earlier discussions on Reynolds number. There is 3D data for Reynolds number of 600 thousand available from both computational and experimental tests. From Figure 16-18 the lift and drag curves is presented. The curves show linear behaviour similar to 2D behaviour. There were some outliers in the data and had to be removed as it gave results that were not physical, such as having two stall angles. The general trend is the same between 2D and 3D and hence removing these outliers are justified [22].

The 2D/3D comparison is that the lift curve is lower with the same intersection at the x-axis, while drag is generally higher [8]. Figure 15 shows how the lift curve changes with AR, where 2D data is approximated as having infinite AR. The lift coefficient decreases with AR as shown in Figure 15. A question might arise on why the stall angle occurs later for 3D airfoils. This is because of the aforementioned wing tip effects. Stall occurs due to flow separation, which again occurs because the flow does not contain enough energy to "stick" to the wing surface. With the flow that occurs from bottom to the top of the wing at the tip, it gets a sideways flow over the wings that manage to maintain the energy required for the flow not to separate. This effect is purely driven by the pressure difference between the bottom and top part of the wing. With high enough AoA, this effect will also inevitably fail and lead to stall [8]. So, although the lift decreases with AR, the stall region occurs over a larger region as shown in the figure, adding a layer of safety. The lift

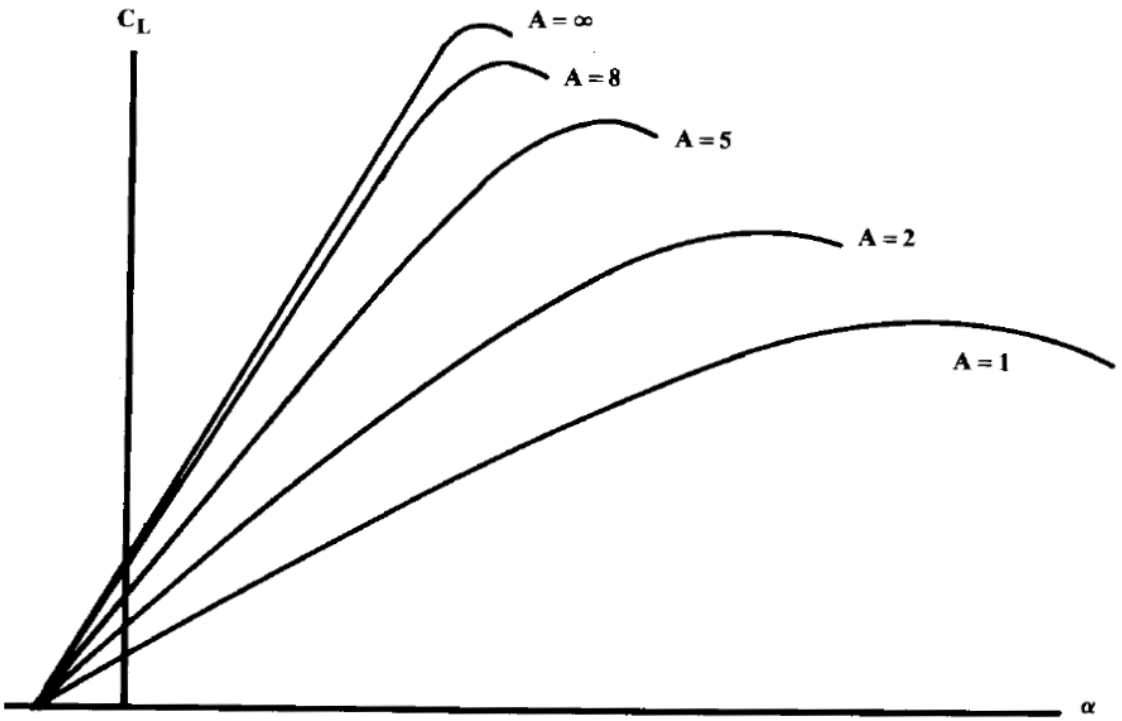

Figure 15: Plots comparing lift curves with different aspect ratios. 2D is assumed to have AR of infinity and the rest are variations of 3D lift curves. Source: [8]

requirement can then be solved by designing airfoils with different lift characteristics. As for drag, the drag increases due to downwash and lift induced drag as explained in chapter 3.2.3. The data referenced in Figure 17-16 is supplied by Hann [1].

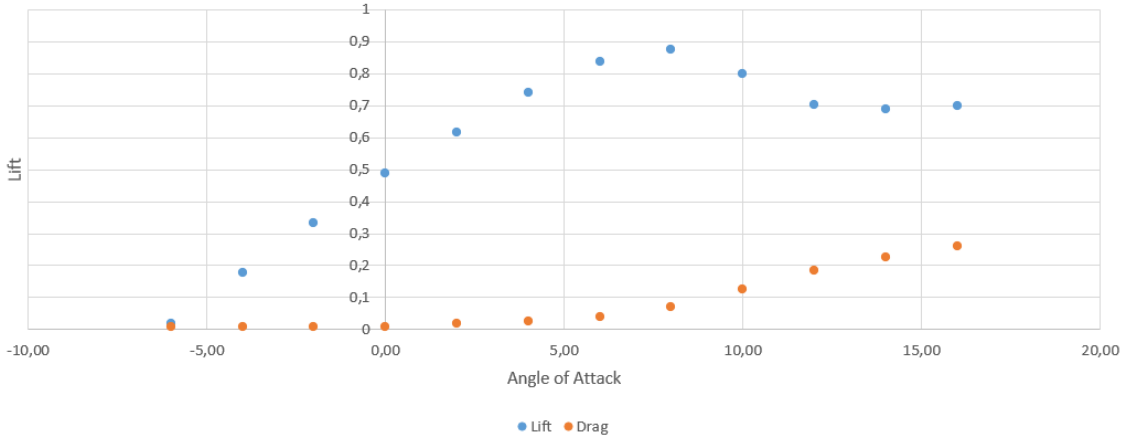

Figure 16: Computational 3D Lift and Drag force Curves for Reynolds number 600 thousand. Source: [1]

3.6 Propeller Performance Degradation Due to Icing

The propeller icing data will use clean steady-state efficiency as reference value. The propeller efficiency depends on the advance ratio, which is the ratio between the freestream fluid velocity and the propeller tip speed. The freestream fluid velocity is often taken as the airspeed of the aircraft, while the propeller tip speed depends on the revolutions per minute (RPM). An increase

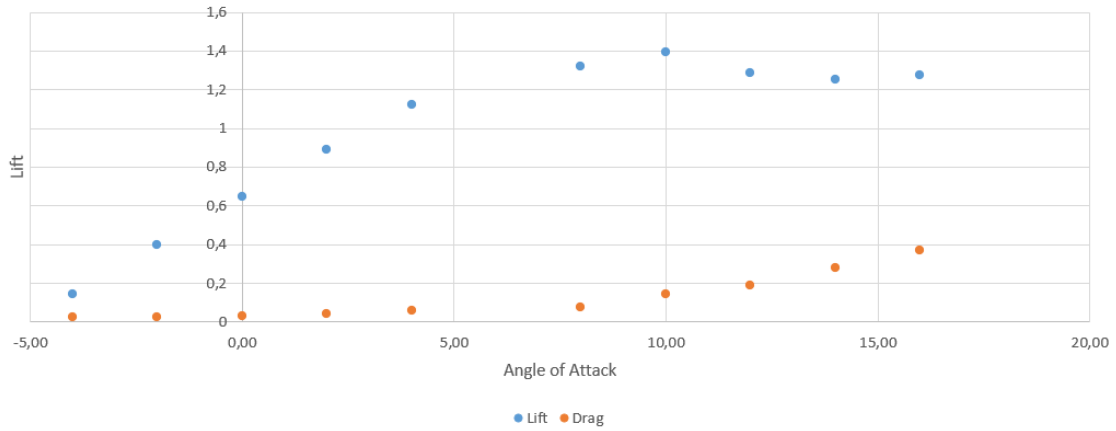

Figure 17: Experimental 3D Lift and Drag force Curves for Reynolds number 1.2 million. Source: [1]

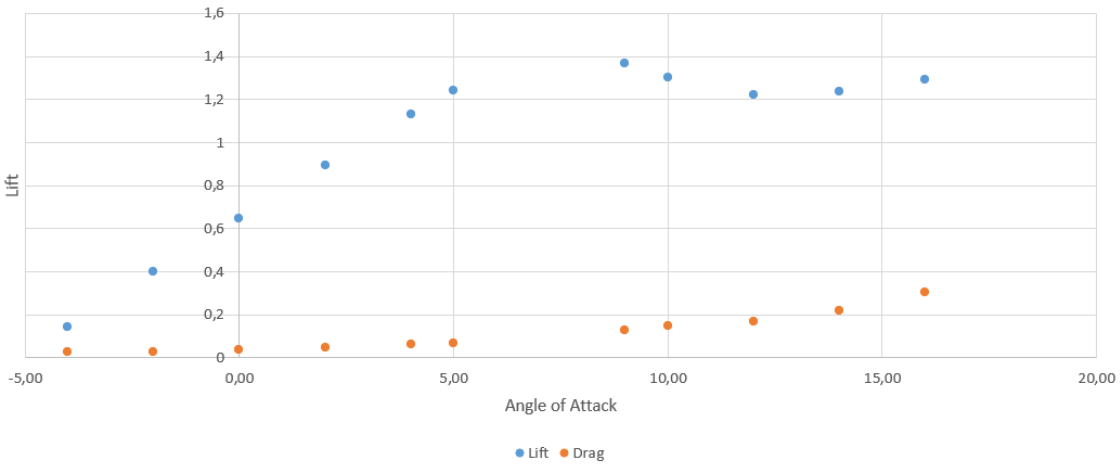

Figure 18: Experimental 3D Lift and Drag force Curves for Reynolds number 600 thousand. Source: [1]

in RPM will increase the airspeed, which generally increases quicker than the propeller tip speed, up until a certain point when the flow becomes unstable and the propeller stalls [30]. Assuming cruise speed of the PX-31 as the reference speed, which is 25 m/s at 5000 RPM the propeller efficiency can be assumed to be 65%. This is in contrast with the efficiency used by Narum [10], which is assumed to be 50%. In the simulations that will be performed in this thesis, there will be a comparison between runs with and without IPS. The runs without the IPS will need to include propeller degradation data. Real life degradation of the propeller is difficult to predict. This is because the efficiency will be oscillatory due to ice shedding from the forces generated by the propeller rotation. Hence, it will oscillate between high and low efficiency as the ice accumulates onto the propeller. The ice on t he propeller can accumulate similarly to the wing or as a thin sheet. If the ice accumulated is thin there will be a tipping point where the ice will shed, making it a complex topic [31]. Some of this complexity includes asymmetrical ice shedding, which can lead to instability as the different blades generate different amount of thrust. This will inevitably give the UAV an uneven flight path. The reason why three bladed propellers are so common in both wind turbine blades and UAVs is that it runs much smoother, as the forces are balanced. To make these forces disperse effectively, the blades have to be close to identical. When ice shedding occurs, this asymmetrical ice shedding can cause each blade to have different shapes, which gives rise to more instability and vibrations. Hence, there is much more physics involved when it comes to UAV propellers, but for this thesis this is not the main topic and hence is not discussed further.

As accuracy for the simulation with the IPS disabled is not as important as for the IPS simulation, some simplifications can be applied. The efficiency degradation plateaus to a constant value after a minute of ice accumulation. Since this constant value is worst case scenario for efficiency and is reached quickly, it is safe to assume a constant value when icing conditions are encountered and steady-state reached. The no IPS run is meant to emphasize how having no IPS is a disadvantage, but might be affected by how much icing is present at a certain day. If icing is not severe, the PSO might have enough freedom to find other routes that can give results that crashes with the fact that there is no IPS. This is because the PSO algorithm currently implemented does not always find global minimum every time, and this might affect results. A more thorough discussion on this will be presented in the path planning section. Additionally, it might not be representative to use the lowest propeller efficiency immediately, it is the only simplification available to implement as it would consume considerable computational resources to model the propeller efficiency accurately and will only yield diminishing returns. This is because it would require timescales to the minute and will require significant computational cost. To end this subchapter on propeller, a discussion on which condition is the worst for propeller efficiency is discussed. This time, lower temperatures degrades efficiency to a much larger degree as seen in Figure 19. It ranges from 15% drop in the higher temperature to 80% drop at lower temperatures. A possible explanation for this is that the ice at lower temperature has higher structural integrity and hence resists ice shedding to a higher degree. This reduced the efficiency to a much higher degree as the propeller ice blocks the airflow to a higher degree. The propeller degradation data will only be used for no IPS runs and the reason for this will be explained in the energy consumption chapter. All propeller data, both efficiency and IPS energy consumption is a contribution from Fajt [7], who is doing a PhD in propeller icing.

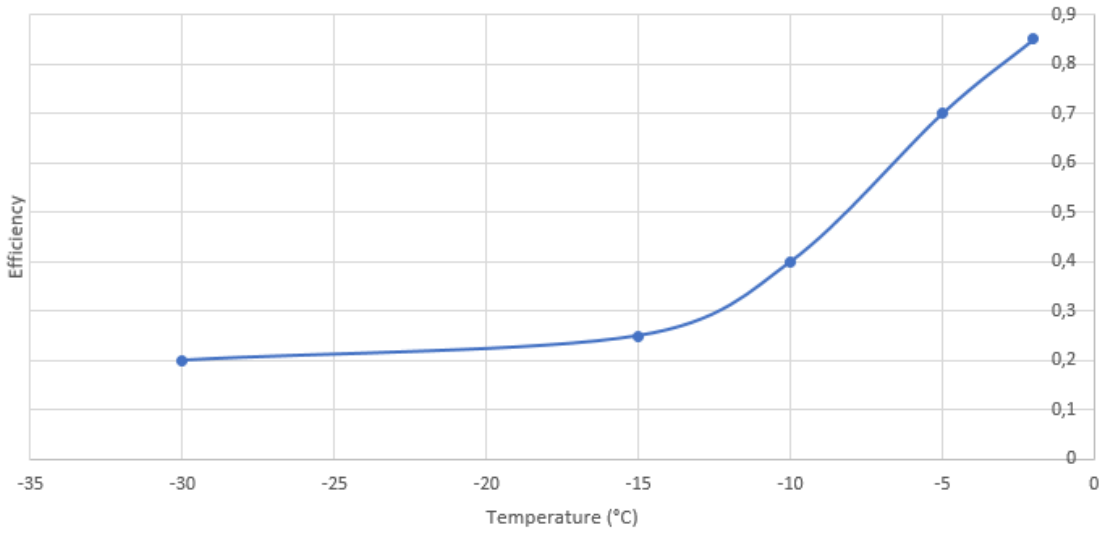

Figure 19: Propeller degradation, here the efficiency in the curve denotes how much the clean efficiency has dropped to. For example for -30 degrees Celsius, 0.2 means the efficiency has dropped by 80%. Source: [7]

3.7 Ice Mass

The ice mass accumulation data is given per meter span. The highest accretion is in the higher temperature range below freezing as this is where the LWC is the highest and hence the wettest. The MVD where the ice mass accumulates the most is at MVD 20. The ice accumulation is the lowest at 40 MVD, most likely due to less variation in droplet size [9]. Hence, high ice accumulation depends on a balance between MVD and LWC. The ice mass accumulation per wing span in meters is given in Figure 20, showing the difference in temperature and MVD.

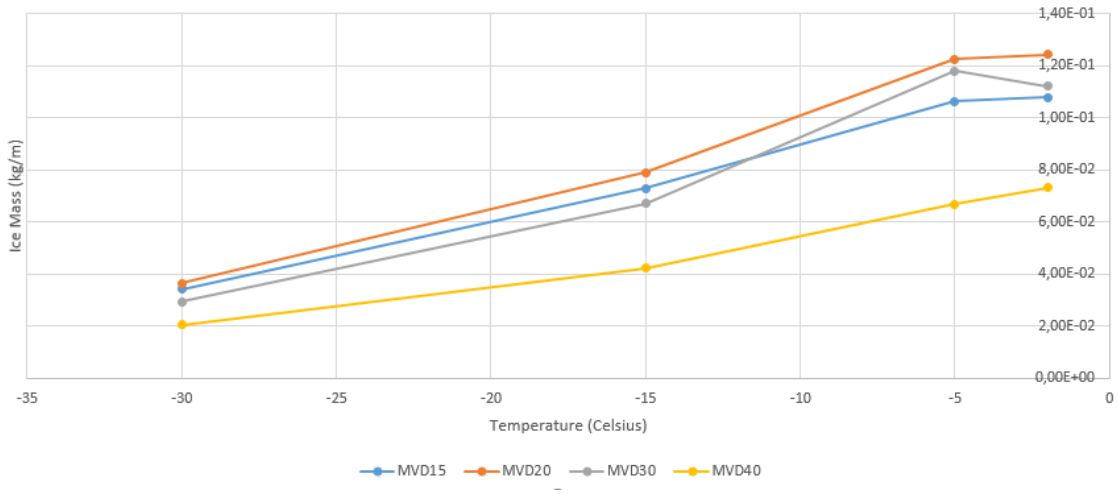

Figure 20: Ice mass per wing span over several temperature ranges for different MVDs. Source: [7]

4 IPS Energy Consumption Model

The implementation of the energy consumption of the IPS changes the initial model implemented by Narum [10]. Initially, the IPS power consumption were based on empirical observations that relates LWC and MVD to power consumption and from it the IPS power consumption was calculated. The IPS is installed on the PX-31 on the leading edge of the wings only, as covering the entire wing would lead to too high energy consumption. However, as discussed from the previous section, the majority of the lift and drag generation is located at the leading edge, making it optimal to place the IPS. The research and design of the IPS was conducted by Hann et al. and the full details can be found at [13]. Some problems associated with only locating the IPS at the leading edge, is that some of the runback water can refreeze further down the wing toward the trailing edge without a way to melt it. This is a complex problem because it can be unpredictable and difficult to measure and is present for both modes of IPS operation [9]. Although there are some methods in dealing with runback ice, this thesis will assume that no runback icing occurs and will also not be discussed further. The IPS have two modes available, anti-icing and de-icing, which is the subject of the next sections.

4.1 IPS Modes

Both modes will only turn on if icing condition is detected to avoid unnecessary energy consumption. It is currently unknown which mode is more energy efficient, which makes it interesting to compare. To test these two modes, energy consumption was measured for different icing conditions. The data currently available is for a particular icing condition with LWC at $0.44g/m^3$ and MVD at 26 microns, which is tested at different temperatures. This is not a problem for the IPS as LWC and MVD does not influence IPS consumption as much as temperature and hence the temperature can be the main indicator for IPS consumption without using MVD and LWC as inputs [13]. This is because the main working principle of the IPS is to increase the temperature above 0 degrees to melt the ice. How much energy is required to increase the temperature above zero depends almost solely on outside temperature. LWC and MVD is more a metric on how much ice gets accumulated and hence how much heat needs to be applied to the IPS. The data used for IPS power consumption for the wings are time-averaged and it is assumed that the IPS is on for 20-30 seconds each time it is turned on to calculate the power. It does not mean the power is multiplied by 20-30 seconds to get the energy however. Since the data is time averaged, the power will be multiplied with the time step between each waypoint to get the actual energy consumed. The IPS consumption is then mostly dependent on the applied power. The two modes will now be introduced and the differences in using lift to drag ratio data will be discussed.

4.1.1 Anti-Icing

The anti-icing strategy of operation is the simplest one. When icing condition is detected, the IPS will run hot enough to avoid any ice to form, which means the surface temperature must be above freezing. This avoids any performance degradation of the aircraft, in exchange for higher energy consumption. The reason for the higher consumption is that the IPS is on for longer and consumes more energy to avoid icing. For colder temperatures, this consumption can be significant. The data suggests that the energy requirements does not increase exponentially, but flattens out. However, since there is a lack of data points, this is only an assumption from the trend that can be observed in Figure 21.

Looking at the data points, the curve for anti-icing can be split into two linear equation at 5 degrees as seen in Figure 21. This is to avoid assuming a quadratic relationship, because the quadratic plot would be concave and hence power would decrease with low enough temperatures, which is not physically correct. The question that arises is why the increase in power requirement is higher up until -5 degrees. In other words, why the power increase this significantly between -2 and -5 degrees? There are some research performed, diving into the physics of ice accretion and the different properties between glaze and rime ice. The glaze ice process is quite a unique case as the initial supercooled liquid freezes instantly, rime ice actually forms first [21]. When the ice freezes latent heat is released. This latent heat is called latent heat of fusion. This latent heat

stems from how much energy is stored in a particular state of matter. Liquid water in this case has a higher energy content compared to ice, which has to be released during phase transition. This energy release prevents all the liquid water from freezing at once at higher temperatures. This leads to the conditions where glaze ice happen to have a water and an ice layer. What happens next is a complex process as many different things can happen. Runback icing can occur, some of the water layer can start to freeze due to convection, which is affected by the temperature and hence affect freezing rates considerably. Nonetheless, at glaze ice conditions, the release of latent heat contributes to melting the initial freezing that occurs together with the IPS, which is why there is quite a large increase between -2 degrees Celsius and -5 degrees Celsius. Glaze and ice horn formation is most frequent between these temperature and it starts to stabilize below -5 degrees [32, 33]. The use of IPS to remove glaze ice is hence much more effective than rime ice, which is also the ice that degrades performance the most and is thus advantageous. As mentioned earlier, temperature will be seen as the main factor for IPS consumption relationships. Hence, LWC will not be a factor in the equation. Although LWC will have an effect on the ice accretion rates, the IPS heating element will be unaffected by these conditions. The heating element will only look at the temperature it needs to raise to melt the ice. Since it is only a strip, the heat conduction of the ice can determine the heat it needs to apply to melt the strip. For glaze ice the thickness of the ice layer is usually small and the water layer will part way and let de-icing occur. Heat conduction for glaze ice is usually higher than rime ice. Rime ice, due to its fast freezing rate, will trap the air around it, making the ice porous. Air is also a bad heat conductor, which require more heat to remove the rime ice [34]. All the reasons discussed contributes to the significant increase in energy between -2 to -5 degrees, which is the transition between glaze and rime ice. As a final note, once the temperature is low enough, the latent heat release affects the freezing rate less and less, which lead to more consistent rime ice formation without forming a water layer. This is related to both temperature and convection rates increasing, leading to faster freeze rates compared to higher temperatures. This can be seen as the reason why the figure stabilizes at colder temperatures. In any case, anti-icing consumes 2-7 times more energy than de-icing depending on temperature, the remaining question is if the cyclical de-icing nature together with aircraft performance degradation will exceed anti-icing consumption.

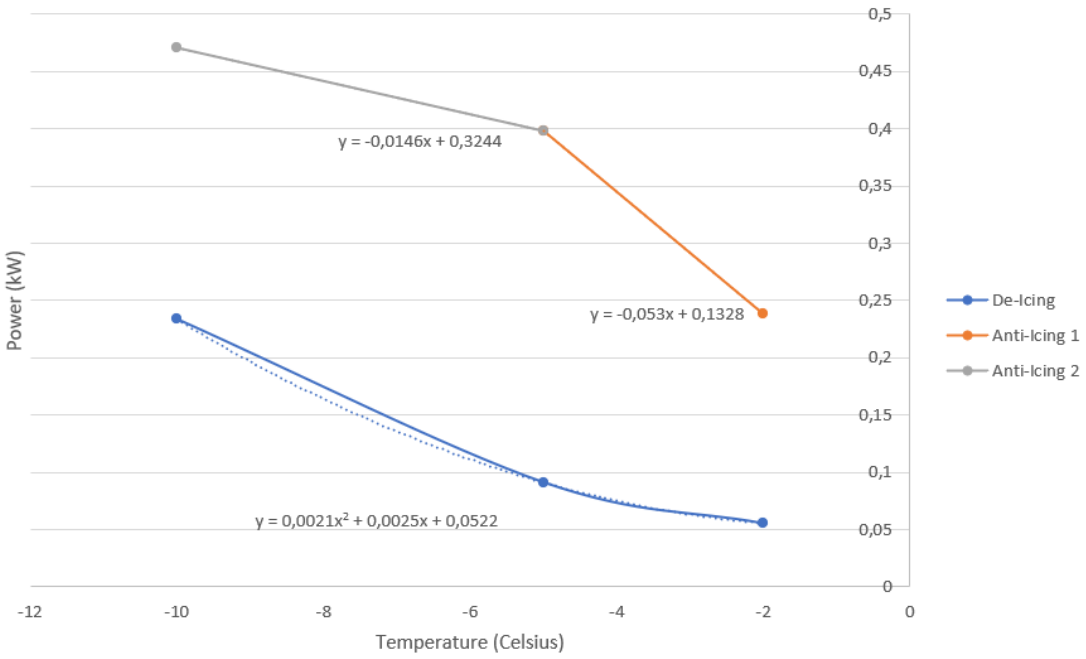

Figure 21: IPS Consumption data for anti and de-icing, using linear and quadratic interpolation to find equations to implement. The figure also shows the equation that will be implemented in the code. Source: [9]

4.1.2 De-Icing

As the de-icing curve in Figure 21 would give a convex curve, a quadratic relationship can be assumed. This can be observed by just how the plot is curving. De-icing is the strategy that is yet to be fully explored and compared with anti-icing. De-icing cyclically heats up the wing to remove ice, with the heating interval being a design parameter. The IPS is usually on every 4 minutes, though this parameter can be changed. However, in this thesis, this design parameter will be assumed to be at 4 minutes as this is the data that is available. There are two methods for removing the ice from the wing, the conventional method or strip de-icing (which is also how ice is removed using anti-icing, despite the name). Strip de-icing mode only has IPS at the leading edge and is effective in removing the ice, as when the ice melts at the leading edge strip, it creates a gap where incoming air can push back the ice and hence take advantage of aerodynamic forces to remove the ice. Together with melting the contact point between the ice and wing surface, the aerodynamic forces overcomes the adhesion effects to loosen the ice from the aircraft. The conventional method requires additional IPS elements, covering a larger surface area, which automatically increases energy consumption. De-icing strategy generally consumes much less energy than anti-icing for heating purposes, but will instead consume more energy in terms of thrust requirements due to increased drag. As icing is now allowed to accumulate on the wing on set intervals, the aircraft performance degradation needs to be taken into account. The use of lift and drag icing data is solely used for this IPS strategy. There will be a combined thrust and IPS energy consumption increase and it needs to be compared with anti-icing mode. Other considerations that needs to be taken into account for future work is whether either mode works better in one situation over the other. For example, it might be worth using anti-icing in glaze ice conditions as the performance degradation is higher under glaze ice, as well as using less energy at glaze ice conditions. De-icing could work better at lower temperatures for the opposite reason.

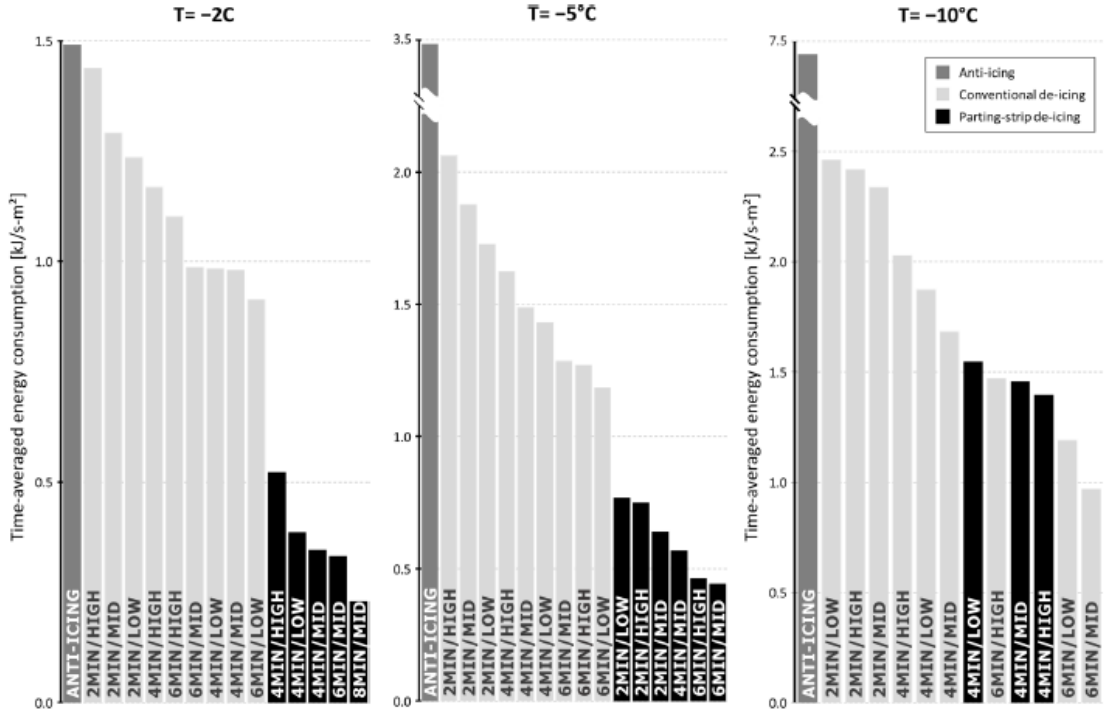

Figure 22: Time-averaged IPS energy consumption for anti-icing and different de-icing intervals. Source: [9]

Figure 22 is taken from the PhD thesis by Hann [9], who among other things, looked at IPS energy consumption for anti-icing and de-icing. Looking at Figure 22, it can be observed that anti-icing uses the most energy as expected and removing ice by strip de-icing being more energy

efficient than conventional methods. Although these results are available, the data has yet to be applied practically together with performance degradation data. The figure only shows IPS energy consumption and not overall consumption together with compensating thrust generation. The low, mid and high notation in the figure is the level of heat flux used, but with no clear trend found by Hann [9]. For this thesis, only mid level flux data is available so only that will be considered. Strip de-icing uses significantly less energy than conventional de-icing up until colder temperatures as seen for $-10°$ C plot in the figure. This could be attributed to higher temperature differences. The IPS will need to heat up to above freezing and higher temperature difference requires more energy. As can be seen in Figure 20, there is actually lower ice mass accumulation for lower temperatures, making the temperature difference the sole determinant for higher energy consumption. Strip de-icing is only at its optimal when the leading edge is exposed and allows the airflow to push the separated ice. If the ice is still in one piece, the leading edge needs to heat enough until strip de-icing can work. The de-icing interval does not show how much the performance have degraded and the only thing that can be concluded is that shorter cycling times gives higher consumption as it is run more often, but with less performance degradation and vice versa. Different cycling times is something to be tested for future work. The data available is as mentioned only available for a specific LWC and MVD, in addition to using mid level of flux and should be more rigorous by covering more value ranges for these parameters. To end the chapter, some final comments on how the IPS is setup and the calculations made is discussed. The leading edge IPS strip is 5 cm wide a wing span of 3.2 m. This gives the effective heating area of 0.16 m^2, as the data is given in kW/m^2. This way, it will be possible to calculate the energy consumed.

4.2 Propeller IPS

By analysing the data, the propeller degrades quickly, within a minute, and hence it would be beneficial to run the IPS on anti-icing mode for the propeller to avoid the propeller degradation completely. It will simplify the implementation of propeller performance in the simulations when IPS is enabled. As for the data, the energy consumption are computationally calculated and assumes $-15°C$. Additionally, some safety margins are added such as including a factor of 1.5 to account for propeller heating, it is assumed that the propeller surface is heated to $10°C$ and only convective heat losses are taken into account. Hence, the energy consumption by the propeller IPS is calculated strictly from first principles of convection and conduction. It calculates what is required to raise the surface temperature of the propeller to 0 and hence melt the ice. It does not take into material properties, only the energy requirement itself, which is why a safety margin is included to account for it indirectly. The data is then extrapolated for colder temperatures. Figure 23 shows the energy consumption in Watts for anti-icing mode. The values are extrapolated assuming linear relationship as a simplification. Experimental values will not be available until after the completion of this thesis so it is the best assumption given the circumstances. Propeller anti-icing has not been implemented in Narum [10], meaning this estimation would be more conservative when implemented.

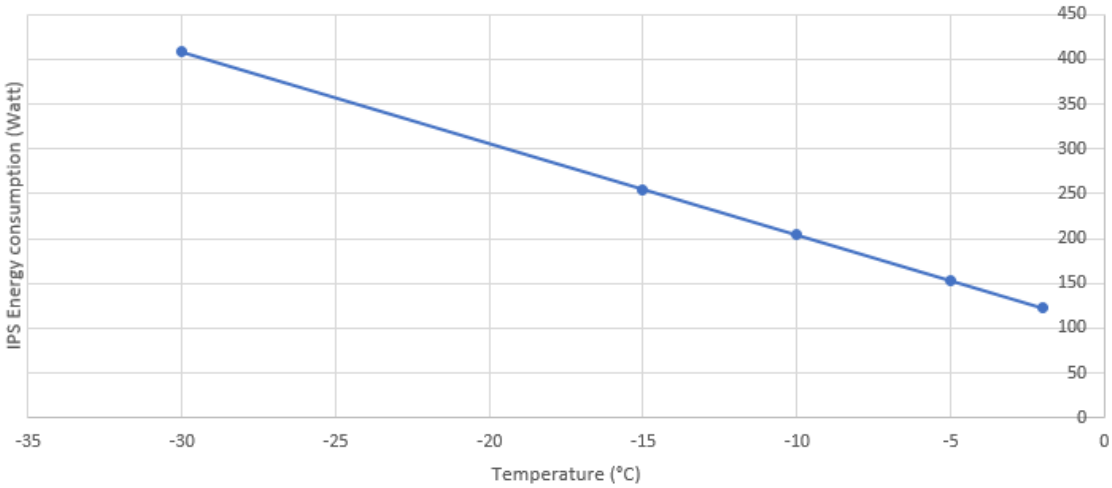

Figure 23: Propeller IPS anti-icing energy consumption plotted against temperature. Data supplied by Fajt [7].

5 Path Planning

The focus of this thesis is not on the control side of the simulation, but it would be useful to present the current path planning method for understanding and completion sake. It is also useful for future work, as the subject focus will shift to path planning in icing conditions. It will give a better overview on the overarching goals and future timeline of the work that will follow in PhD work. This chapter will focus on presenting the details of the current path planning method.

5.1 Narums Path Planning Implementation

This section will look into explaining the path planning implementation by Narum. The current path planning implementation use PSO, from the works by Eberhard and Kennedy and the overview by Wang et al. [35, 36], to calculate the optimal path in terms of minimizing the cost function, which is either flight time or energy consumption. It achieves this by utilizing a pseudo-random swarm. The swarm consists of many individual points in space that keeps track of the path that has the most potential in minimizing the cost function. Due to the pseudo-randomness of the method, it is possible that one iteration will not give an optimal path, but only the best one for that iteration. Because of this, multiple iterations are required to give a better estimate of the optimal path. The only constant of the path planner are the waypoints that are set before executing the simulation. The waypoints do change depending on the route, but at a set route the waypoints will be constant. The PSO can then be run with the swarm going within a confined space that is limited by the user. This allows the PSO to go as far out as the defined space, both vertically and horizontally to find the best path possible for that iteration. The PSO will however, not explore the whole space as the PSO has to follow a default path where the swarm expands from. Unless necessary, the PSO will stick relatively close to this default path and is part of the reason why global minima is not found at every iteration. One downside that has been mentioned at the start of the thesis, is that because the PSO is pseudo-random it will give a different answer every time if the parameters are kept the same as in Narum [10]. As a consequence of this randomness, the PSO method does not yield global minimum answers for every run. The PSO does yield minima, but whether or not it is the global minima is uncertain unless enough iterations are run, which can consume considerable computational resources. Hence, it is possible that sometimes some results is not as expected. For example in the results that Narum found, the energy cost in the no IPS case is lower than the IPS case. This could be attributed to the difference between energy consumed by the IPS. It might also be because the PSO now "explores" solution space more to avoid icing and manages to find a better solution. This is just some of the quirks of the PSO, and finding improvements both for increased "exploration" and hence finding global minimum is something reserved for future work. In any case, Tiller [16] in his thesis has managed to implement a method that makes the PSO more consistent by eliminating this pseudo-randomness and hence reproducible to make it more comparable to changes or additional implementation to the code. However, unless the number of iterations are increased, the same solution will be found and hence the PSO will possibly be stuck to a local minima. In this thesis, the number of iterations used for finding a solution is set to 256. This is deemed to be a sufficient number of iterations as the PSO scales with the number of iterations to know when it needs to explore less and go towards convergence. Some other iterations were tested, such as 1000 iterations, but comparing the solution to 256 showed minimal improvement and hence to save computational resources 256 was chosen. It could be possible that even more iterations would yield closer to global minimum, but the uncertainty on this is too big and there are no guaranteed way to ascertain if global minimum has been reached. Hence, at the current stage, increasing the number of iteration is not an optimal choice. Hence, for future work, it will be beneficial to explore methods that can give an indication of global minimum.

The results from Narum [10] made several simulations for testing. The UAV was to deliver emergency hospital supplies from one Norwegian city to another. As an example, the best path between Bodø and Tromsø for both energy optimal and time optimal paths are shown both horizontally and vertically in Figure 24-25 respectively.

Looking at these figures, it is possible to observe the many considerations that the simulation takes. For example if the optimal path is indeed the straightest one. In most cases, the simulation

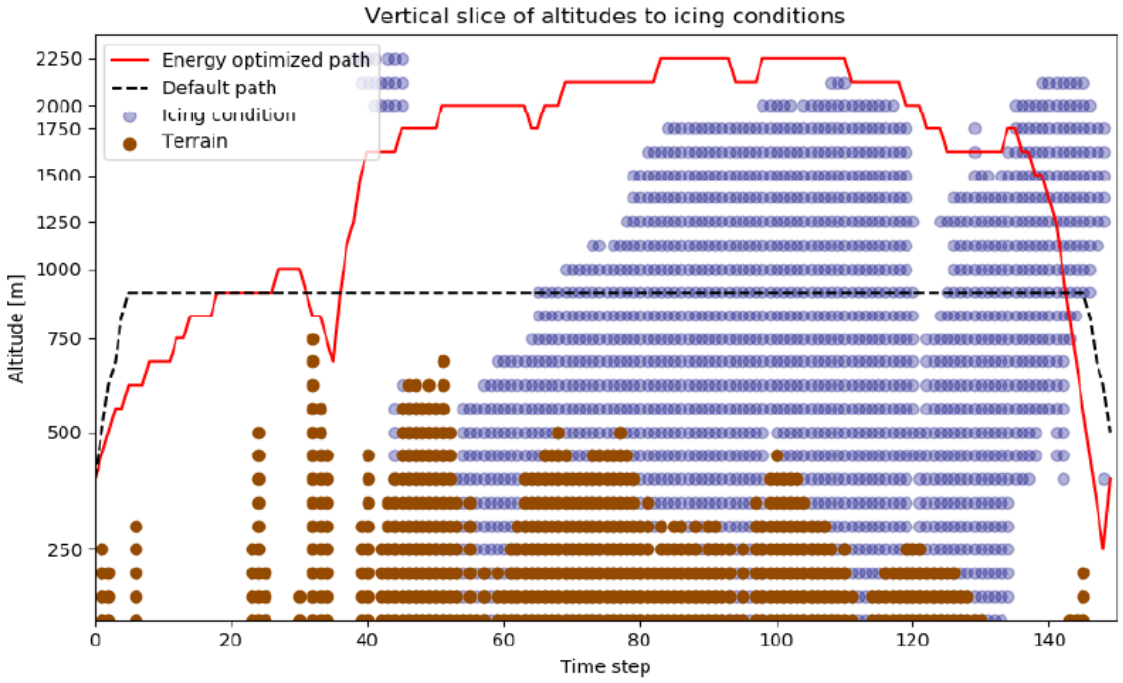

Figure 24: Vertical slice of energy optimal path between Bodø and Tromsø. Source:[10]

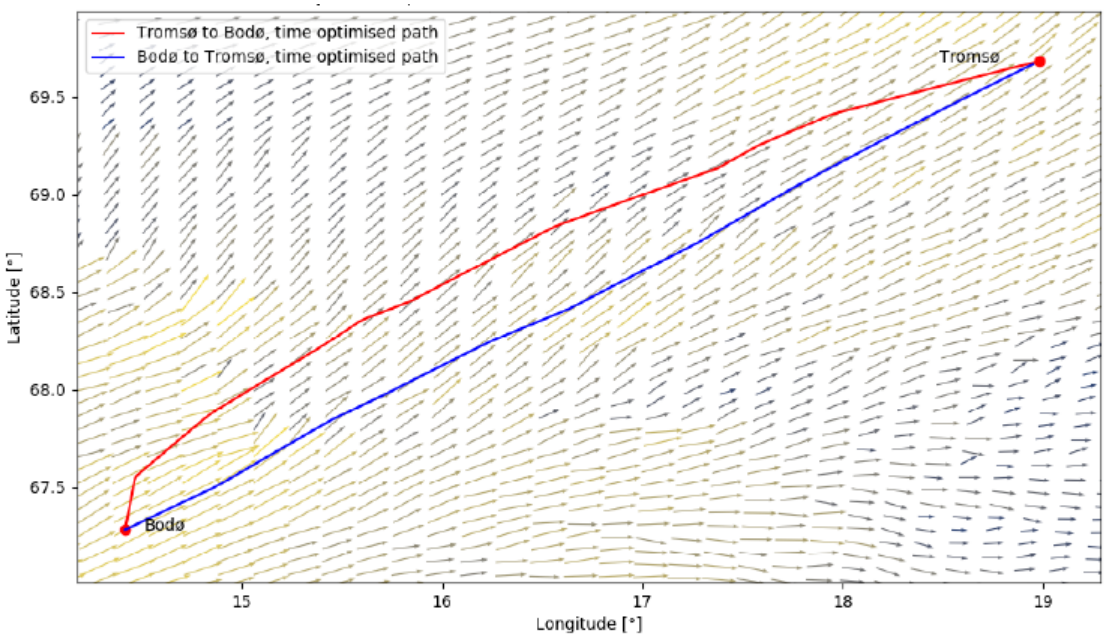

Figure 25: Horizontal slice of time optimized path between Bodø and Tromsø. The wind pattern is from an altitude of 1200 m. Source: [10]

will consider taking advantage of the wind and going through icing conditions rather than moving around it to save energy consumed. Figure 25 shows the effect of wind on time optimised path, depending on which direction the aircraft is travelling. The arrows in the figure shows the wind direction, which allows the Bodø-Tromsø route to be almost straight, by taking advantage of the wind. The other direction needs to take a longer detour to presumably avoid the strongest winds, the path tries to find where the wind is weakest to minimize headwind. An important note is that these horizontal and vertical slices are taken from a particular altitude or longitude. Hence, it is

possible that choosing one slice is not representative to the path. It could be possible to consider a 3D plot with all of this taken into account, but it is deemed to give cluttered plots with too much information at this time. Hence, in this thesis, the paths will be presented in the cleanest manner without icing or wind information. However, a 3D plot would be beneficial if plots with condensed information can be made. It will be reserved for future work to figure out a less cluttered way to represent all the information in a 3D plot. The information will for this thesis be summarized in a table instead, presenting parameters such as icing duration and energy consumption breakdown between propeller consumption, IPS consumption and propeller consumption due to icing.

To summarize with results taken from Narum [10] with three scenarios, default, energy and time optimisation. The default straight route as seen in Figure 24 uses 2-3 hours longer and almost double the energy consumption than the other two between Tromsø-Bodø. The difference between energy and time optimised paths is not as remarkable, but time optimised path is faster by one hour and only consume 5 Ampere-hours (Ah) more. This is only one scenario presented here of the six different routes tested by Narum [10]. The other scenarios is much more varied, with small difference and anywhere inbetween, with the Bodø-Tromsø route being close to identical in performance. The results have a huge dependency, as predicted, to the weather conditions. There is also not a huge difference between energy and time optimised paths. However, it can be important if the mission is time-dependent or if multiple trips are necessary, where the energy optimised path enables these multiple trips. Hence, detailed analysis of the paths are not usually worth it, as it can be mission sensitive.

Using this methods leads to potentially limitless paths available depending on the iteration. It can also be concluded that global optimal path is most likely never achieved. It is however not necessary as mission completion should be the main focus. With that said, the method used is ultimately quite flexible. The conditions that makes the mission impossible does not have a clear definition, but the overarching goal of the research made here is to ultimately minimize operation envelope that make missions impossible. These envelopes depends on the aircraft in question and due to the large catalogue of aircrafts available, will not be discussed further. Ultimately, the PSO method is a very robust method that has seen much research due to its exploratory nature, using the statistical nature of the method to find many possible paths.

5.2 Tillers Path Planning Implementation

The rebuilt path planning implementation by Tiller [16] in his thesis looks to make an algorithm that has better documentation. The algorithm by Narum was written with the mindset of self-use, which made it difficult to use without spending significant time interpreting the algorithm. Tiller wrote the algorithm from scratch to make it more readable such that it would be easier for collaboration, while updating the PSO and how weather data is processed. Additionally, it changes how the PSO behaves. Narums implementation has a default path that the PSO uses to expand its swarm from. This generally restricts the PSO swarm behaviour, making it explore less than optimal. In Tillers implementation, the default path will now be initialized randomly multiple times within the same test run, such that it can explore more possibilities. There are disadvantages by implementing the PSO this way, but this is dealt with and discussed in Tillers thesis, which is written at the same time as this thesis, so the reader is referred to Tillers thesis for the details [16]. When this thesis is finished, it is Tillers implementation that will be used. The ensemble weather data will need to be re-implemented as future work with this implementation, together with everything else that has been implemented in this thesis so far.

6 Simulations

The simulation environment combines everything presented in the last few chapters. Some of these remain unchanged from the work by Narum [10], some are changed with additional model implementations. The changes and new implementations made have already been mentioned in the previous chapters. This chapter aims to include the rest of the program with implemented equations. It also goes into more detail on how the new energy model is implemented code-wise in C++. To be able to start simulating, the simulation program needs to initialize the world and its boundaries where the drone will operate. This world sets the boundaries for the PSO method, including all weather and geographical data. The space the simulation occupies can be visualised as a three-dimensional grid, which is the most common method of discretization for computers, to give a certain accuracy or resolution of the solution. In this case, the grid size depends on the number of ensemble weather predictions used as implemented by Tiller [17] in his project report. The first section briefly goes into data acquisition and how the data is treated in the functions of the program, particularly the PSO.

Table 1: Table documenting where data is from, how it is implemented and what condition in the code it is used

Reference	**Data**	**Implementation**	**When is the data used in the simulation?**
[9]	IPS energy consumption data	Linearly interpolated between data points. Split into two linear regions, one higher than -5 degrees, one less than -5 degrees.	Used whenever IPS is included in the simulation and icing condition is detected
[7]	Aerodynamic performance degradation data	Trilinear interpolation between data points and assuming constant ice accretion rates per minute	Used whenever icing condition is detected and anti-icing mode is not used as anti-icing mode assumes that the ice is fully melted at all times
[7]	Ice accretion data	Bilinear interpolation between data points of ice mass. Assumes proportional accretion rates per minute	Used whenever icing condition is detected and anti-icing mode is not used as anti-icing mode assumes that the ice is fully melted at all times
[7]	Propeller performance degradation data	Assumes linear relationship with extrapolated data from first principles, using standard convection equations	Only used for the case where IPS is disabled and when icing condition is detected
[7]	Propeller IPS consumption data, anti-icing mode only	Implemented linearly and separated into two regions, one above and below -12 degrees.	Used whenever icing conditions is detected and IPS is enabled

6.1 Data Acquisition

The data acquisition here pertains to the meteorological data for a given mission, which is used to initialize the parameters of the world. The data is extracted from Norwegian MET, as part of their forecast model. Norwegian MET has two datasets that are relevant for this project, each containing weather parameters. There is one dataset that is the ensemble dataset, but only for some weather parameters, and one for all weather parameters but deterministic and hence not significant in a statistical sense. The ensemble contains the general weather data, while the deterministic dataset contains the icing parameters. The two dataset does not contain the same resolution either, which require interpolation to fill in the gaps. Model wise, the implementation in the code separates the general ensemble and icing data. The icing data usage is as presented by Narum, while the new ensemble data is as presented by Tiller. The objective with the ensemble weather prediction

implemented by Tiller [17] in his project report, is to be able to predict the weather in statistical manner, using climate data for the area. The deterministic dataset is equivalent to a day to day weather forecast, which in itself does not give a good picture of the actual climate conditions of the area. Hence, the implementation of ensemble weather data is important for a more accurate picture of the weather the drone can expect to encounter. The ensemble weather data implementation is not part of this thesis, and hence will not be discussed further, but the interested reader is referred to the project report by Tiller [17] or any other papers on ensemble weather forecasts such as [37].

6.1.1 Particle Swarm Optimisation

The PSO implementation consists, as mentioned previously, of many particles that explores the environment, to try and find the best solution. Each particle has its own parameter vector that contains waypoint coordinates in x and y-directions, airspeed and climb angle. These parameters are updated in each iteration. There is also a weighting associated with each particle, denoting how much the particle will "explore" to find a better solution in space. This will initially be large and shrink nearing the end of a user given iteration limit, such that the program can converge. The space is also limited by the user, so the particles are not able to go outside the world boundary, which is taken care of by making the particle move back inside the boundary by reflecting it back with the same angle it approached the boundary. This initialization of boundaries and limits is also where the velocity, angles and physical constraints are defined, which is something the user can choose. In this case, these constraints are chosen to be the same as the limits of the PX-31.

6.2 Cost Functions

To get an indicator for how well the different scenarios and missions are performing, a cost function is implemented for this purpose [38]. There are some user defined criteria that would make the function go to infinity, such as going out of bounds of the defined space or running out of fuel. This will automatically assign it as an infeasible solution. The way to find which is the best route for that particular iteration is just to compare this function with each other. By assigning an initial cost function value, this value will be compared with the rest of the paths and finding the lowest value for either energy usage or flight duration. As mentioned earlier, the route is not guaranteed to be global minimum, but in most cases this will not be necessary as long as the mission is feasible. The cost function for time and energy optimisation is different and will be presented as is from Narum.

6.2.1 Minimizing Energy Usage

The energy optimisation function as defined by Narum is given as:

$$COST_{Energy} = C_{cut} - C_{end} + \frac{2 * (F_{full} - F_{remain})\eta_{tot}\rho_{fuel}E_{fuel}}{V_{exp} + V_{nom}} \tag{25}$$

where C_{cut} and F_{full} is the max battery discharge capacity and fuel level at start of the route respectively, while C_{end} and F_{remain} is the remaining battery and fuel level at the end of the route. The other terms such as η_{tot}, ρ_{fuel} and E_{fuel} is total system efficiency, fuel density kg/m^3 and total fuel energy per kg respectively. The V_{exp} and V_{nom} are exponential and nominal voltages at end of route, which denotes the nominal charge the remaining fuel can supply. There are many energy terms here that are not related to this thesis and pertains the battery and fuel system, and as noted earlier, is not in the scope of this thesis and will not be discussed further. The full details can be found in the thesis by Narum [10]. One comment that can be made is that the iced airfoil will affect the energy consumption, but affects the equation indirectly through extra thrust generation and IPS consumption.

6.2.2 Minimizing Flight Duration

Minimizing flight duration is a much simpler affair and gives the equation:

$$COST_{time} = \sum_{i=0}^{N-1} t_i \tag{26}$$

where t_i is the time for discretisation step i. This is just simple summation of total time taken for a particular route, but does also take into account that the aircraft is able to complete the route with the energy it has. This is detailed in Narum [10].

6.3 Software Implementation of Icing Data

The implementation of the energy model using iced airfoil data is discussed in this section. The relationships used is relatively simple, but is slightly challenging in trying to combine all of them together to a coherent model. This section is broken down into four topics, the discretization of the data, implementation of the aerodynamic model, IPS energy consumption and the propeller model. Of these, the aerodynamic model will be the most complicated due to the amount of data required for implementation.

6.3.1 Discretization of Data

The discretization of data pertains to breaking down the data in discrete steps, so the computer is able to process it. A computer is not able to process continuous data and requires a certain amount of significant numbers within each step to properly process and use the data. This can be done manually through breaking down a variable, for example AoA into steps defined by the user, such as to the tenth or hundredth decimal place. Each of these steps will correspond to a lift and drag coefficient that can be used further. This is the look-up table (LUT) method. Another method is to describe the model with an equation. This equation uses variables such as temperature to calculate a value such as energy consumption directly. Both of these approaches have their pros and cons. Both methods can clamp the input variable to restrict itself within a given boundary. This is more important when using equations that tend to be defined over a larger domain. Equations are usually easier to deal with if the equation is relatively simple and does not require large datasets that needs to be put into the memory of the computer for lookup. This is however only possible if it is possible to construct a simple equation. Some models can tend to be too complex to generate such an equation and a LUT might be easier to implement in that case. The disadvantage with the LUT is the size of the table. A method that simplifies the LUT is real-time interpolation with the values available, making it semi-lookup. This means that the table contains key data values and any values inbetween will be interpolated. The downside is that any values outside the range of the key data points will not be available and will require extrapolation. For this thesis, any values that fall outside the range of the key data points will be clamped to the nearest data point as a simplification. The interpolation method used will be presented in the next sub-chapter. For this thesis, a combination of methods will be used depending on the simplicity of the equations that can be generated from data. It will be attempted to keep relationships linear or quadratic.

6.3.2 Implementation of Aerodynamic model and Ice mass

The aerodynamic model is the most complex implementation wise, due to the fact that it is dependent on three different variables, AoA, MVD and temperature. These three variables determine the lift and drag of an airfoil with ice. Technically, there is a fourth variable in time, as time determines the total accumulation of icing. The data supplied gives performance degradation when icing is allowed to accumulate for 20 minutes. It will be assumed that the accumulation rates are constant and linear, meaning any icing below or above the 20 minute frame will be calculated by linear relationship. An example for this is for de-icing, where in this case the ice is allowed to accumulate cyclically for 4 minutes. To calculate the appropriate degradation and not the full 20 minute of ice accretion, the degradation is multiplied by 4/20. Any other time is also available by just substituting 4 with any other time that the ice is allowed to accumulate. This is all dealt with in a linear manner, through all the data tested at different MVD, temperature and AoA. How to calculate across these three variables plus time is explained below.

It would be simplest to implement the modified semi-LUT for this purpose, by interpolating between key values. With the data supplied by Fajt [7] for different iced airfoil conditions, the method employed uses the data as fixed points and if data between these points is needed, a simple linear interpolation is used to calculate the needed value. In this case, trilinear interpolation will be used to be able to interpolate and discretize the data and calculate parameters such as desired lift which can then calculate corresponding angle of attack. The drag can also be found by using the calculated lift coefficient, which uses the angle of attack calculated to find corresponding drag coefficient. Since lift due to icing depends on AoA, MVD and temperature, trilinear interpolation is a good method to implement. This linearizes every point between the three variables as desired and finds the desired value. The method can be visualised as a cube, where every value is stored within that cube, with each extremes in the data acting as the vertices and the boundaries of the cube. Each variable is along one axis of this cube and each value can be interpolated and found. A detailed account on the trilinear interpolation method can be found in the article by Haynes et al. [39].

The implementation for ice mass is less complex than that for the aerodynamic model, but still has some complexity. This is because the ice mass depends on both the temperature and MVD, making it dependent on two variables and hence instead of trilinear interpolation uses bilinear interpolation to calculate the inbetween values. Time is also a factor here and is dealt with similarly as explained above. The data shows that the ice accumulation is a few percent of the aircraft, which contributes to increasing lift requirements. The thrust requirements is also increased, but indirectly through the drag increase of the performance degradation, due to a change in shape rather than a consequence of increased mass. At first glance the mass might seem negligible enough, but it can compound energy consumption if left alone for long enough. A detailed account on the bilinear method can be found in the article by Haynes et al. [39]. The methods themselves are not presented in this chapter as the methods are commonly used and can be easily found or in this case the article referenced.

6.3.3 Implementation of IPS energy consumption

The implementation of the IPS energy consumption is divided into two, one for the wing and one for the propeller. As mentioned in the previous chapter, IPS energy consumption is mostly dependent on the outside temperature and less so by MVD and LWC. This makes the IPS energy consumption much more simple to implement than the aerodynamic model as it only depends on one variable, the temperature. This is the case for both the propeller and wing IPS. However, while the energy consumption for the wings are experimentally measured, the propeller is computationally modelled. With what was discussed in the propeller degradation model section, a few safety margin measures have been applied and it is possible that the energy consumption for the propeller IPS can be overestimated. As this is a conservative number, the results will not deliver overly optimistic values. In the future, a more accurate approach would be beneficial, as more accurate values could potentially extend the operational range. The propeller IPS consumption equation for anti-icing is implemented as follows:

$$IPS_{prop}[W] = -10.2T + 102 \tag{27}$$

where T is for air temperature and W is Watts. As mentioned in the previous chapter, due to how sensitive the propeller is to ice, the IPS on the propeller only runs in anti-icing mode. The IPS equations for the wing is divided into anti-icing and de-icing, which respectively is implemented as:

$$IPS_{wing,anti-icing,-5<T<0degC}[kW] = -0.053T + 0.1328 \tag{28}$$

$$IPS_{wing,anti-icing,T<-5degC}[kW] = -0.0146T + 0.3244 \tag{29}$$

$$IPS_{wing,de-icing}[kW] = 0.0021T^2 + 0.00257T + 0.0522 \tag{30}$$

where again T is air temperature and kW is kilowatts. Since these values are time-averaged, after calculating the IPS consumption for a given temperature, it is only required to multiply these values with the time taken in icing condition. In the simulation, the conditions from waypoint to waypoint is assumed constant. Subsequently, each time step is calculated directly for each of these waypoint to waypoint segments. If the segment has icing, then the time will be known, making it easy to calculate the energy used by the IPS. The energy can then be calculated and summed. The anti-icing is divided into two linear equations as this fits the trend better. That is because the equation that is received from trend calculations gives a concave curve. This will inevitably lead back down to zero energy consumption given high enough temperature. Hence, it has been split into two. For de-icing this problem is avoided as the curve that results from the equation is convex and the line generally fits better. By implementing the IPS consumption this way, the upward trend of energy consumption with temperature happens, which is as expected. All data used to find these relationships is supplied by Hann [9].

6.3.4 Implementation of Propeller performance degradation model

For the propeller performance degradation model, a simple linear relationship will be implemented. The details have been mentioned earlier, assuming that no ice shedding occurs as this complicates the process for all cases. It is also only used for when the IPS is disabled scenario because of how fast the propeller degrades. The implementation does not need to be as accurate as it is only for comparison and to see the effect of how not using IPS on the propellers will affect the path. As seen from Figure 19, the curve can be separated into to linear equations, one from -12 degrees and lower and one from -12 degrees and higher. The temperature will be the input and will output the drop in efficiency, which will be multiplied with the thrust equation. The efficiency degradation equations implemented are simple and presented as follows:

$$\eta_{prop,deg} = 0.0033T + 0.3 \tag{31}$$

$$\eta_{prop,deg} = 0.0566T + 0.9709 \tag{32}$$

Here T is temperature and Eq.(31) is the equation for -12 degrees and lower while Eq.(32) is the equation for -12 degrees and higher. As these equations will only be used when icing is detected, there is no need to clamp the temperature when it reaches above 0 degrees, as no icing occurs above this temperature. It is also not necessary to clamp the temperature from below as it will be assumed that temperature measurements will always give reasonable physical temperature. The data used to find these relationships is supplied by Fajt [7].

As a final note, when the IPS is disabled, the icing is essentially continuous throughout the entire route after the UAV encounters the first icing condition. Meaning there will always be degradation after a first encounter with icing as no IPS is available. It is also assumed that no positive temperatures will be encountered for melting to occur. The propeller degradation equation is used during icing condition, but what about when it comes out of icing? This is a much more difficult question to answer as there are many variables to consider afterwards, such as ice shedding. What propeller degradation should be chosen in this case, as the propeller degrades quickly and hence can have a range of values. The solution is to test every 10%, ranging from 50%-90% degradation outside of icing. This effectively explores how propeller degradation affects the algorithm and can grant insight into the behaviour of the code. This range is applied to the energy optimisation. Since this will mostly affect energy consumption, the time optimisation will test fewer cases, the 70% and 90% degradation. You might ask why to not just carry over the degradation from the icing condition. It was considered, but the propeller degradation has quite fast dynamics and can change quickly. By testing a range of values will showcase how propeller degradation can affect the results better. It will also indirectly show the severity of icing on the propellers.

7 Results and Analysis

In this chapter, the results will be divided into two sections, energy and time optimised. The results will then be discussed by comparing the different test scenarios and discussing possible improvements. A discussion when comparing two scenarios is also needed if the results are unexpected, which will be made clear when looking at the results. As will be shown, optimisation for energy and time might not give the same results. The results will focus on using weather data from one day on 14.March 2020, the trip being between Tromsø-Bodø and Bodø-Tromsø. This is not right after each other, and each simulation is made as if they left at the same time from their respective cities.

7.1 Energy Optimised Path

In this section, the energy optimisation will be discussed. A Table over key results will be presented, such as icing times, total energy consumption and energy consumption breakdown for IPS and propeller consumption. These results are important to highlight what is not immediately apparent in the paths simulated. The key parameters will be discussed as they become relevant. The energy cost used by Narum is in Ah, but the energy will be presented in kilo-Watt-hours (kWh) as this unit is less ambiguous. This is because to calculate Ah requires calculating the voltage difference between exponential and nominal voltage. This means that the UAV draws the power at different voltages, which will ultimately change how much Ah is consumed at different operating conditions. This is not repeated in this thesis as kWh is arguably better for comparison. The kWh is better for comparison because it is a unit without ambiguity. It is energy consumed in absolute value and does not require interpretation. Ah is good to use when talking about battery capacity drawn at a constant voltage, but not so much when voltage varies, especially not for comparison sake. The convergence plot will still be in Ah however, as this is what the algorithm is minimizing against for the current iteration of the code. It is also required when comparing against Narums results at the end of the chapter. As mentioned in earlier chapters, the simulation is divided into steps, each with their own power and time. These are multiplied to get energy and converted into kWh manually. In any case, this does make it a bit easier to compare between energy and time optimised scenarios directly.

Table 2: Table over key parameters for different scenarios - Energy Optimisation

Mission	Scenario	Cost (kWh)	IPS Energy Consumption (kWh)	Flight Time (hr:mm:ss)	Icing Time (hr:mm:ss)
Tromsø-Bodø	Combined IPS modes	2.08kWh	0.15kWh	04:20:25	00:33:19
Bodø-Tromsø	Combined IPS modes	1.08kWh	0.05kWh	02:13:57	00:08:36
Tromsø-Bodø	IPS Disabled	2.03kWh	N/A	05:14:42	02:23:56
Bodø-Tromsø	IPS Disabled	1.05kWh	N/A	02:36:08	01:28:07
Tromsø-Bodø	No Icing 2D	1.83kWh	N/A	04:04:15	00:00:00
Bodø-Tromsø	No Icing 2D	0.98kWh	N/A	02:10:41	00:00:00
Tromsø-Bodø	No Icing 3D	1.59kWh	N/A	04:38:36	00:00:00
Bodø-Tromsø	No Icing 3D	0.72kWh	N/A	02:15:04	00:00:00
Tromsø-Bodø	Anti-Icing Only	1.95kWh	0.06kWh	04:17:27	00:06:08
Bodø-Tromsø	Anti-Icing Only	1.11kWh	0.04kWh	02:14:59	00:03:52
Tromsø-Bodø	De-Icing Only	1.98kWh	0.144kWh	03:58:08	00:30:51
Bodø-Tromsø	De-Icing Only	1.05kWh	0.056kWh	02:10:44	00:08:36

Two parameter not presented in the table are airspeed and average flight path altitude. These could be important as the airspeed does determine how much power to consume from the engine at anytime. However, there are too many other parameters that can affect energy consumption in combination with airspeed. For example, it is possible for the UAV to fly at a higher airspeed having clean wings and have less energy consumption than at slower speeds, but have iced wings. Wind speed is also part of airspeed, which with tailwind means that the UAV is currently drawing less power, or with headwind is drawing more power for the same airspeed. It is too difficult to really determine how airspeed affect energy consumption as it depends on the drag (which is dependent on icing and AoA) and wind speeds. Airspeed is simply not representative in terms of determining energy consumption without having every parameter accompanying this information. Because of these reasons, flight time is also not a good indicator for energy consumption. The UAV velocity simply have too much dependencies that can affect it both as an advantage and disadvantage, making it an unreliable indicator. As for the average flight path altitude, it is in some cases important because altitude is a factor for air density. As can be seen in Eq. 21, the drag depends on the air density and as altitude is increased it decreases, leading to lower drag. The difference in a few hundred meters does however not change density significantly. Hence, the average flight path altitude is also not included in the table. Temperature is also a factor in air density, but since it is on the same route, the temperature can mostly be assumed to be similar along the route. It might be colder at higher altitude giving denser air, but pressure also decreases with altitude and hence mostly cancels each other out. This relation can be estimated using the ideal gas equation where all of these parameters are proportional to each other [22].

7.1.1 Tests with IPS Disabled

To make this clear, when it is stated no IPS, it means that the IPS is disabled and hence not used for these test runs. This is to showcase the benefits of implementing IPS to the UAV.

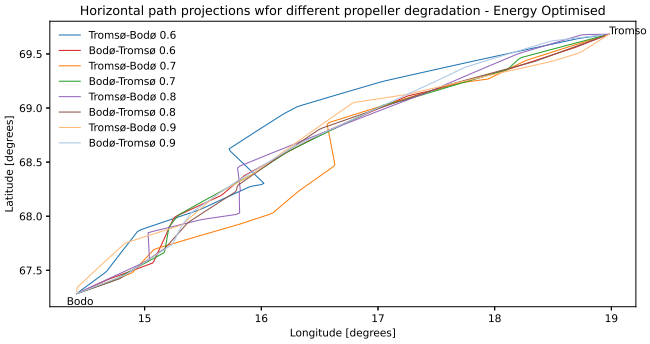

(a) Horizontal Path Projection disabling IPS

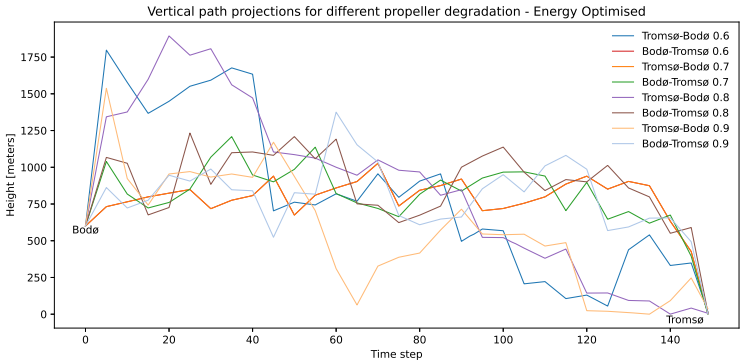

(b) Vertical Path Projection disabling IPS

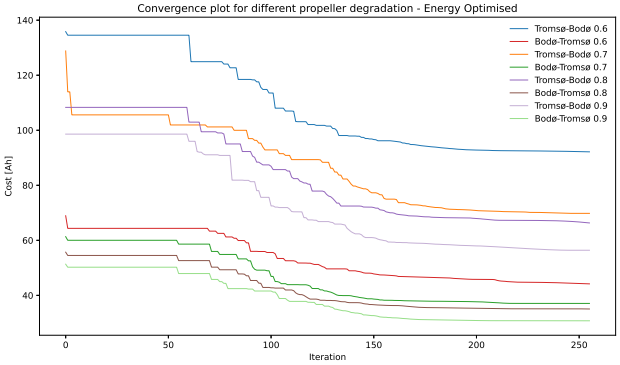

(c) Cost Convergence Plot disabling IPS

Figure 26: IPS disabled results - Energy Optimisation

Figure 26 show path projections and cost convergence plots for Tromsø-Bodø and Bodø-Tromsø flights when IPS is disabled. There are quite a few differences just by which route is taken This can easily be observed in Figure 26a on horizontal path projections and Figure 26b on vertical path projections. There are quite a few reasons for this with the main one being that the UAV experience the wind differently due to its relative path. As mentioned in earlier chapters, wind can account for as much as 50% on total airspeed of the UAV. The paths are ultimately quite similar with some exceptions. It basically comes down to taking advantage of winds, avoiding icing, or even going through icing as the winds are more favourable. There is a number of information that can be extracted from these plots. The horizontal path is taking advantage of favourable conditions It can also be used to compare ground distance covered between the different scenarios. Ground distance is also not representative of flight time nor energy consumption as this depends on the weather condition the UAV takes.

From the cost convergence plot, which in this case tracks energy consumption in Ampere-hours (Ah), the Bodø-Tromsø route consumes a lot less energy. This could, for example, be because it got more favorable wind in form of tailwind, while the opposite occurs for Tromsø-Bodø (more headwind). The difference can also be seen when comparing flight times in Table 2, where the Tromsø-Bodø almost has double the flight time compared to Bodø-Tromsø for all test scenarios. It is important to note that the initial no IPS test scenario consistently gave less energy consumption compared to the other scenarios as seen in 2. Explanations on why this happened is known and changes were made to the algorithm to deal with this inconsistency. The updated results will be presented with explanations next. This fixes the same issue that Narum encountered and will no longer be an issue for future simulations.

The problem was pinned on one particular issue. Because the algorithm is based on a waypoint

to waypoint system, with each containing their own icing condition and icing exposure time, the algorithm resets the ice accumulation between each waypoint and hence does not reflect ice accumulation correctly. This especially bad when there is back to back icing between several waypoints. The icing times should then be added between these waypoints, but instead this resets and icing is not as severe as it should be. Another issue identified, is that the icing condition between these waypoints could differ widely in terms of MVD and temperature, yielding a highly nonlinear mixed ice accretion. Data on mixed ice accretion from two different icing conditions are not available and is difficult to model. Hence, the current solution is to assume that every new icing condition, it resets the icing to that particular condition with the accumulated icing time. This potentially yields a drastic change in drag values and is not completely accurate. However, given the lack of data on combined ice accretion for different icing conditions it is the best solution available. In the best case scenario, the energy consumption will average out, as the drag would sometimes be higher than it should be and vice versa. For future work, an icing severity index should be implemented as to be able to model this nonlinear ice accretion more accurately. This icing severity index is not implemented here as it is outside the scope of this thesis. Additionally, the ice mass accumulation should also be higher, which would then require a higher AoA which again yields higher drag. It is also hard to really get a good grasp on the icing severity if, for example, between waypoints, the air temperature went positive, how much would the ice melt? Would the exposure to positive temperatures be long enough for the ice to melt? These are some questions that needs to be addressed. If the UAV is kept below freezing, the ice will not melt, but lead to more ice build-up on the UAV. This is especially true for glaze ice, because as mentioned earlier, glaze ice will have a water surface of certain thickness. As it gets exposed longer to freezing temperatures, more will freeze and change the geometry of the ice, leading to an increase in drag. In fact, as an IPS is not available to remove the ice, the ice should never disappear, only be kept constant or continuously accumulating. Hence, any ice the UAV accumulates, will most likely last for the entire trip. As for conditions with positive temperature, it is mostly a question of dynamics of icing. At colder weather conditions, these positive temperatures will be unlikely and probably be negligible if it does occur, such as flying close to a volcano. However, the volcano scenario yields other problems which is out of the scope of this thesis. If positive temperature pockets does occur to have an effect on melting the ice, it will most likely be close to the freezing point where glaze ice occurs. Once out of the hot pocket of air, will ultimately make the process even more complex, with the melting and refreezing to glaze ice, potentially making even more complex shapes. This is also out of scope of this thesis.

This continuous ice accumulation problem only applies when testing for this exact scenario. When IPS is used, the icing is assumed to reset as the IPS takes care of the ice from one waypoint to the next. The ice accretion can then also be assumed linear because the algorithm assumes that there is no ice at the start of each waypoint. The problem is then only connected to the no IPS case. To deal with this problem, several measures were taken in the code to try to make the simulation closer to real life. First, the icing time is considered accumulative throughout the flight. Even though the UAV is not in icing condition all the time, the water layers at lower temperatures will freeze continuously throughout the flight, degrading performance further. Ice mass is also assumed to increase at this time as the water layer is not represented in the code. However, during testing, the factor that affected the UAV the most is how much the propeller is degraded after flying through icing conditions. As mentioned in chapter 4, the propeller degradation is sporadic due to cyclical ice shedding (due to vibrations), the ice integrity and steady-state ice accretion. These are all unknown factors in the algorithm and data was unfortunately not available to model and simulate properly. Instead, a series of propeller degradation values were chosen to see how different values change the overall results as mentioned in chapter 6. The icing on the propeller should get worse with time as more ice accumulates. However, due to propeller ice shedding as a a consequence of vibration of the propellers, there should be a lower bound. It would be difficult to model this process of continuous ice accumulation, followed by ice shedding restarting the process. It is important to note that when ice shedding occurs, only the outermost layers would shed and hence some degradation would always be present after the UAV has encountered icing. This is also reflected in the algorithm, where the degradation only starts after a first encounter with icing. The assumption that only the outermost ice layer is shed from the propeller is because it is as-

sumed that the ice layer close to the propeller has a larger adhesive force. Otherwise the ice would manage to shed fully from the propeller before the critical point was reached. It would diminish the usefulness of the IPS if the propeller could manually shed itself from ice, as it would possess natural de-icing properties. This is known to not be the case and hence some ice would always remain. Data on accurate ice accumulation on the propeller is currently not available. Hence a constant degradation is assumed when the UAV is not in icing conditions, as there should be some degradation at all times when the IPS is disabled. When the UAV is in icing, the degradation will follow the degradation equation as implemented in chapter 6. It is only during icing the degradation changes, while it is kept constant otherwise. It is not known what constant degradation should be chosen and hence it is tested for a range of values.

The values ranges from 50-90 % propeller degradation, and the lower the value, the higher the energy consumption because degradation factor is divided by the power. The percentages given here are for how much the power needs to be increased to give a certain thrust. The lower bound set here at 50% is due to the algorithm failing to give a solution at this value. This is most likely because the UAV is not able to draw the required power at this degradation. For example the UAV exceeded the upper voltage rating of the batteries. It was not attributed to battery capacity as capacity was not close to being reached at 60% propeller degradation. The upper bound was chosen to be 90%, as 100% (no degradation) is unlikely when icing is present. As the algorithm fails at 50%, 60% is the most conservative value. To clarify, when we say 60%, it means the propeller has degraded by 40%, while when we say 90% the propeller has only degraded by 10%. This is as mentioned in chapter 3. With these changes the updated results now shows more consistent values as shown in Table 3. In the bare minimum cases when the IPS is disabled, the propeller degradation should be set at 90%, as the minimum degradation. The results become consistent just by setting it to this minimum degradation. The degradation can be set higher, if higher safety margins is required to a particular mission. If the icing severity is known in advance, the degradation can be chosen as appropriate.

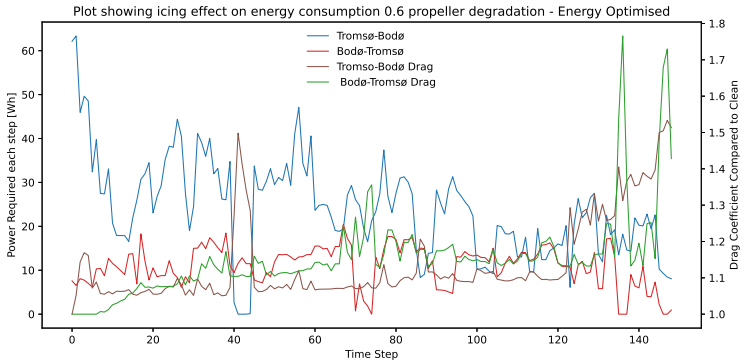

(a) Propeller Degradation 0.6

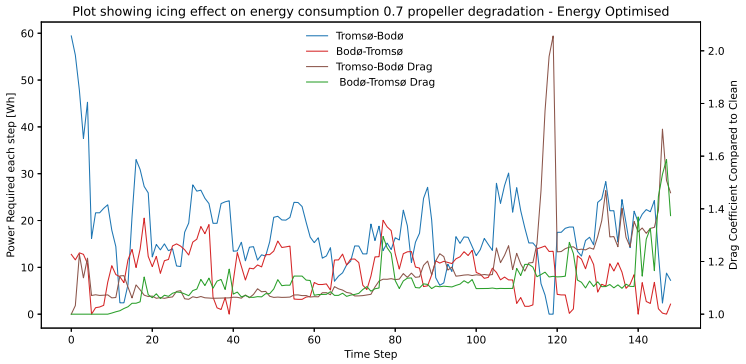

(b) Propeller Degradation 0.7

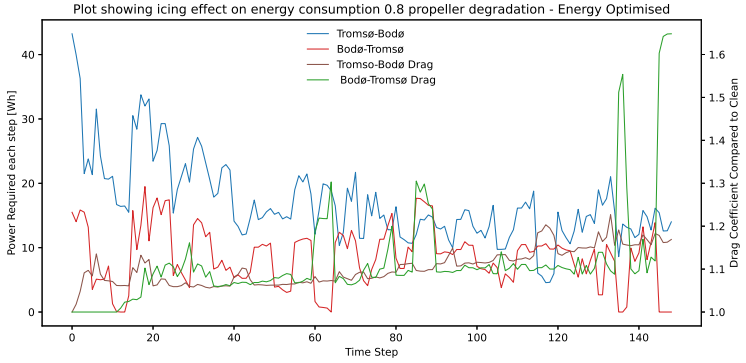

(c) Propeller Degradation 0.8

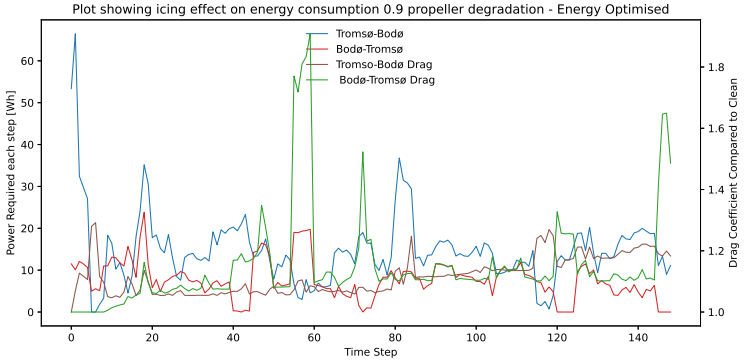

(d) Propeller Degradation 0.9

Figure 27: Comparing Icing Effect with Different Degrees of Propeller Degradation - Energy Optimisation

Table 3: Table over updated results when IPS is disabled - Energy Optimisation

Mission	**Propeller Degradation (%)**	**Cost (kWh)**	**Propeller Consumption due to Icing (kWh)**	**Flight Time (hr:mm:ss)**	**Icing Time (hr:mm:ss)**
Tromsø-Bodø	90%	2.20kWh	0.216kWh	04:18:56	00:13:40
Tromsø-Bodø	80%	2.52kWh	0.22kWh	04:21:27	00:09:28
Tromsø-Bodø	70%	2.68kWh	0.332kWh	04:08:20	00:22:43
Tromsø-Bodø	60%	3.57kWh	0.35kWh	04:48:49	00:31:55
Bodø-Tromsø	90%	1.15kWh	0.14kWh	02:11:27	00:09:30
Bodø-Tromsø	80%	1.27kWh	0.11kWh	02:12:12	00:10:42
Bodø-Tromsø	70%	1.37kWh	0.123kWh	02:10:27	00:16:32
Bodø-Tromsø	60%	1.64kWh	0.192kWh	02:12:32	00:15:24

Table 3 shows three things. First, it shows how different propeller degradation will affect the energy consumption of the UAV. Second, it now shows icing times that are more consistent. Lastly, it shows how much icing affects the propeller consumption. When comparing the icing time of Table 2 and 3 the difference is obvious. Now that the penalty of encountering icing is high enough,

the algorithm will do its best to avoid icing. Hence, the longest duration of icing is 30 minutes rather than almost half the duration of the flight. Icing time is highest for the largest penalty of 60% because, paradoxically, the penalty is already so high as to give the algorithm more options by going into icing conditions which effectively grants lower degradation. It can also be observed that as the degradation factor approaches no degradation, the energy consumption approaches the other scenarios as expected. The flight time also varies and is not linear with regards to the degradation. The UAV has the longest flight time for 60% degradation, but the flight time does not necessarily decrease with less degradation. The only result that should matter in this case is that cost decreases with less degradation, which it does. Every case in Table 3 have the changes implemented, which shows that the propeller degradation play the largest role when it comes to performance degradation. The question on the effects of wing degradation does come up with this in mind. It could simply be that wing requires much more severe icing to be affected compared to the propeller and it does show the importance of at least having a propeller IPS implemented. This is true by experience, as the propeller degrades quicker than the wings, as mentioned in earlier chapters, by having the most important task of generating thrust. One thing to keep in mind when testing for different propeller degradation as in Table 2, is that the usage of these values might not be entirely accurate. It is only to highlight the importance of modelling propeller degradation properly when testing for no IPS. Any of these values could be correct, as the propeller degrades quickly (within a minute) as mentioned in the propeller section of chapter 3. It depends on how the ice accumulates at this minute. Lastly, Figure 27 shows how icing affects propeller energy consumption at every time step for different propeller degradation. An interesting observation is how drag is not always increasing, which is a consequence of the resetting of ice condition as mentioned earlier. In some cases the icing will be worse, in other cases it will be lower. The plot is a good indicator of when the UAV is flying in similar or different icing conditions, but only for when the IPS is disabled. The left y-axis shows the energy consumption at a particular step, while the right y-axis shows drag increase. In this plot, 1 is the baseline clean drag coefficient and the plot shows correctly for the drag plots that it is never 1 after the UAV encounters icing. Any other number, for example 1.5 in the plot, means that there is a 50% increase in energy consumption due to icing. Figure 27 gives a general idea on how drag affects energy consumption at each step, but also where icing occurs and its severity for non IPS disabled scenarios. There is a lot of information in these plots that can be extracted from it. The overall propeller energy consumption due to icing is presented in Table 3, which is as expected, highest for the IPS disabled scenario. It does not present IPS consumption, as obviously, IPS is disabled.

For future work, it would be beneficial to be able to detect propeller icing severity, which then gives the propeller degradation. However, since propeller IPS is available, it is not a priority as it would only be used for the IPS disabled case. During the modification of the code, tests were made to compare whether the wings or propeller degradation had the most impact. The propeller was shown to be the most impactful and if IPS is available for both wings and propeller, propeller should always get priority if the battery is low. The consequences of propeller degradation is just too severe. This includes increased energy consumption from ice, but also affects the system overall with vibrations that could affect safety. It just shows how important it is compare cases with and without IPS to fully showcase the benefits. A final point to make, is how much effort should be put into modelling the scenario with IPS is disabled. It is a reference case to highlight how important the IPS is for the UAV. This scenario will showcase the benefit of IPS the more accurate the model becomes, but with diminishing returns. The most intensive work will be in modelling the nonlinear ice shapes, but might not be worth doing as it will require considerable amount of resources. The results shown here is arguably enough to showcase the benefits of the IPS. Whether any additional modelling is worth it is something to determine in the future.

7.1.2 Comparison between Using Anti-icing Only and De-icing Only

Figure 28 show path projections, cost convergence and propeller energy consumption due to icing plots when testing for anti-ice only mode and de-ice only mode respectively. When comparing anti-icing and de-icing run between Tromsø-Bodø, it is possible to see that the icing time for de-icing only in Table 2 is much higher compared to anti-icing only, which leads to a higher IPS energy

consumption. De-icing only still comes quite close to anti-icing only scenario due to its flight time being significantly lower than anti-icing only. It makes sense that icing exposure is higher for de-icing compared to anti-icing, due to de-icing having lower IPS power consumption, but with a penalty having icing and performance degradation. When comparing the Bodø-Tromsø route for example, energy consumption is now less for de-icing only scenario. Flight time is relatively close with a few minutes difference for the same routes. One reason that can affect results and influence how "adventurous" the PSO decides to be, is the default route implemented by Narum [5]. This default route influences how far away the PSO should explore and in most cases chooses not to explore too far if not absolutely necessary. This is a disadvantage with the algorithm and can potentially lead to better solutions being avoided. However, this is something Tiller [17] has found a solution to when overhauling the code and should not be a problem for future simulations. The implemented solution is to randomize this default path, forcing the algorithm to explore more. In any case, this difference is enough to influence the results the other way. This reinforces that anti-icing and de-icing have their respective strengths and weaknesses. The Bodø-Tromsø route for de-icing might penalize icing condition less, allowing it to move through a quicker route, while there is a higher penalty for anti-icing when it comes to icing. A conclusion that can be drawn is that the algorithm can be sensitive.

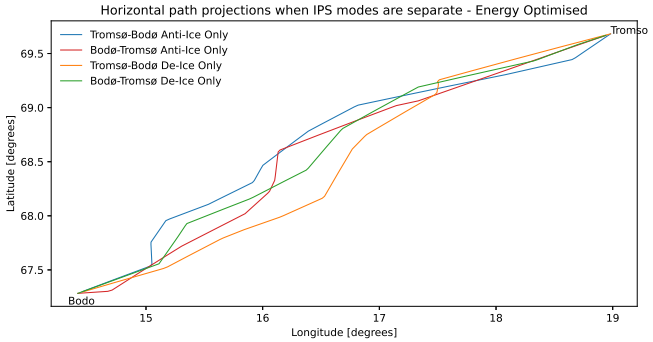

(a) Horizontal Path Projection comparing Anti-Ice only and De-Ice only

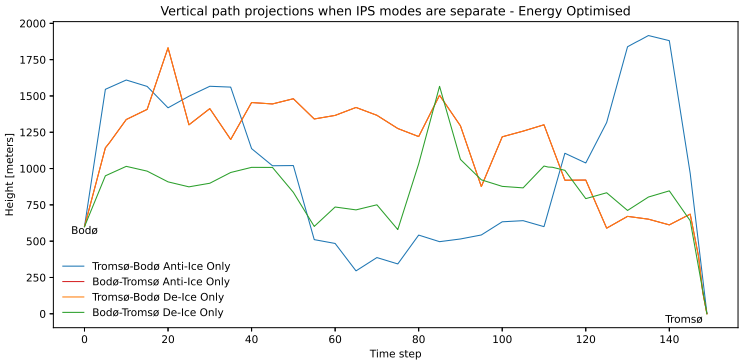

(b) Vertical Path Projection comparing Anti-Ice only and De-Ice only

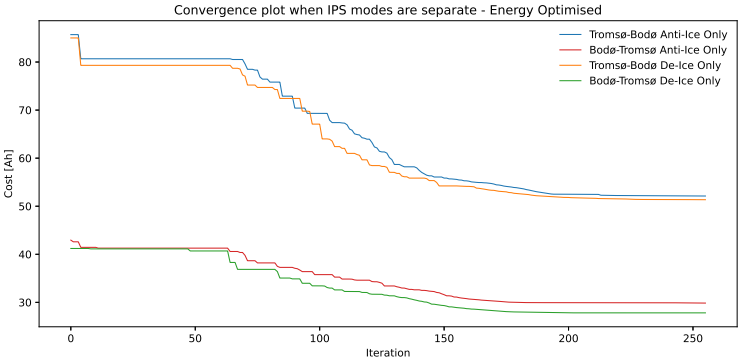

(c) Cost Convergence Plot Comparison between Anti-Ice only and De-Ice only

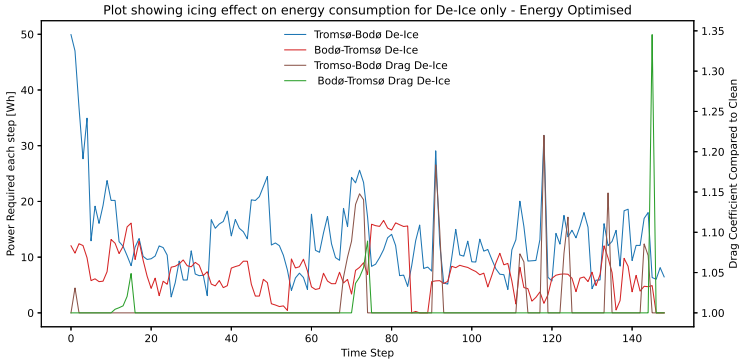

(d) Propeller consumption due to icing for De-Icing Only

Figure 28: Anti-Ice only and De-ice only test results - Energy Optimisation

Table 4: Table over Energy Consumption breakdown when IPS modes are used separately - Energy Optimisation

Mission	Scenario	Cost (kWh)	Propeller Consumption due to Icing (kWh)	IPS Consumption (kWh)
Tromsø-Bodø	Anti-Icing Only	1.95kWh	0kWh	0.06kWh
Bodø-Tromsø	Anti-Icing Only	1.11kWh	0kWh	0.04kWh
Tromsø-Bodø	De-Icing Only	1.98kWh	0.022kWh	0.144kWh
Bodø-Tromsø	De-Icing Only	1.05kWh	0.002kWh	0.056kWh

The horizontal path projection is mostly not interesting. It shows how the UAV manoeuvres in terms of either taking advantage of the highest tailwind, avoiding strong headwinds or icing to minimize energy consumption. This is why the path taken in all horizontal path projection plots such as Figure 28a is rarely the straight path. This is no mistake but by design. It would be possible to showcase how the wind is distributed in these figures such as Figure 25, but as mentioned earlier, it would only show wind for one particular altitude. This would not be particularly representative just by seeing Figure 28b for how often the UAV changes altitude. Hence, it would be beneficial to graph a 3D plot that show the wind distribution over the path for future work. A plot of this nature would contain a lot of information and due to time constraint, would take too much time in finding a good solution to condense this information. The horizontal wind distribution would in most cases be sufficient when presenting this information due to the tailwind/headwind argument. Vertical winds would be beneficial in reducing AoA for climbs. However, in the weather conditions that the UAV is tested in (cold weather), updrafts would be rare as updrafts is generated by warm air rising from the ground as the ground and hence air is being heated by the sun. If the ground is heated enough by the sun, the overall temperature would most likely be too high for icing to occur. Hence, it is assumed that vertical winds is relatively negligible compared to horizontal winds. The vertical path projection gives average flight path altitude information, which can attribute some of the smaller energy consumption differences presented.

The convergence plot shown in Figure 28c shows iterations of how cost reduces as the PSO finds better solutions. It can be observed that by 100 iterations for this scenario the plot is already converging. This is because the algorithm is set up such that the simulation scales with the number of iterations. For the PSO to be able to converge in the end, the PSO needs to explore less and less and hence closer and closer to the current best solution. Hence, it is still not possible to tell if it is a global minimum as the algorithm restricts itself early and not every possibility is explored. When comparing the icing exposure times for anti-icing and de-icing only scenarios, it seems like it is optimal to minimize icing as much as possible. With the exception of Tromsø-Bodø de-icing scenario, the icing times are less than 10 minutes. It is hard to identify any advantage from using anti-icing or de-icing only when it comes to optimising energy consumption. However, as will be shown later, it is not in energy optimisation where this comparison pays off, but rather in the time optimisation.

7.1.3 Using a Combination of Anti-icing and De-icing

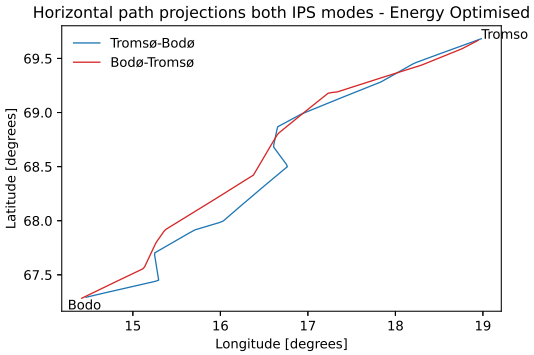

(a) Horizontal Path Projection-Both IPS modes

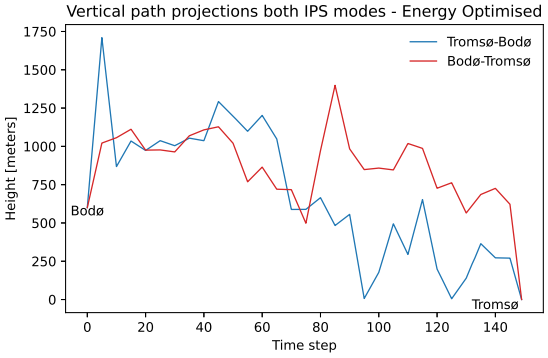

(b) Vertical Path Projection-Both IPS modes

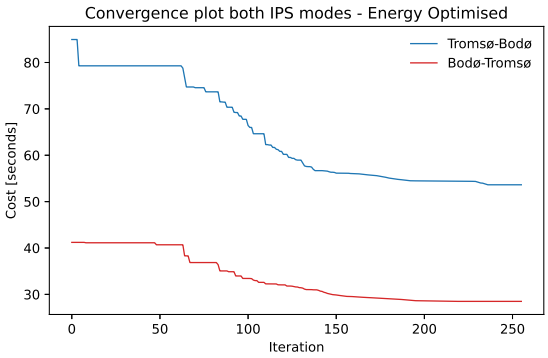

(c) Cost Convergence Plot-Both IPS modes

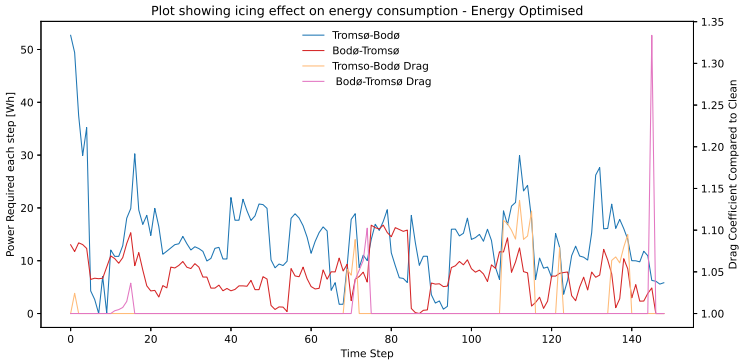

(d) Propeller Consumption due to Icing

Figure 29: Combined IPS mode results - Energy Optimisation

The combined IPS mode scenario where the algorithm decides which mode to use based upon whichever mode consumes the least energy at each waypoint is presented here. For energy optimised scenarios, the combined IPS modes does not produce any large differences between using only one of the IPS modes only. In fact, the Bodø-Tromsø combined IPS and De-icing only is almost exactly the same, which indicates that de-icing is indeed best for this route. Tromsø-Bodø has higher icing time at 33 minutes, but still being on par with energy consumed with other IPS scenarios. The combined IPS scenario is inbetween anti-ice and de-ice only scenario in terms of IPS energy consumption. By using a combination of anti-icing and de-icing, it looks like the UAV is able to take more chances as it can use the best mode possible for each situation. The current results show that the Tromsø-Bodø route is higher of the three IPS scenarios, while the Bodø-Tromsø route is in the middle, which is not really what you would expect. The flight time and IPS energy consumption is higher than for de-icing only. The energy consumption is, however, close enough to each other that the results can be attributed to the randomness of the PSO algorithm.

Table 5: Table over Energy Consumption breakdown with combined IPS modes - Energy Optimisation

Mission	**Cost (kWh)**	**Propeller Consumption due to Icing (kWh)**	**IPS Consumption (kWh)**
Tromsø-Bodø	2.08kWh	0.0164kWh	0.15kWh
Bodø-Tromsø	1.08kWh	0.0012kWh	0.05kWh

7.1.4 Comparison between Using Clean 2D and 3D Aerodynamic Performance Data

For the 2D and 3D comparison tests, when no icing is stated, means that icing is ignored in the simulation. Since only clean 3D data is available, a variable that checks for whether or not icing is tested is implemented. Hence, for these particular runs, the algorithm pretends that icing does not exist to be able to compare the two datasets.

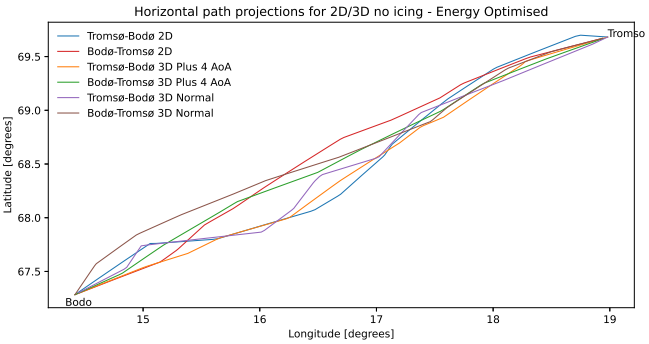

(a) Horizontal Path Projection - 2D/3D

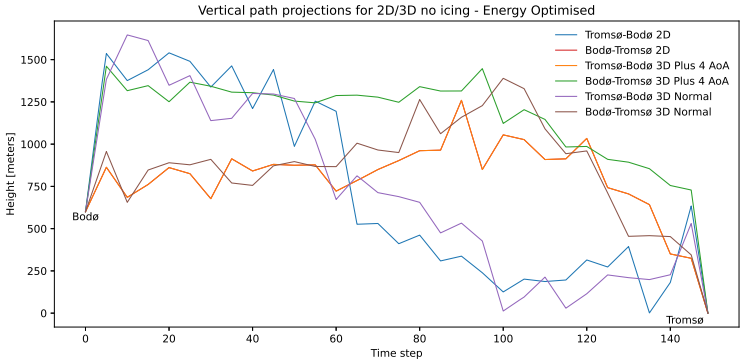

(b) Vertical Path Projection - 2D/3D

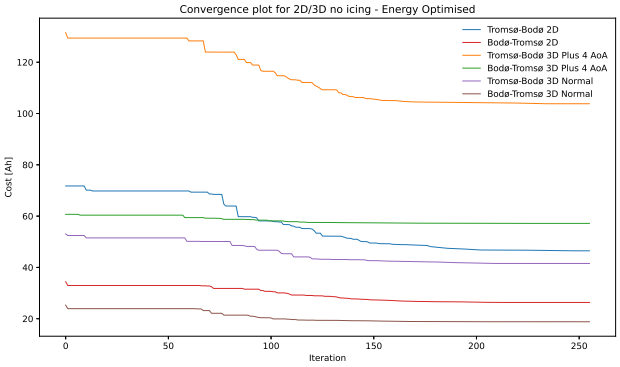

(c) Cost Convergence Plot - 2D/3D

Figure 30: 2D/3D No Icing results - Energy Optimisation

This section compares the usage of 2D and 3D data and to look at the viability of using 2D data over the more realistic 3D data. As presented in the section for 2D and 3D data, the drag of 3D data is higher by a much larger margin. However, Table 2 shows that 3D tests gives consistently lower costs than 2D tests. There is an explanation for this inconsistency and some readjustments were required to deal with this problem. In examining the code, there is one equation that can change the power:

$$T = D + W \sin\left(\gamma_a + (AoA * \frac{\pi}{180})\right) \tag{33}$$

Here T is thrust, D is drag force, W is weight, $_a$ is air flight path angle and AoA is angle of attack. The fraction at the end of the equation is conversion from degrees to radians. Although drag in the 3D case is higher for all angles, the operating AoA is much lower for the 3D case than 2D. While for the 2D case the operating AoA is around 3 degrees, the operating range for the 3D case is around 0 degrees. It is possible that this can lead to the second term being negative, subtracting from required thrust and hence, power consumption becomes less. Looking at the raw data for the 2D and 3D case, this indeed seem to be the case as the power required for each step is mostly lower. There are a few steps where the power required is higher, but this is in the minority, leading to the 2D case to calculate a higher energy cost. The 3D data is as mentioned in earlier chapters

not from physical experiments, but from computational fluid dynamics. A mistake was identified when comparing between the CFD modelled aircraft and the PX-31, is that the wings of the PX-31 is manufactured with a negative incidence of -4 degrees. This was not taken into account in the CFD model and hence the data and the lift curve is slightly wrong. It has been confirmed by the manufacturers that the data supplied by Hann is close to the PX-31 values, with the exception of the AoA values. It is also confirmed by the manufacturers that the UAV operates at cruise AoA values of 0-2 degrees, relative to the wing incidence angle and the air streamline. Hence, the PX-31 operates at an AoA of 4-6 degrees. By adding 4 degrees to the AoA values supplied by Hann, while keeping the corresponding lift values and rerunning the algorithm, now gave expected results. This should not be a problem since we only look at the data with regards to the wing. The wing with the same airfoil will still give the same lift characteristic. As mentioned in earlier chapters, the wing is the main lift generating surface, whereas the fuselage only contributes minimally. It is still possible that just adding 4 degrees will yield some discrepancies in the data. This is because by modelling in 3D, the lift characteristic curve might not be the same at 0 degree incidence or 4 degree incidence when using CFD. This is just how sensitive the CFD can be sometimes. Whether or not this is the case, is however, unknown. We can only assume that by adding plus 4 degrees to the AoA that the 3D effects between 0 and 4 degrees will not be changed significantly. We essentially approximate that similar lift coefficient values will be achieved. Given the circumstances it was the best solution as rerunning the CFD simulation was not possible with the time remaining, as mentioned in earlier chapters, the data was provided externally by Hann [1]. Although the PX-31 operate between 0-2 degrees at cruise conditions, the computed 3D lift coefficient deviates the closer to stall we get. Hence, it was chosen to add the lower bound instead of the upper bound of AoAs. By adding 4 degrees instead of 6 degrees, the reference aircraft in the simulation operates somewhere between 2-3 degrees AoA. This is similar to the AoA operating conditions of the 2D data. Hence, when the thrust equation is used, the same amount will be added or subtracted in the equation. This makes it more comparable in terms of comparing the two datasets directly.

The updated results now almost gives the exact ratio between the drag of the 2D and 3D for the energy consumed as can be seen in the updated results in Table 6. It shows just how much 3D effects can affect the performance of the UAV. With that in mind, is it justified to use 2D data instead of 3D data for the simulation? It does depend on the application, but in most cases, the design process with simulations does not represent real life a hundred percent. In most modelling and simulation cases, it is enough to have the dynamics correct and accounting for the largest forces that can lead to failure. In this case, the UAV requires having enough battery capacity to account for the increase in drag and hence energy consumption. The algorithm show that the battery capacity should most likely be more than double than the 2D consumption. The design flight range is however something that is designed for and should be taken into account at that stage. As presented in chapter 3, the PX-31 has a maximum estimated flight time of 10-13 hours, presumably for clean condition as nothing else has been stated in brochures. The aircraft is also designed with 3D data, which is very close to the data provided by Hann. The maximum flight time duration of a clean run should then be close to 10-13 hours in the simulations as well. The maximum flight time between Tromsø-Bodø is less than half of this, so it should not be a problem to use 2D in this case. However, caution is required when flight times approach maximum flight time and realistically much lower when icing is present. 2D data stops being viable for this condition and should be stopped at 10 hours or less depending on desired safety margins. This will require further exploration, particularly with 3D icing data, which is not currently available. This also shows that the problem was connected to the thrust equation. It shows the importance of getting the AoA correctly and is a part of the design process of aircrafts, as 3D effects needs to taken into consideration.

Figure 30 show quite varied path projections, with some scenarios having a longer ground distance by inspection of the horizontal path projection. However, there is not much else that can be concluded from these plots. The convergence plot has an interesting curve for the Bodø-Tromsø route with plus 4 added AoA, by showing little improvement between iterations. There is not anything wrong with this, as it could simply result from the algorithm starting close to the optimal solution.

Table 6: Table over updated results for 2D/3D tests - Energy Optimisation

Mission	**Scenario**	**Cost (kWh)**	**Flight Time (hr:mm:ss)**
Tromsø-Bodø	2D No Icing	1.83kWh	04:04:15
Bodø-Tromsø	2D No Icing	0.98kWh	02:10:41
Tromsø-Bodø	3D No Icing Normal	1.59kWh	04:38:36
Bodø-Tromsø	3D No Icing Normal	0.72kWh	02:15:04
Tromsø-Bodø	3D No Icing 4 Degrees Added to AoA	3.94kWh	04:09:21
Bodø-Tromsø	3D No Icing 4 Degrees Added to AoA	2.15kWh	02:16:06

With this ends the discussion on simulations with focus on optimising energy. The next section will discuss and focus on optimising time. This shifts the cost to minimising flight time.

7.2 Time Optimised Path

This section follows in similar manner to the previous section, only this time, the optimisation parameter is time. With that regard, there are some expectations in terms of the results. This means that the algorithm should be less averse to flying through icing if it is indeed the faster path. This sections also opens with a Table of values which will be discussed as the parameter becomes important.

Table 7: Table over key parameters for different scenarios - Time Optimisation

Mission	**Scenario**	**Cost (hr:mm:ss)**	**Energy Cost (kWh)**	**IPS Energy Consumption (kWh)**	**Icing Time (hr:mm:ss)**
Tromsø-Bodø	Combined IPS modes	03:52:33	1.92kWh	0.16kWh	00:30:02
Bodø-Tromsø	Combined IPS modes	01:53:48	1.038kWh	0.09kWh	00:16:21
Tromsø-Bodø	No IPS	04:10:04	1.93kWh	N/A	00:47:24
Bodø-Tromsø	No IPS	01:56:02	1.34kWh	N/A	00:23:21
Tromsø-Bodø	No Icing 2D	03:49:07	1.72kWh	N/A	00:00:00
Bodø-Tromsø	No Icing 2D	01:57:44	1.043kWh	N/A	00:00:00
Tromsø-Bodø	No Icing 3D	03:49:07	1.61kWh	N/A	00:00:00
Bodø-Tromsø	No Icing 3D	01:57:44	1.046kWh	N/A	00:00:00
Tromsø-Bodø	Anti-Icing Only	03:47:41	2.39kWh	0.68kWh	01:11:57
Bodø-Tromsø	Anti-Icing Only	01:56:37	1.25kWh	0.23kWh	00:19:48
Tromsø-Bodø	De-Icing Only	03:51:11	1.95kWh	0.2kWh	00:33:43
Bodø-Tromsø	De-Icing Only	01:56:31	1.23kWh	0.184kWh	00:21:33

A quick glance when comparing the results for energy and time optimisation is that the time optimisation does indeed give reduced flight times for all scenarios compared to the energy optimised tests. This is encouraging as it shows that the algorithm is working in that regard. The icing exposure time is also generally much higher to achieve a faster time, but does oddly enough yield a lower energy consumption than when optimised for energy for some scenarios. The reader might think there is an inconsistency with this, but this might not actually be the case. Although icing exposure is increased and hence an increase in IPS energy consumption follows, the flight time saved can also influence energy consumption to a large degree. The lower energy consumption is mostly for the Tromsø-Bodø route. It is possible that due to headwind and longer flight times, it will lead to more variation in the results, which can potentially yield paths that give lower energy consumption. The randomness of the PSO does open up the possibility to give these results. The difference is small where the consumption is indeed lower when optimised for time. It is also possible that the weather condition yields icing that is not severe enough to give widely different results between the two optimisations. Icing must be more severe as to penalize icing more, which would make the algorithm to explore more to get results that are significantly different. The fact that not all of the scenarios yield lower energy consumption is enough to show that it is not an inconsistency, but it works as intended with the given weather conditions and route. It might also be that optimising for time is in certain cases the optimal solution for both cases.

As shown in the results so far, global minimum is not reached for every case. This can be directly observed between the combined IPS, anti-icing only and de-icing only Tromsø-Bodø route. Despite the combined IPS being more flexible between choosing the best IPS mode, it is the slow-

est of the three scenarios. It does consume the least amount of energy, which is what is expected however. It might be an artifact of the algorithm that yield these results. For example, anti-icing generally penalizes icing more and hence, the algorithm becomes more "adventurous" in trying to find a better solution, which is in fact the case. With the trade-off of using more energy, it explored more and got a better results than the other two IPS scenarios. As we can see from comparing the results of combined IPS and de-icing, the results are quite close to each other. It does make sense because de-icing is generally less energy intensive and hence is less averse to icing. This makes the combined IPS mode be as "adventurous" as de-icing in exploring for better solutions. It is possible that this points to a slightly faulty approach in the code for time optimisation. It is possible that there are elements of energy optimisation in the time optimisation when choosing the best IPS mode to use, and restricts options. The random default route initialization implemented by Tiller [16] should alleviate this issue, as it will be able to explore more solutions without being restricted to another scenarios parameters.

7.2.1 Tests with IPS Disabled

Again to repeat what is stated earlier, when it is stated no IPS, it means that the IPS is disabled and hence not used for these test runs. This is to showcase the benefits of implementing IPS to the UAV.

Table 8: Table over updated results when IPS is disabled - Time Optimisation

Mission	**Propeller Degradation (%)**	**Cost (hr:mm:ss)**	**Energy Cost (kWh)**	**Propeller Consumption due to Icing (kWh)**	**Icing Time (hr:mm:ss)**
Tromsø-Bodø	90%	04:20:14	3.06kWh	0.599kWh	00:24:59
Tromsø-Bodø	70%	04:10:36	3.12kWh	0.79kWh	00:44:34
Bodø-Tromsø	90%	01:57:45	1.5kWh	0.534kWh	00:21:31
Bodø-Tromsø	70%	01:59:26	1.89kWh	0.673kWh	00:14:17

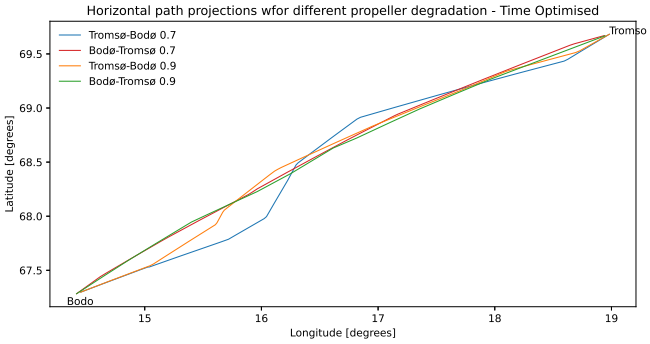

(a) Horizontal Path Projection

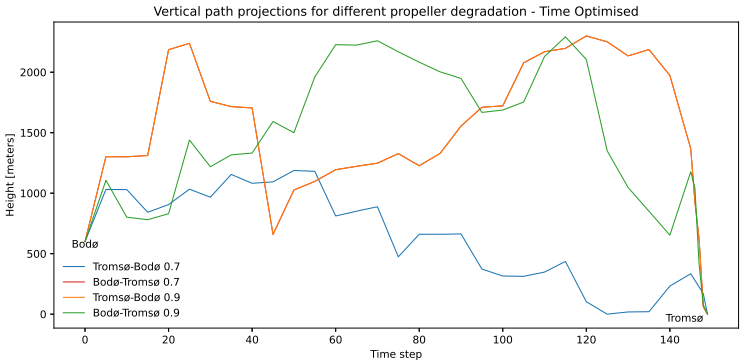

(b) Vertical Path Projection

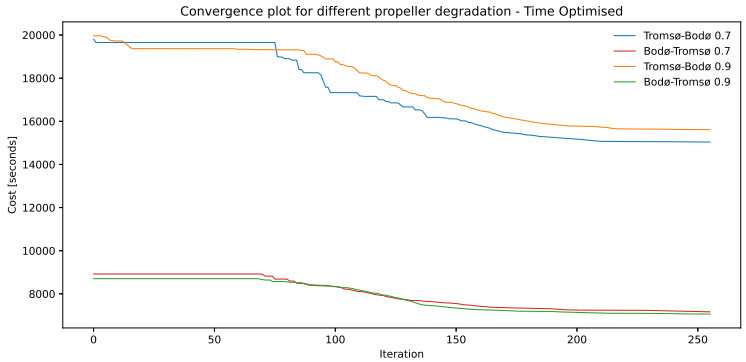

(c) Cost Convergence Plot

Figure 31: IPS disabled results - Time Optimisation

The energy cost is similar to other scenarios, as seen in Table 7. This is is inconsistent as icing should increase energy consumption significantly more now that time is the focus as icing is not as hazardous in the eyes of the algorithm. Although time is the focus in this section, the energy cost still needs to be consistent when comparing with other scenarios. The flight time is longest for the Tromsø-Bodø route as expected without IPS system. The Bodø-Tromsø route is however, the shortest. This is due to the same problems as discussed in the energy optimisation section.

By implementing the same changes as discussed in the energy section, Table 8 now show more consistent values. The Tromsø-Bodø route still has the longest route, but also highest energy consumption with a significant margin as expected. The results are similar for Bodø-Tromsø route by having the highest energy consumption, but while the flight time is still longest, it is quite close to other scenarios. This could simply be because of the significant tailwind helping the UAV get to its destination, showing the benefits of taking advantage of the wind. The propeller consumption due to icing is now higher than the energy optimisation as expected as optimising for time is now the goal. Icing time follows similar trend as for energy optimisation and exhibit quite different icing times for different scenarios. There is nothing particularly wrong with this, as time is again the focus and icing time should not be an indicator for anything unless it is too high. Figure 31 shows path projections and convergence plots. There is no new information that results from this, as horizontal path mostly follows similarly as for energy in general, while being slightly different for vertical path projections. Figure 32 again shows the propeller consumption due to icing. Since the drag plot focuses on increase of propeller energy consumption due to icing, we test for fewer cases for the time optimised cases. We still test for cases with two different degradation values to see how it changes the results. The same information as discussed in the energy section can be drawn from these plots. The drag plot show the main difference between every scenario for both energy and time optimisation. It shows where icing is the most severe, but also that it is worth flying

through to achieve best time. It would be useful to analyze these plots to get some general idea on the weather conditions encountered. However, adding more key parameters in a plot already filled with information will only make it more confusing. The main result of propeller consumption due to icing is presented in Table 8.

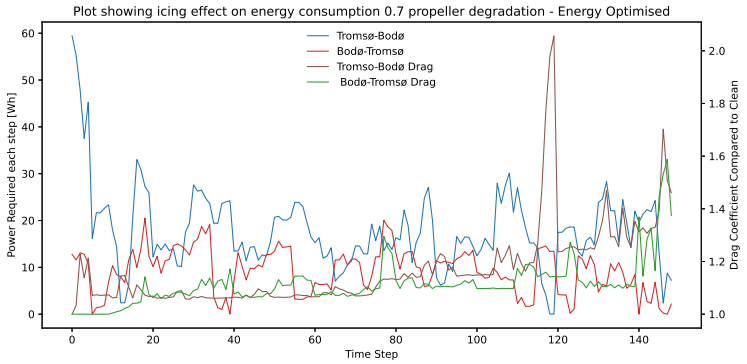

(a) Propeller Degradation 0.7

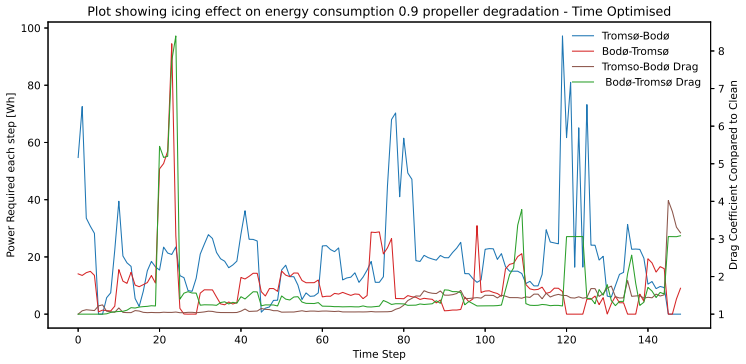

(b) Propeller Degradation 0.9

Figure 32: Comparing Icing Effect with Different Degrees of Propeller Degradation - Time Optimisation

7.2.2 Comparison between Using Anti-icing Only and De-icing Only

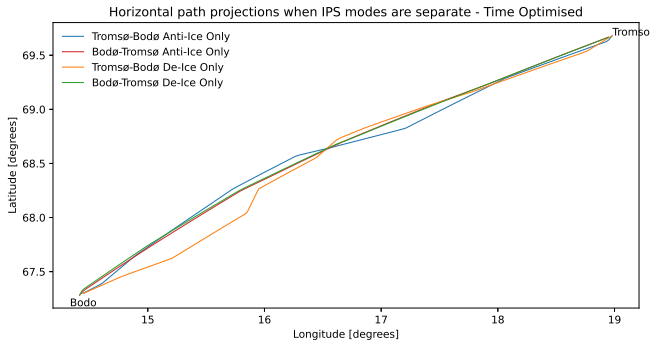

(a) Horizontal Path Projection

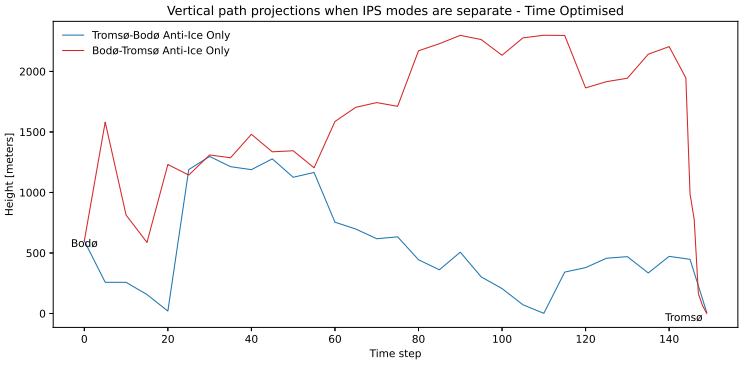

(b) Vertical Path Projection

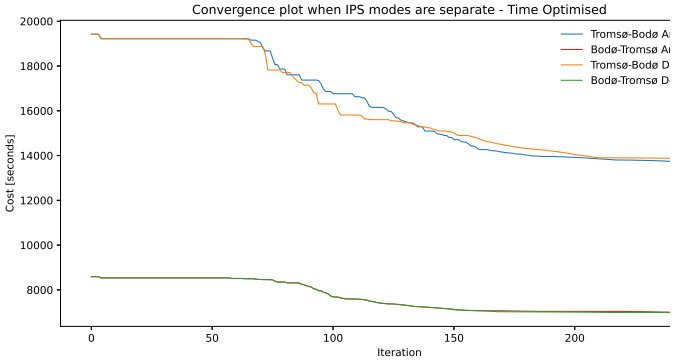

(c) Cost Convergence Plot Comparison between Anti-Ice and De-Ice

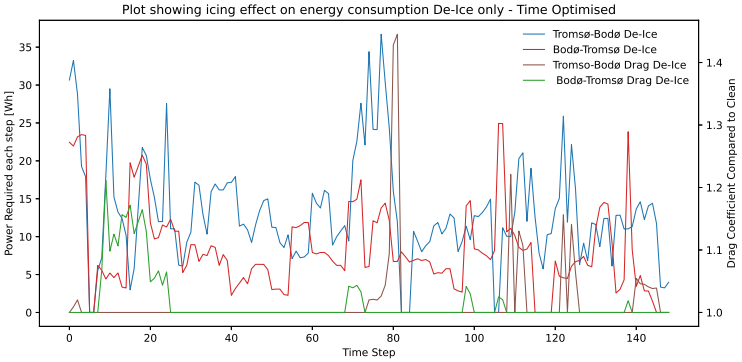

(d) Propeller consumption due to icing for De-Icing Only

Figure 33: Anti-Ice only and De-Ice Only test result comparison - Time Optimisation

In the horizontal projection, Figure 33a and indeed in most of the horizontal path projection for most time scenarios, the path now varies less than for energy optimisation. In fact, the path projection tries to keep as straight as possible, which is, in most cases, is the fastest path. It is only in Figure 34a and the de-ice path in Figure 33a where the algorithm make the most turns in the path. Even then the deviation from the straight path is not big. The results shown in the horizontal path projections here shows why there are more turns in the energy optimisation tests. Since for time optimisation icing is penalised less and having the same weather conditions, the turns made in Figure 26a-30a is to avoid icing. If there are path deviations it is probably to take advantage of wind when optimising for time. Table 9 shows the energy consumption breakdown for these scenarios. All the propeller consumption due to icing is transferred to the IPS consumption for anti-icing only scenario. Even then, the propeller consumption due to icing is quite low as shown for the de-icing case. The anti-icing just goes through every icing condition if it is indeed the faster route.

Table 9: Table over Energy Consumption breakdown when IPS modes are used separately - Time Optimisation

Mission	**Scenario**	**Cost (kWh)**	**Propeller Consumption due to Icing (kWh)**	**IPS Consumption (kWh)**
Tromsø-Bodø	Anti-Icing Only	2.39kWh	0kWh	0.68kWh
Bodø-Tromsø	Anti-Icing Only	1.25kWh	0kWh	0.23kWh
Tromsø-Bodø	De-Icing Only	1.95kWh	0.016kWh	0.2kWh
Bodø-Tromsø	De-Icing Only	1.23kWh	0.014kWh	0.184kWh

Comparing the bottom four entries of Table 7 with the same routes, the results are close. The Bodø-Tromsø route barely inches in the favor of de-icing, while it is much more clearly in the favor of anti-icing for the Tromsø-Bodø route. The Bodø-Tromsø route is as close as it can get in terms of energy cost, which comes down to the difference in IPS energy consumption. It shows very clearly at the same icing conditions that de-icing consumes less energy even with longer icing exposure times for Bodø-Tromsø route. For the Tromsø-Bodø route the results are not as close. Anti-icing with much longer icing times consumes much more energy in general, but manages to be faster, as expected. It could simply be that the wind in the pockets of icing is more favourable and hence the algorithm chooses to use the IPS more. Figure 33d shows much larger variations than in Figure 32, but this is because the IPS for de-icing allows cyclical accumulation and melting. The curve goes up and back down to clean values after each cycle. Anti-icing melts the ice at all times and hence is always at clean wing conditions.

7.2.3 Using a Combination of Anti-icing and De-icing

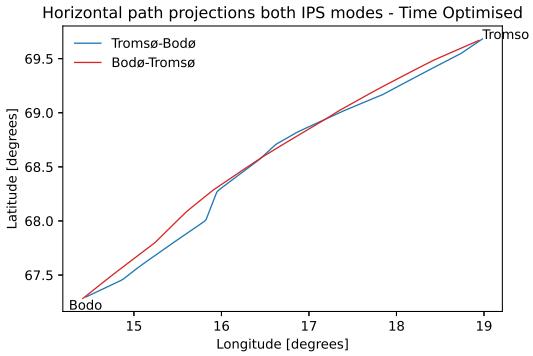

(a) Horizontal Path Projection

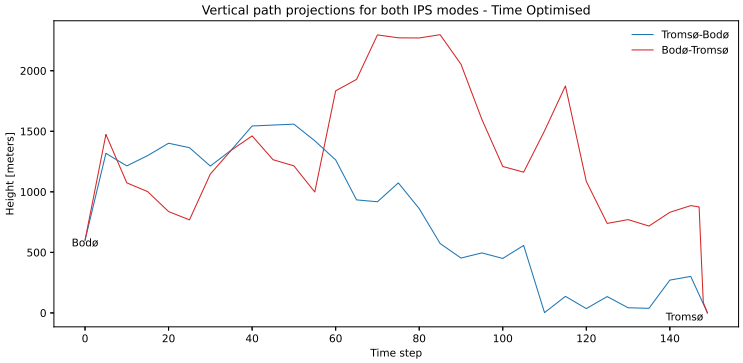

(b) Vertical Path Projection

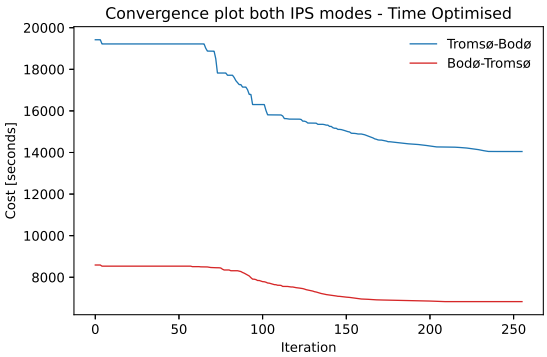

(c) Cost Convergence Plot

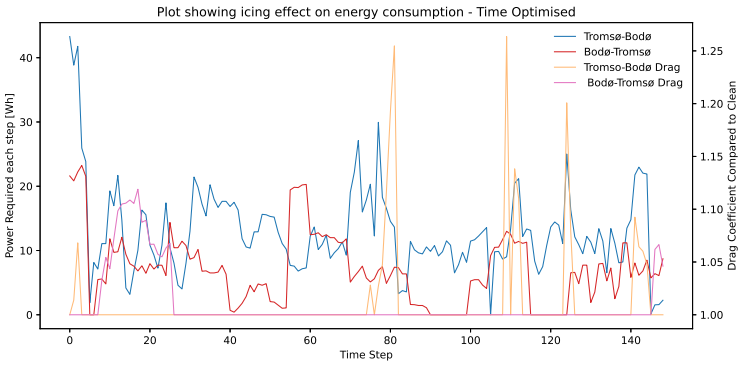

(d) Propeller Consumption due to Icing

Figure 34: Combined IPS mode results - Time Optimisation

The combined IPS mode give the best combination of flight time and energy cost. Although for the Tromsø-Bodø route it is the slowest of the IPS scenarios, it gives the best balance, with lowest energy consumption. For the Bodø-Tromsø route, the time and energy is the lowest out of all scenarios. In conclusion, the combined IPS scenario is the most flexible and should give optimal results in most cases. Table 10 shows the energy breakdown for this scenario. It has similar consumption as de-icing, but having less icing time. Figure 34 again shows the path projection, convergence and propeller consumption plots. There is nothing noteworthy happening and is similar to the other scenarios.

Table 10: Table over Energy Consumption breakdown with combined IPS modes - Time Optimisation

Mission	**Cost (kWh)**	**Propeller Consumption due to Icing (kWh)**	**IPS Consumption (kWh)**
Tromsø-Bodø	1.92kWh	0.0173kWh	0.16kWh
Bodø-Tromsø	1.08kWh	0.006kWh	0.09kWh

Time optimisation does show the potential of the IPS more. Unless remote surveillance is the goal, a quadcopter is much more suitable for idle surveying. It is most likely because conserving energy is much more complex, requiring the algorithm to consider more factors, while for time it just needs to get there fast as possible without draining its power capacity. It is also a lot less

interesting, because it is possible for the algorithm to improve the energy consumption in many ways only to yield small savings, while for time it has more options, simply because just using the IPS consumes energy for the energy optimisation.

7.2.4 Comparison between using Clean 2D and 3D Aerodynamic Performance Data

To repeat what was said earlier, when no icing is stated, means that the algorithm pretends that icing does not exist to be able to compare 2D and 3D data, as only 3D data for clean wings is available.

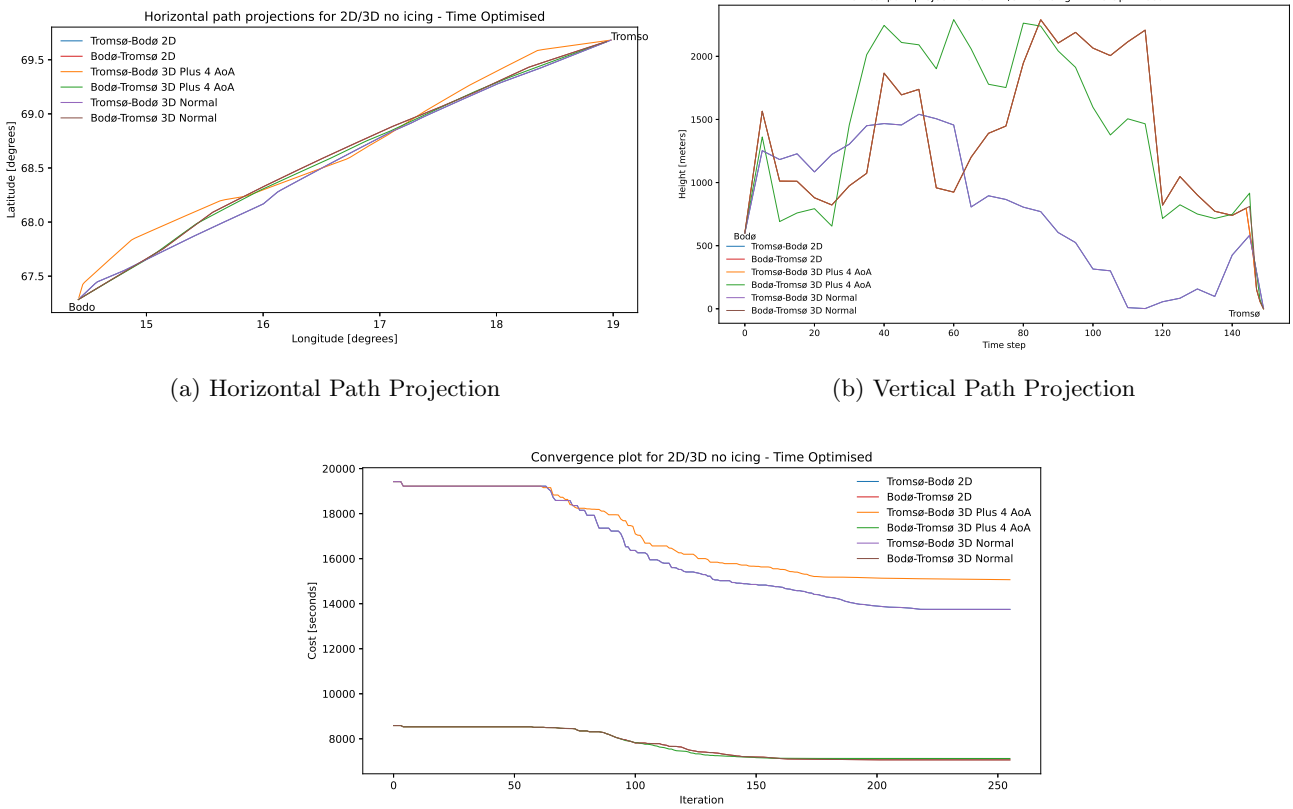

(a) Horizontal Path Projection

(b) Vertical Path Projection

(c) Cost Convergence Plot

Figure 35: 2D/3D No Icing Results Comparison - Time Optimisation

Table 11: Table over updated results for 2D/3D tests - Time Optimisation

Mission	**Scenario**	**Cost (hr:mm:ss)**	**Energy Cost (kWh)**
Tromsø-Bodø	No Icing 2D	03:49:07	1.72kWh
Bodø-Tromsø	No Icing 2D	01:57:44	1.043kWh
Tromsø-Bodø	No Icing 3D	03:49:07	1.61kWh
Bodø-Tromsø	No Icing 3D	01:57:44	1.046kWh
Tromsø-Bodø	3D No Icing 4 Degrees Added to AoA	04:11:07	4.37kWh
Bodø-Tromsø	3D No Icing 4 Degrees Added to AoA	01:58:46	2.37kWh

Similar to the energy section, by adding 4 to the AoA values, the flight time and energy cost now becomes more consistent with the higher drag of the 3D data. Due to increased drag, it takes the Tromsø-Bodø route longer than most scenarios. The Bodø-Tromsø route is still quite similar in time, because of favourable the winds are. In any case, the energy cost is more consistent. As you might have seen, some plots throughout the results have some paths missing. This is because two paths are overlapping, which is also what happens in this case. The route between 2D and unchanged 3D data give overlapping paths between Tromsø-Bodø. There is no propeller consumption or IPS consumption in this case as icing is ignored. The plots does not add anything again and is generally just the path taken. The horizontal path projection is quite close to each other, while the vertical path has more variations.

With that said, this ends the section with regards to time optimisation.

7.3 Comparing Narums Results

Profile	Expended energy	Time spent	Fuel left	Battery cap left	Tot. time in ice	Avg. height	Tot. path length
1 - D	116.739Ah	6h14m29s	0.518L	14.873Ah	1h18m51s	1320m	328.0km
1 - E	63.713Ah	4h30m19s	2.365L	12.075Ah	0h12m20s	1059m	349.9km
1 - T	68.805Ah	3h36m22s	1.923L	20.337Ah	0h42m34s	1199m	342.7km
2 - D	47.503Ah	2h15m56s	2.779L	15.771Ah	0h24m55s	1320m	328.0km
2 - E	32.924Ah	2h2m27s	3.155L	19.004Ah	0h0m42s	1237m	333.5km
2 - T	35.986Ah	1h52m3s	3.170L	15.490Ah	0h19m42s	1290m	334.1km

Figure 36: A table over Narums results for the same route and day as presented in this chapter. Source: [5]

We end the chapter with a comparison between the results presented in this thesis and Narums results. Comparing results is not entirely 1 to 1 because every run for Narum is random, as seeding was yet to be implemented. It also does not have ensemble weather forecasting and it is possible the weather condition in Narums thesis is worse. It is still useful to compare to see where the new implementations have made an impact. Figure 36 shows Narums results, where profile 1 is the Tromsø-Bodø route and profile 2 is the Bodø-Tromsø route. The D, E and T notations are default path, energy optimised and time optimised respectively. The default path is the straightest path possible and is where the PSO uses as a baseline which is shown in Figure 24. The three parameters to compare is expended energy and time spent. There were no similar default path tests performed in this thesis and hence is incomparable. It does show how badly the default path performs and reinforces the need for better path planning. The energy consumption show the same trend where time optimised consumption is higher than energy optimised consumption. The overall energy consumption is higher in general when comparing with the convergence plots in this thesis. This is a consequence of incorporating a higher propeller efficiency (15% increase, hence 15% decrease in energy consumed), a more accurate weather forecasting model and IPS energy consumption model. For the Tromsø-Bodø route, it exhibits longer flight time for energy optimisation, but a significantly shorter flight time when optimised for time. It could be that the wind forecast more favourable to yield the much shorter flight time. However, as mentioned earlier, the comparison is not 1 to 1 and some margin of error, $\pm 20 minutes$ should be expected. The results are much closer for the Bodø-Tromsø route, where the shortest flight is on par with what is presented in this thesis. All in all, Narums results is quite different to the results presented in this thesis. It should give a general idea on how the implementation has affected the algorithm, but it should be used as a direct comparison as too much is changed between the two algorithms.

This ends the chapter. There has been a lot of information to digest, but all that is left is to conclude the thesis.

8 Conclusion

To conclude, this thesis has presented a lot of information to process and hence a summary of the most important information is in order. This thesis dealt with the topic of UAV icing, which is important due to the huge growth in the UAV industry. To make the UAV as safe and efficient as possible, dealing with icing becomes important. This is because some of the potential applications for UAVs is transportation of packages and people. To avoid accidents, icing needs to be dealt with as the UAV can fail with too much icing. Packages can fall out of the sky or fail while there is a passenger onboard. The UAV itself can crash onto people which is dangerous in the urban environment. This thesis focuses on the aerodynamic performance degradation in the path planning of UAVs in icing conditions, which is to find the best path through an icy environment, either avoiding it or by utilizing the onboard IPS. To simulate the paths requires having an understanding on how icing affects the aerodynamics of the UAV. This thesis works to implement the performance degradation of the wings, propellers and IPS energy consumption of both the wings and propellers. It is also a part of the thesis to document the changes made and where the data used for implementation comes from. Before this can be implemented, the physics of icing and aerodynamics needs to be explained.

As a short summary on the deep dive of the physics of the problem, it will be split into 3 parts, icing conditions, aerodynamic performance and IPS energy consumption. The icing conditions explains some of the main parameters that influence how icing is formed and the type of ice. There are 3 main parameters, temperature, MVD and LWC. These three parameters affect the severity of icing, which can be split into three parts, rime ice, glaze ice and mixed ice. Of these glaze ice is the worst due to the horns that can form on the leading edge of the wings, which contribute to a large drag increase. Mixed ice can also form horns, but can go either way in terms of being more rime than glaze. Rime ice preserves the airfoil shape better and is thus less severe. Glaze ice usually forms at higher temperatures, while rime ice forms at colder temperatures. Rime ice forms by freezing quickly, trapping air bubbles and maintaining the airfoil shape. Glaze ice freezes slower which gives more uneven shapes by allowing wind to affect the freezing process. Icing is detected by checking for relative humidity, LWC and temperature is in certain icing ranges. Temperature must be below freezing, LWC can not be too small or heavy as it will either follow streamlines or fall as rain and relative humidity needs to be high enough for icing to occur. Since MVD is fixed by LWC and temperature it is not used to check for icing.

As for aerodynamic performance degradation, the keywords are early flow separation due to icing (happens more for glaze ice and horns) and drag increase. Icing affects the wing performance in specific ways. The more severe the icing is, the less lift the wings will generate for a given AoA. Stall angle also reduces. As the lift coefficient is mostly constant throughout the route, drag is the main issue. Drag can increase significantly depending on how long the ice is allowed to accumulate and the severity of icing. The drag can increase anywhere from 10-100% depending if it is glaze or rime ice, where glaze ice nearly doubles drag when ice is allowed to accumulate for 20 minutes. This increase in drag ultimately increases energy consumption, which can affect mission success. Propeller degradation is just as bad and can decrease efficiency up to 80%.

The IPS energy consumption is divided into anti-icing and de-icing. For the propeller, only anti-icing is used due to how fast the propeller degrades, while for the wing both are available. The IPS energy consumption only depends on the temperature and for simplicity assumes linear relationship between data points. Some of the IPS data is separated into two linear regions, which is explained in more detail in the energy consumption section why this is valid. The colder the temperature, the higher the IPS energy consumption, as it requires more energy to heat to positive temperatures.

Finally, in presenting the results, there are a few scenarios that are of interest. It is of interest to compare anti-icing and de-icing by themselves. To see if there are conditions where one is better than the other. It was found that neither IPS mode was better than the other, but depends on the conditions encountered. It is also interesting to see results when the IPS is disabled as a reference case. There were also testing performed between using 2D and 3D aerodynamic data

to see if it was viable to use 2D data, as 3D drag characteristics is higher. The tests were split into minimizing energy or flight time. For both of these the results showed that the no IPS run had too many inconsistencies, but changes were implemented to solve this issue. The problem was identified by how the PSO operates, based on a waypoint to waypoint system. The weather conditions between waypoints was assumed constant and transitioning to the next waypoint resets the icing, making the icing seem less severe than it actually was. By implementing changes such as continuous ice accumulation times and testing for different propeller degradation, the results clearly showed the benefits of having IPS. The 2D and 3D results were also not as expected as using 3D data gave lower energy cost than 2D despite having higher drag characteristics. The problem was identified to the thrust equation that had angle of attack as a variable. The 3D data operated at a lower angle of attack, which can make a term negative in the equation and hence resulting in a lower power requirement. This is collaborated by looking at the raw data. Another issue was that the CFD model was not entirely correct. The PX-31 wing incidence is made with -4 inclination, while the cruise AoA of the PX-31 is at 0-2 degrees AoA. This was not modelled in the CFD model and hence gave correct lift coefficients, but at the wrong AoA values. Due to time constraint, the CFD simulation could not be performed on time. Instead, a good estimate was achieved by adding 4 to the AoA values, giving results that was as expected with higher energy consumption when using 3D data. It is concluded that 2D data is okay to use, but only in cases far from maximum flight time of the aircraft, especially when icing is present. When the UAV is pushed to the limit of its endurance together with icing, 2D is no longer viable and 3D data should be used. By using 3D icing data, the results should give higher energy cost and longer flight times for all scenarios. 3D icing data was not available during the thesis and hence could not be tested.

The results presented, did not show any definite overall best scenario. In fact, the scenarios where IPS was used were quite close to each other, with only minor advantages. The differences were small enough to attribute the results to the randomness of the simulation. Another theory is that the weather on the test day was not varied enough to yield icing condition severe enough to fully test each IPS mode. For the time optimised tests, the different IPS scenarios showed expected results. The simulation did not penalize icing as much, but prioritized better flight time. Anti-icing did give better flight times than de-icing for the Tromsø-Bodø route, while the Bodø-Tromsø routes gave small differences between every scenario. It is possible that anti-icing with its larger energy cost lead the simulation to explore more, while de-icing is more restricted. The time optimisation might have some innate energy optimisation baked into the algorithm that restricts how "adventurous" it gets. This is hopefully alleviated with the random default path implemented by Tiller. The comparison between anti-icing and de-icing was inconclusive, but de-icing was found to give the best balance between energy expenditure and flight time for the given weather conditions. Anti-icing has higher power ratings at low icing severity, while de-icing overtakes anti-icing if the icing is severe enough. The results did not show when de-icing power ratings overtakes anti-icing power ratings. Further investigations is required and testing should be performed in more varied weather conditions for more conclusive answers. Anti-icing was the only IPS scenario to give significantly higher energy cost for time optimised simulations. This is as expected due to its higher power ratings. For the 2D/3D and IPS disabled cases, the results were as expected after implementing changes to make the results more consistent. They gave consistently higher energy cost and flight time. With that said, a lot was learned from this thesis on the behaviour of the simulation. The documentation in this thesis will help in developing it further in the future.

9 Future Work

9.1 Model Improvements

Due to the overhaul of the code by Tiller, the implementations made in this thesis need to be re-implemented in the new code. The ensemble weather forecasting also needs to be re-implemented. The things learned from implementing the performance degradation and IPS energy consumption will help in implementing it quicker. The new code also functions differently and things that were not possible before might now be possible. This needs to be explored further. Other improvements includes being more consistent in calculating energy consumption, transitioning into kilo-Watt-hours instead of Ampere-hours.

9.2 Path Planning Improvements

Some path planning improvements have already been implemented by Tiller, which makes the PSO explore more by randomizing the initial default path. This allows the PSO to explore more potential solutions. It remains to make the solution more consistent by making the simulation find the global minimum.

9.3 No IPS Improvements

As mentioned in the results chapter, there remain quite a few improvements to the IPS disabled scenario. This includes implementing an icing severity index to model the propeller degradation more accurately. It is also beneficial to model the ice formation for more accurate degradation modelling. It remains to determine how much effort is worth to make the no IPS case more accurate before returns become diminishing.

9.4 Moving Forward

The main aim is to be able to make the simulations more and more accurate. More experimental data should be used for this and it is possible with enough data that some machine learning could be used to improve the simulations. The experimental data will come from testing in an icing wind tunnel. There might also be more focus on thermodynamics and to be able to model the heat transfer better. As the project moves along, the simulation will expand into including splash backs, run back icing and super large droplets. The icing formation should also be modelled better to achieve more accurate path planning. Finally, 3D plots with wind and icing should be implemented, such that it is easier to see the pathing decisions made by the algorithm.

References

[1] R. Hann, R. J. Hearst, L. R. Sætran, and T. Bracchi, "Experimental and numerical icing penalties of an S826 airfoil at low reynolds numbers," *Aerospace*, vol. 7, no. 4, pp. 1–18, 2020.

[2] FAA, "Icing Design Envelopes (14 CFR Parts 25 and 29 , Appendix C)," *Regulation*, no. April, 2002.

[3] M. B. Bragg, A. P. Broeren, and L. A. Blumenthal, "Iced-airfoil aerodynamics," *Progress in Aerospace Sciences*, vol. 41, no. 5, pp. 323–362, 2005.

[4] R. W. Beard and T. W. McLain, *Small unmanned aircraft: Theory and practice*. 2012.

[5] E. Narum, "Mission Planning for Fixed-Wing UAVs in Wind and Icing Conditions," 2020.

[6] C. Humphreys-Jennings, I. Lappas, and D. M. Sovar, "Conceptual design, flying, and handling qualities assessment of a blended wing body (BWB) aircraft by using an engineering flight simulator," *Aerospace*, vol. 7, no. 5, 2020.

[7] N. Fajt, R. Hann, and T. Lutz, "The Influence of Meteorological Conditions on the Icing Performance Penalties on a UAV Airfoil," *8th European Conference for Aeronautics and Space Sciences (EUCASS)*, no. July, 2019.

[8] D. Raymer, *Aircraft Design: A Conceptual Approach, Sixth Edition*. Amer Institute of Aeronautics, 2018.

[9] R. Hann, *Atmospheric Ice Accretions, Aerodynamic Icing Penalties, and Ice Protection Systems on Unmanned Aerial Vehicles*. 2020.

[10] E. Narum, R. Hann, and T. A. Johansen, "Optimal Mission Planning for Fixed-Wing UAVs with Electro-Thermal Icing Protection and Hybrid-Electric Power Systems," *2020 International Conference on Unmanned Aircraft Systems, ICUAS 2020*, pp. 651–660, 2020.

[11] BIS Research Inc., "Global Unmanned Aerial Vehicle (UAV) Market: Focus on Class, Components, Applications, and End User - Analysis and Forecast, 2020-2025," 2020.

[12] R. Hann and T. A. Johansen, *Unsettled Topics in Unmanned Aerial Vehicle Icing*, vol. EPR2020008. 2020.

[13] R. Hann, K. Borup, A. Zolich, K. Sorenson, H. Vestad, M. Steinert, and T. A. Johansen, "Experimental Investigations of an Icing Protection System for UAVs," no. August, pp. 1–7, 2019.

[14] R. Hann, A. Wenz, K. Gryte, and T. A. Johansen, "Impact of Atmospheric Icing on UAV Aerodynamic Performance," 2017.

[15] A. R. Hovenburgh, *Flight Performance Optimization for Small Unmanned Aerial Vehicles Using Path Planning Methods*. 2020.

[16] M. Tiller, *Path Planning for Fixed-Wing UAVs in Wind and Icing Conditions*. PhD thesis, Norwegian University of Science and Technology, 2021.

[17] M. Tiller, T. A. Johansen, and R. Hann, *Path Planning for Fixed-Wing UAVs in Wind and Icing Conditions*. PhD thesis, Norwegian University of Science and Technology, Trondheim, 2020.

[18] J. F. Manwell, J. G. McGowan, and A. L. Rogers, *Wind Energy Explained: Theory, Design and Application*. 2010.

[19] D. McLean, *Understanding Aerodynamics: Arguing from the Real Physics*. 2012.

[20] S. E. Bansmer, *Aircraft Icing - A challenging problem of fluid mechanics*. 2020.

[21] X. Zhang, X. Wu, and J. Min, "Aircraft icing model considering both rime ice property variability and runback water effect," *International Journal of Heat and Mass Transfer*, vol. 104, pp. 510–516, 2017.

[22] J. D. Anderson, *Fundamentals of Aerodynamics SI*, vol. 1984. 2011.

[23] D. Li, R. Li, C. Yang, and X. Wang, "Effects of surface roughness on aerodynamic performance of a wind turbine airfoil," *Asia-Pacific Power and Energy Engineering Conference, APPEEC*, no. 2007, 2010.

[24] M. Costes and F. Moens, "Advanced numerical prediction of iced airfoil aerodynamics," *Aerospace Science and Technology*, vol. 91, pp. 186–207, 2019.

[25] S. Min and K. Yee, "New roughness-induced transition model for simulating ice accretion on airfoils," *AIAA Journal*, vol. 59, no. 1, pp. 250–262, 2021.

[26] T. Shannon and S. T. McClain, "An Assessment of LEWICE Roughness and Convection Enhancement Models," *SAE Technical Papers*, vol. 2019-June, no. June, pp. 128–139, 2019.

[27] J. Winslow, H. Otsuka, B. Govindarajan, and I. Chopra, "Basic understanding of airfoil characteristics at low Reynolds numbers (104–105)," *Journal of Aircraft*, vol. 55, no. 3, pp. 1050–1061, 2018.

[28] G. Narayan and B. John, "Effect of winglets induced tip vortex structure on the performance of subsonic wings," *Aerospace Science and Technology*, vol. 58, pp. 328–340, 2016.

[29] R. T. Whitcomb, "A design approach and selected wind tunnel results at high subsonic speeds for wing-tip mounted winglets," *Nasa Tn D-8260*, no. July, pp. 1–33, 1976.

[30] Q. R. Wald, "The aerodynamics of propellers," 2006.

[31] R. J. Scavuzzo, M. L. Chu, and C. J. Kellackey, "Impact ice stresses in rotating airfoils," *Journal of Aircraft*, vol. 28, no. 7, 1991.

[32] G. F. Naterer, "Multiphase transport processes of droplet impact and ice accretion on surfaces," *Cold Regions Science and Technology*, vol. 65, no. 1, pp. 5–12, 2011.

[33] T. Liu, K. Qu, J. Cai, and S. Pan, "A three-dimensional aircraft ice accretion model based on the numerical solution of the unsteady Stefan problem," *Aerospace Science and Technology*, vol. 93, p. 105328, 2019.

[34] P. Lavoie, D. Pena, Y. Hoarau, and E. Laurendeau, "Comparison of thermodynamic models for ice accretion on airfoils," *International Journal of Numerical Methods for Heat and Fluid Flow*, vol. 28, no. 5, pp. 1004–1030, 2018.

[35] R. Eberhart and J. Kennedy, "New optimizer using particle swarm theory," in *Proceedings of the International Symposium on Micro Machine and Human Science*, 1995.

[36] D. Wang, D. Tan, and L. Liu, "Particle swarm optimization algorithm: an overview," *Soft Computing*, vol. 22, no. 2, 2018.

[37] J. Du, J. Berner, R. Buizza, M. Charron, P. Houtekamer, D. Hou, I. Jankov, M. Mu, X. Wang, M. Wei, and H. Yuan, *Ensemble Methods for Meteorological Predictions*. 2018.

[38] J. Nocedal and S. Wright, *Numerical optimization, series in operations research and financial engineering*. 2006.

[39] A. L. Haynes and C. E. Parnell, "A trilinear method for finding null points in a three-dimensional vector space," *Physics of Plasmas*, vol. 14, no. 8, 2007.